

https://dspace.org/

On the detectability of multiple input multiple output (MIMO) radar signals using conventional electronic warfare support (ES) receivers

Huang, Yen-Hsiang

2016

http://hdl.handle.net/10539/22667

Huang, Yen-Hsiang (2016) On the detectability of multiple input multiple output (MIMO) radar signals using conventional electronic warfare support (ES) receivers, University of the Witwatersrand, Johannesburg, <http://hdl.handle.net/10539/22667>

Downloaded from a DSpace repository. https://dspace.org/

ON THE DETECTABILITY OF MULTIPLE INPUT MULTIPLE OUTPUT (MIMO) RADAR SIGNALS USING CONVENTIONAL ELECTRONIC WARFARE SUPPORT (ES) RECEIVERS

Yen-Hsiang Huang

A research report submitted to the Faculty of Engineering and the Built Environment, University of the Witwatersrand, Johannesburg, in fulfilment of the requirements for the degree of Master of Science in Engineering.

Johannesburg, 2016

Declaration

I declare that this research report is my own, unaided work, unless otherwise acknowledged. It is being submitted for the degree of Master of Science in Engineering in the University of the Witwatersrand, Johannesburg. It has not been submitted before for any degree or examination in any other university.

Signature of candidate

_____ day of _____ year _____

day *month* *year*

Abstract

Multiple-Input Multiple-Output (MIMO) radar is a more general form of phased array radar, where each antenna in the array transmits linearly independent or mutually orthogonal signals. Sustained growth in computational power as well as the decline in the cost of integrated radio frequency (RF) components has made MIMO more viable than in the past. The potential emergence of practical MIMO radar has prompted an investigation into the detectability of MIMO radar signals using existing conventional Electronic warfare Support (ES) receivers such as the Crystal Video Receiver (CVR) and a specific type of superheterodyne receiver (superhet) known as the Zero IF Receiver (ZIFR). Literature on the detectability of MIMO radar signals is extremely scarce and this investigation aims to offer insights into the detectability of MIMO radar signals by means of computer simulations.

The fundamental theory necessary for this research includes phased array radar theory, MIMO array radar theory and ES receiver signal detection theory. The detection of MIMO radar signals is compared to a reference phased array case to provide relative context. This investigation focusses on co-located Uniform Linear Arrays (ULA) based radar systems. The result of interest is the relative Signal-to-Noise Ratio (SNR) at which each type of radar can be detected by the ES receiver. Therefore, a lossless transmission, without loss of generality, is assumed. Constraints such as the equal transmit power over all antenna elements in the arrays, are used for a fair comparison. Many different array simulation setups are simulated. These setups are achieved by varying the number of elements in the array and the inter-element spacing. The phased array radar transmitted complex linear chirp signals, and the MIMO radar transmitted Hadamard sequences, interpolated using a Constant Envelope Linear-Route-of-Unity (CE-LRU) technique. The CVR and ZIFR detection thresholds were determined for a Probability of False Alarm (PFA) of 10^{-4}.

For all of the setups, the phased array radar was found to be more detectable than the MIMO radar at values of Probability of Detection (PD) below 0.6. The in phase coherent combination of phased array radar signals in its main beam resulted in a signal gain caused by the constructive addition of the signals. This gain thus increases with the number of antenna elements. In contrast, the MIMO signals also add coherently, but the instantaneous phase for each signal is a function of the transmitted signal as well as the direction of propagation relative to the array face. The set of orthogonal signals thus add constructively and destructively, resulting in the average signal power remaining approximately constant

despite the number of antenna elements increasing. The difference in detectability of the phased array radar over MIMO radar therefore increases as the number of antenna elements is increased, due to the fact that each element is constrained to transmit a fixed power.

Comparing the performance of the ZIFR and CVR, the ZIFR outperforms the CVR. This is due to the fact that the ZIFR implements a quadrature ES receiver, and was able to detect both types of radar signals at a lower SNR than the CVR. However, both ES receivers struggle to detect MIMO radar signals in comparison to detecting phased array radar signals and this performance margin widens as the number of transmitting elements is increased. This result suggests that research into dedicated techniques for the detection of MIMO radar signals using ES receivers may be necessary should the need arise to detect MIMO radar signals in future. This is the first quantitative analysis of the detectability of MIMO radar signals using conventional ES receivers that the author is aware of.

Acknowledgements

I would like to express my sincere gratitude towards my supervisors Professor Anton van Wyk from the University of the Witwatersrand and Jacques Cilliers from the Council for Scientific and Industrial Research. Together, they were able to push me across the finish line.

I would like to thank Professor Anton van Wyk for getting me started with antenna array theory, for eventually getting me into an analytical mindset, and for sharing his knowledge and wisdom. Next, I would like to thank Jacques Cilliers for taking over the responsibility of supervising my research, for always being available to me for consultation, for all the late night Skype discussions, for the interesting tangent discussions, for adding some real world knowledge into my research, and for putting up with all my nonsense in general. I would also like to thank the University of the Witwatersrand for awarding me the Postgraduate Merit Award and to the CSIR for granting me the Ledger Bursary.

Thank you to my family and friends who supported me through this degree and this research. A special thanks to my loving mom, Chiung-O Huang, and my caring dad, Tsung-Chen Huang, to whom I am grateful for everything in the world. Together, they have afforded me all sorts of amazing opportunities in my life, including the opportunity to study a postgraduate degree. Thanks to my sister, Lin-Chun Huang, for always being there for me and for inspiring me to take my education this far.

Finally, I would like to thank my (new) wife, Ying-Hsi Chien, for supporting, motivating and encouraging me every step of the way, for accepting all the nights I wanted to stay in and get some work done, and for planning most of our wedding while I was writing up.

I hereby dedicate this work to everyone that made this possible.

Contents

1 Introduction 1

1.1 Problem Statement 3

1.2 Research Objective 4

1.3 Research Contribution 5

1.4 Approach Overview 5

1.5 Conclusion 6

2 Background Theory 7

2.1 Radar Signals 8

2.1.1 Propagating Plane Waves 8

2.1.2 Far-Field 8

2.1.3 Narrowband Signal Approximation 10

2.2 Phased Array Model 13

2.2.1 Narrowband Phased Arrays 14

2.2.2 Received Signal Model 17

2.2.3 Statistical Assumptions 18

2.2.4 Beamforming 18

2.2.5 Array Antenna Pattern 19

2.2.6 Phased Array Beamforming Techniques 20

2.3 MIMO Arrays 21

2.3.1 Narrowband MIMO Arrays 23

2.4 MIMO Array Signal Generation 24

2.4.1 Hadamard Matrix 25

2.4.2 Signal Interpolation 25

2.4.3 Constant Envelope Linear Root-of-Unity Filtering 28

2.5 ES Receivers 29

2.5.1 Crystal Video Receiver (CVR) 30

2.5.2 Superheterodyne Receiver 30
2.6 Signal Detection in ES receivers 32
2.6.1 CVR Detection Model 34
2.6.2 ZIFR Detection Model 37
2.7 Conclusion 39
3 Simulation Setup 40
3.1 Phased Array Signal Generation 42
3.2 MIMO Array Signal Generation 45
3.3 Theoretical Patch Antenna Implementation 48
3.4 CVR Implementation 49
3.5 ZIFR Implementation 53
3.6 Simulation Setup for Antenna Pattern Comparison 55
3.6.1 Ideal Omnidirectional Phased Array Antenna Patterns 56
3.6.2 Ideal Omnidirectional MIMO Array Antenna Patterns 61
3.6.3 Theoretical Patch Phased Array Antenna Patterns 66
3.6.4 Theoretical Patch MIMO Array Antenna Patterns 70
3.7 Conclusion 72
4 Results, Analysis and Discussion 73
4.1 Discussion of Emphasized Detection Results 74
4.2 Discussion of Overall Detection Results 79
4.2.1 Comparison of the Detection Performance of the CVR and the ZIFR 79
4.2.2 Comparison of the Detectability of MIMO and Phased Array Radar 80
4.2.3 Comparison of the ES Receiver's Detection Result to a Theoretical Benchmark 81
4.2.4 Comparison of ES Receiver and Radar Detection Ranges 82
4.2.5 Overall Detection Results 85
4.3 Conclusion 90
5 Conclusion 91

6 Future Recommendations 93

References 95

List of Figures

Figure 2.1: A basic radar system block diagram. 7
Figure 2.2: Antenna array receiving a signal transmitted by an omnidirectional point source. 9
Figure 2.3: Narrowband approximation for a typical search radar operating at 1 GHz. ... 12
Figure 2.4: Antenna array spatially sampling a wave. 14
Figure 2.5: Distances and angles between a point source and antenna array elements. ... 15
Figure 2.6: MIMO radar architecture illustration. 22
Figure 2.7: MIMO array spatial convolution effect. 22
Figure 2.8: Interpolation block diagram. 25
Figure 2.9: Numeric example of a sinusoid signal being interpolated by a factor of L. ... 27
Figure 2.10: CE-LRU filtering [32]. 28
Figure 2.11: CE-LRU block diagram. 29
Figure 2.12: CVR system overview. 30
Figure 2.13: Superhet system overview. 31
Figure 2.14: ZIFR system overview [35]. 32
Figure 2.15: Four possible signal detection outcomes. 33
Figure 3.1: Semicircle (180°) range. 40
Figure 3.2: Example of phased array radar beam stepping operation. 43
Figure 3.3: PD comparison of phased array main beam versus side lobes, for the case of 4-element array. 44
Figure 3.4: Complex chirp signal example. 45
Figure 3.5: MIMO signal generation example. 47
Figure 3.6: Bandwidth comparison between the MIMO signal and the complex chirp. .. 48
Figure 3.7: Theoretical patch antenna pattern. 48
Figure 3.8: Overview of CVR implementation. 49
Figure 3.9: CVR detection threshold error correction for $P_{fa}=10^{-4}$. 52
Figure 3.10: Overview of the ZIFR implementation. 53
Figure 3.11: ZIFR detection threshold error correction for $P_{fa}=10^{-4}$. 55
Figure 3.12: Four-antenna element phased array 0.5λ inter-element spacing. 57
Figure 3.13: Four-antenna element phased array with 1.0λ inter-element spacing. 58
Figure 3.14: Four-antenna element phased array with 2.0λ inter-element spacing. 58
Figure 3.15: Four-antenna element phased array with 4.0λ inter-element spacing. 58
Figure 3.16: Eight-antenna element phased array with 0.5λ inter-element spacing. 59

Figure 3.17: Eight-antenna element phased array with 1.0λ inter-element spacing. 59
Figure 3.18: Eight-antenna element phased array with 2.0λ inter-element spacing. 59
Figure 3.19: Eight-antenna element phased array with 4.0λ inter-element spacing. 60
Figure 3.20: Sixteen-antenna element phased array with 0.5λ inter-element spacing. 60
Figure 3.21: Sixteen-antenna element phased array with 1.0λ inter-element spacing. 60
Figure 3.22: Sixteen-antenna element phased array with 2.0λ inter-element spacing. 61
Figure 3.23: Sixteen-antenna element phased array with 4.0λ inter-element spacing. 61
Figure 3.24: Four-antenna element MIMO array with 0.5λ inter-element spacing. 62
Figure 3.25: Four-antenna element MIMO array with 1.0λ inter-element spacing. 63
Figure 3.26: Four-antenna element MIMO array with 2.0λ inter-element spacing. 63
Figure 3.27: Four-antenna element MIMO array with 4.0λ inter-element spacing. 63
Figure 3.28: Eight-antenna element MIMO array with 0.5λ inter-element spacing. 64
Figure 3.29: Eight-antenna element MIMO array with 1.0λ inter-element spacing. 64
Figure 3.30: Eight-antenna element MIMO array with 2. 0λ inter-element spacing. 64
Figure 3.31: Eight-antenna element MIMO array with 4.0λ inter-element spacing. 65
Figure 3.32: Sixteen-antenna element MIMO array with 0.5λ inter-element spacing..... 65
Figure 3.33: Sixteen-antenna element MIMO array with 1.0λ inter-element spacing..... 65
Figure 3.34: Sixteen-antenna element MIMO array with 2.0λ inter-element spacing..... 66
Figure 3.35: Sixteen-antenna element MIMO array with 4.0λ inter-element spacing..... 66
Figure 3.36: Four patch antenna element phased array with 0.5λ inter-element spacing. 67
Figure 3.37: Four patch antenna element phased array with 4.0λ inter-element spacing. 68
Figure 3.38: Eight patch antenna element phased array with 0.5λ inter-element spacing.68
Figure 3.39: Eight patch antenna element phased array with 4.0λ inter-element spacing.68
Figure 3.40: Sixteen patch antenna element phased array with 0.5λ inter-element spacing. 69
Figure 3.41: Sixteen patch antenna element phased array with 4.0λ inter- element spacing. 69
Figure 3.42: Four patch antenna element MIMO with 0.5λ inter-element spacing. 70
Figure 3.43: Four patch antenna element MIMO with 4.0λ inter-element spacing. 71
Figure 3.44: Eight patch antenna element MIMO with 0.5λ inter-element spacing. 71
Figure 3.45: Eight patch antenna element MIMO with 4.0λ inter-element spacing. 71
Figure 3.46: Sixteen patch antenna element MIMO with 0.5λ inter-element spacing. 72
Figure 3.47: Sixteen patch antenna element MIMO with 4.0λ inter-element spacing. 72
Figure 4.1: CVR detection results of a 4-element phased array at 0.5λ spacing. 74
Figure 4.2: CVR detection results of a 4-element phased array at 4.0λ spacing..... 74

Figure 4.3: CVR detection results of an 8-element phased array at 0.5λ spacing. 75
Figure 4.4: CVR detection results of an 8-element phased array at 4.0λ spacing..... 75
Figure 4.5: CVR detection results for 4-element versus 8-element phased arrays. 76
Figure 4.6: CVR detection results of a 4-element MIMO array at 0.5λ spacing. 76
Figure 4.7: CVR detection results for a 4-element MIMO array at 4.0λ spacing. 77
Figure 4.8: CVR detection results of an 8-element MIMO array at 4.0λ spacing. 77
Figure 4.9: CVR detection results of a 4-element versus 8-element MIMO array. 77
Figure 4.10: CVR detection results of a 4-element patch antenna phased array at 4.0λ spacing. 78
Figure 4.11: CVR detection results of a 4-element patch antenna MIMO array at 4.0λ spacing. 78
Figure 4.12: CVR detection results of 4-element phased array versus the 4-element MIMO array using patch antennas. 79
Figure 4.13: Comparison of the spectra at various points in the processing chain of CVR versus ZIFR with a 16-element phased array case with 0.5λ inter-element spacing. 80
Figure 4.14: Detectability of simulation results versus theoretical benchmarks for interpolated Hadamard codes with lengths of 8, 11, 13 and 16. 82
Figure 4.15: Comparison of detection ranges of radar versus ES receivers. 85
Figure 4.16: Overall CVR PD result averaged over all DOAs. 86
Figure 4.17: Overall ZIFR PD result averaged over all DOAs. 87
Figure 4.18: Comparison of CVR versus ZIFR PD results (4.0λ only) for the case of ideal omnidirectional antenna array elements. 88
Figure 4.19: Comparison of CVR versus ZIFR results (4.0λ only) for the case of patch antenna array elements. 89

List of Tables

Table 1. Simulation setup for phased arrays by varying number of antenna elements and inter-element spacing. 41
Table 2. Simulation setup for MIMO arrays by varying number of antenna elements and inter-element spacing. 41
Table 3: Typical example of search radar parameters. 42
Table 4: Parameters for simulation of the radar. 42
Table 5: Patch antenna simulation setups. 49
Table 6: MIMO array illustrated transmitted signals. 62
Table 7: Illustrated simulation results for the CVR. 73
Table 8: Detection Probability and detectability for $P_{fa}=10^{-4}$ [38]. 81
Table 9. Example radar and ES receiver parameters. 84

Nomenclature

Acronyms

CDF	Cumulative distribution function
CE-LRU	Constant Envelope Linear-Root-of-Unity
CVR	Crystal Video Receiver
DIB	Data Independent Beamformer
DOA	Direction of Arrival
EA	Electronic Attack
EP	Electronic Protection
ES	Electronic warfare Support
EW	Electronic Warfare
FIR	Finite Impulse Response
IF	Intermediate Frequency
LPI	Low Probability of Intercept
LRU	Linear Route-of-Unity
MIMO	Multiple Input Multiple Output
PAPR	Peak-to-Average Power Ratio
PD	Probability of Detection
PDF	Probability Density Function
PFA	Probability of False Alarm
PRI	Pulse Repetition Interval
RF	Radio Frequency
SNR	Signal-to-Noise Ratio
SOB	Statistically Optimum Beamformer
ULA	Uniform Linear Array
ZIFR	Zero IF Receiver

Mathematical Symbols

β	Complex amplitude
Δ	Antenna length
δr	Plane wave approximation error
λ	Wavelength
μ	Statistical mean
ϕ	Phase
ω	Angular frequency
σ	Standard deviation
σ^2	Variance
τ	Time delay
θ	Direction of arrival
a	Steering for a single antenna element
b	Antenna pattern
b_f	Array response
B	Signal bandwidth
c	Speed of wave propagation
D	Antenna array length
d	Antenna array inter-element spacing
E_t	Amplitude detection threshold
f	Frequency
F	Cumulative Distribution Function
G	Gain
G_{nc}	Noncoherent integration Gain
h	Filter coefficient
I	In-phase component
L	Interpolation factor
M	Number of signal sources
m	Signal modulation function
n	Number of filter coefficients
N	Number of antenna elements in an antenna array
P_d	Probability of detection
P_{fa}	Probability of false alarm
Q	Quadrature component

r	Distance from source to antenna array
s	signal
t	Time
T	Period
w	Complex weight
x	Received signal
$\mathbf{k}$	Wave vector
$\mathbf{r}$	Position vector
$\mathbf{A}$	Steering matrix for multiple sources
$\mathbf{a}$	Steering vector for an antenna array receiving a signal
$\mathbf{H}$	Hadamard matrix
$\mathbf{h}$	Vector of filter coefficients
$\mathbf{I}$	Identity matrix
$\mathbf{R}$	Covariance matrix
$\mathbf{s}$	Set of signals
$\mathbf{w}$	Vector of complex weights
$\mathbf{x}$	Vector of received signals
$\mathbf{Y}$	MIMO array received signal
$\mathbf{z}$	Additive noise and interference
$\mathbf{y}$	Beamformer output

1 Introduction

Radio detection and ranging, known more commonly as radar, is a technique which employs radio frequency radiation detect objects. This is achieved by transmitting radio waves and analysing the echoed returns from the objects to determine the object's properties such as range, altitude, direction and speed [1]. Radar is commonly associated with defence applications. Logically, it is advantageous to be alerted to the approach of a potential threat before the threat is within striking distance in a combat scenario. The alert allows for longer timelines, and thus better preparation to deal with the incoming threat, for example preparing a weapon system to intercept an incoming threat beyond that of the weapon system's visual range. Conversely, the ability to detect the deployment of any defence measures provides the attacker with the information necessary to counteract or evade the defence measures.

Radar is an all-weather, long range sensor and thus plays a major role in Electronic Warfare (EW). Adamy defines EW as "*the art and science of preserving the use of the electromagnectic spectrum for friendly use while denying its use to the enemy.*" [2]. The Armed Forces of the United States of America defines EW with three subdivisions: Electronic warfare Support (ES), Electronic Attack (EA) and Electronic Protection (EP). The corresponding definitions for each subdivision are quoted respectively [3]:

ES: "*Actions tasked by, or under direct control of, an operational commander to search for, intercept, identify, and locate or localize sources of intentional and unintentional radiated electromagnetic energy for the purpose of immediate threat recognition, targeting, planning, and conduct of future operations.*"

EA: "*Use of electromagnetic energy, directed energy, or anti-radiation weapons to attack personnel, facilities, or equipment with the intent of degrading, neutralizing, or destroying enemy combat capability and is considered a form of fires*[1]."

EP: "*Actions taken to protect personnel, facilities, and equipment from any effects of friendly or enemy use of electromagnetic spectrum that degrade, neutralize, or destroy friendly combat capability.*"

An example of a typical cycle of EW in the context of a basic radar system is as follows. The defender deploys a radar for threat warning purposes. The attacker deploys a radar

[1] "fires" refers to any form of attack on the enemy with the intent to do damage. In this case, an electromagnetic attack.

detection system, such as a radar intercept receiver, to detect the radar and identify the type of radar which has been deployed (ES). The attacker then uses the information obtained to counteract the defence measures, for example jamming the radar (EA). The result is a cycle of innovation between the attacker and defender where each one tries to gain an advantage over the other.

It is interesting to note that the concept upon which radar is based is not a man-made innovation, and had already existed in many forms in nature. For example, nocturnal animals such as bats use ultrasonic ranging techniques to navigate and forage for food in the darkness of night. Conversely, the different types of insects, which are hunted by the bats, have ultrasonic hearing and are able to perform evasive manoeuvres to escape the bats. Studies have shown that the hunter and prey constantly adapt to try and better each other in the fight for survival [4]. The manmade EW conflict is thus reflected in nature as well.

There are many ways to implement a radar system. One of the common radar architectures is the phased array radar. Phased arrays are antenna arrays in which the relative phase of each antenna element is manipulated such that the direction of the antenna beam is changed electronically instead of mechanically. Phased arrays can be either active or passive. Passive phased arrays have an electronically controlled phase shifter directly behind the antenna elements. This is as opposed to the significantly more complex active phased arrays which have transmit/receive modules instead of phase shifters [1]. Compared to mechanical steering, the electrical steering allows for agile beam operation, which is sometimes referred to as “inertia-less” operation. Phased arrays are also more cost effective in the long term and perform better than their single antenna mechanically steered counterparts [5].

A radar architecture, known as multiple-input-multiple-output (MIMO) radar, has been called a generalisation of phased array radar [6]. Each transmit antenna element in a MIMO array transmits a signal from a set of linearly independent signals as opposed to phased arrays where each antenna element transmits the same signal scaled by a complex weight [7]. MIMO radar is therefore more computationally intensive than its phased array counterpart, and the emergence of MIMO architecture is as a result of the sustained growth in computational power as well as the decline in the cost of integrated radio frequency (RF) components. There is an on-going debate whether or not MIMO radar is actually feasible when its phased array counterpart can achieve similar if not better results with less complexity for certain application [6]. It should be noted that it is difficult to fairly compare phased arrays and MIMO arrays, and this is evident in the current literature on the subject.

The emergence of MIMO radar and its potential implementation in future EW logically initiates the next step of the typical EW cycle. This calls for an investigation into the detectability of MIMO radar signals using existing conventional ES receivers. A comprehensive investigation will offer insights as to whether or not existing ES devices are able to detect MIMO radar signals, and if new development in this area is necessary.

Research in the field of MIMO radar is predominantly confined to theoretical work and focusses on improving the performance of MIMO radar and its ability to detect targets. It should be noted that it is difficult to fairly and conclusively compare MIMO radar to its phased array counterparts, and the lack thereof is evident in literature [6]. MIMO radar can be broadly classified into two categories: statistical MIMO radar and coherent MIMO radar. Statistical MIMO radar uses widely spaced antenna elements to achieve spatial diversity. Each individual element induces an independent scattering response from the target, resulting in diversity gain [8]. Coherent MIMO radar involves closely spaced antenna elements, for example co-located arrays. In this configuration, the target's scattering response for each antenna is assumed to be approximately equal [9]. A primary advantage to closely spaced, co-located elements is the resulting large virtual antenna aperture, which improves the angular resolution.

Practically, MIMO radar is still expensive compared to its phased array counterpart. MIMO radar experimental data is therefore scarce in literature. Cost-effective ways of developing and testing MIMO radar techniques are therefore still being investigated.

The classification of MIMO and conventional radar signals using existing ES devices is a recent topic in literature. In 2013, Howard *et al.* have begun investigations into the characterization of radar transmitters using spatially distributed receivers. The rank of the transmitted signals is used to differentiate between MIMO and conventional radars [10]. During this study, no literature could be found which discusses the detectability of MIMO signals.

In summary, this investigation aims to evaluate the detectability of MIMO radar signals using conventional ES receivers. It also aims to serve as a basis for a more comprehensive investigation into the battle between MIMO radar and the detection thereof from an EW point of view.

1.1 Problem Statement

Conventional phased array radars scan a high-gain, narrow "pencil" beam across a range of angles. This stands in contrast to the MIMO radar, which has a lower-gain, "floodlight"

beam per element, and each element transmits an orthogonal signal. These signals combine coherently in space and can thus fluctuate depending on the instantaneous values of the amplitudes and phases of each element's signal as well as the direction of propagation. This fluctuation caused by the constructive and destructive interference between the set of signals leads to a form of intra-pulse amplitude modulation on the radar pulse which can reduce the amount of energy available to the ES receiver for signal detection. The performance of conventional ES devices in detecting the MIMO radar signals is therefore uncertain, and is the primary motivation of this dissertation.

An investigation into the detectability of a MIMO radar using conventional ES receivers will be performed. More specifically, co-located uniform linear arrays (ULA) will be investigated as the radar transmit and receive antennas. Various ULA setups will be explored where the number of antenna elements and the inter-element spacing are the parameters which will be varied. Conventional ES devices such as the crystal video receiver (CVR) and the superheterodyne receiver (hereafter referred to as "superhet") will be used as a basis for this investigation. More specifically, the superhet used in this investigation is the zero IF receiver (ZIFR), which mixes the signal down to baseband, but retains the phase information of the signals. Hereafter, all instances of "superhet" refers specifically to the ZIFR. For a conclusive analysis, the performance of the ES devices will be evaluated in comparison to a reference case. The detectability of MIMO radar signals will therefore be compared to the detectability of the corresponding phased array counterpart. Constraints on the MIMO and phased arrays need to be devised to allow for fair comparison between the two cases. This investigation will be conducted by means of computer simulations.

1.2 Research Objective

The key objective of this research is to scientifically evaluate the performance of conventional ES receivers when detecting MIMO radar signals. The detection of MIMO signals will then be compared to the detection of phased array radar signals. To achieve this objective, the scope and objectives of the research must cover:

- The investigation of the relevant background theory of wave propagation, signal properties, classical phased arrays, MIMO arrays, MIMO signal generation, conventional ES devices and signal detection theory;
- The discussion and development of a suitable narrowband phased array model, narrowband MIMO array model, CVR model and ZIFR model;

- Derivation of threshold for ES receiver to maintain a specified Probability of False Alarm (PFA);
- The investigation of the performance of the ES devices when detecting MIMO radar signals and phased array radar signals;
- The analysis and discussion of the ES detection results; and
- The laying of a theoretical foundation for further investigation.

The investigation will be exclusively performed via computer simulations.

1.3 Research Contribution

This investigation has resulted in the following contributions to field of ES:

- The formulation of a fair comparison case between a phased array radar and its MIMO counterpart with the following constraint: each antenna element transmits the same power; the same number of antenna elements; the same inter-element spacing; unity peak-to-average power ratio for the radar signals; and the same radar signal bandwidth.
- The derivation of an approximation for the receiver detection threshold for the CVR and ZIFR, with an error margin of approximately 11 % for a PFA of 10^{-4}. Furthermore, it is demonstrated that by varying the detection threshold, the 11% error can be eliminated.
- The generation of MIMO radar signals by interpolating Hadamard Matrix values using the Constant Envelope Linear Route-of-Unity technique.
- The comparison of the detectability of phased array radar signals versus MIMO radar signals using conventional ES receivers such as the CVR and the ZIFR.
- The comparison of the detectability of phased array radar signals versus MIMO radar signals, where the antenna arrays consisted of ideal omnidirectional antenna elements and theoretical patch antennas.

The results of this investigation has been summarised as a paper, which was accepted and presented at the 2015 IEEE Radar Conference, Johannesburg [11].

1.4 Approach Overview

This section presents the organisation of the remaining chapters of this dissertation and provides a brief outline of the contents of each chapter.

The necessary background theory is presented in Chapter 2. The theory includes: wave propagation, signal properties, phased arrays, MIMO arrays, MIMO signal generation, the CVR, the superhet, the ZIFR and signal detection theory. The development of suitable signal models for phased arrays, MIMO arrays and the ES receivers are also presented.

The simulation setup for this investigation is described in Chapter 3. This includes the phased array implementation, the MIMO implementation, the CVR implementation and the ZIFR implementation. Various array setups are investigated by varying the numbers of antenna elements in the array and the inter-element spacing. Two antenna patterns are used in the simulations: the ideal omnidirectional antenna pattern and the theoretical patch antenna pattern. The antenna patterns of the setups are presented to provide insight into the simulation results.

The simulation results are presented in Chapter 4, along with the analysis and the discussion of the results. Chapter 5 presents a conclusion to this investigation. Finally, Chapter 6 provides recommendations for future investigations.

1.5 Conclusion

This chapter introduced the role of radars and ES receivers in the broad field of EW. Furthermore, the motivation for the investigation into the detectability of MIMO radar signals using conventional ES receivers is attributed to the sustained growth in computational power as well as the decline in the cost of integrated RF components. As a result of the technological advancements, MIMO arrays may emerge as a practical option for radars. The investigation's scope and objectives are discussed and the investigation's contributions to the field of ES receivers are presented. Finally, an overview of the remaining chapters of this dissertation is summarised.

2 Background Theory

This chapter presents the fundamental theory most relevant to this investigation. A basic radar block diagram is illustrated in Figure 2.1. The fundamental components of a radar system include: the transmitter, the transmitting antenna, the receiver, the receiver antenna, and the radar display [1]. This investigation primarily focuses on the signal transmission aspect of the radar transmitter and the signal detection aspect of the ES receiver. The propagation environment is therefore neglected and lossless transmission, without loss of generality, is assumed. The various model developments assume that antenna elements are ideal and omnidirectional and that the mutual coupling between antenna elements is negligible. However, this investigation will be extended to non-ideal antenna elements such as a theoretical patch antenna element.

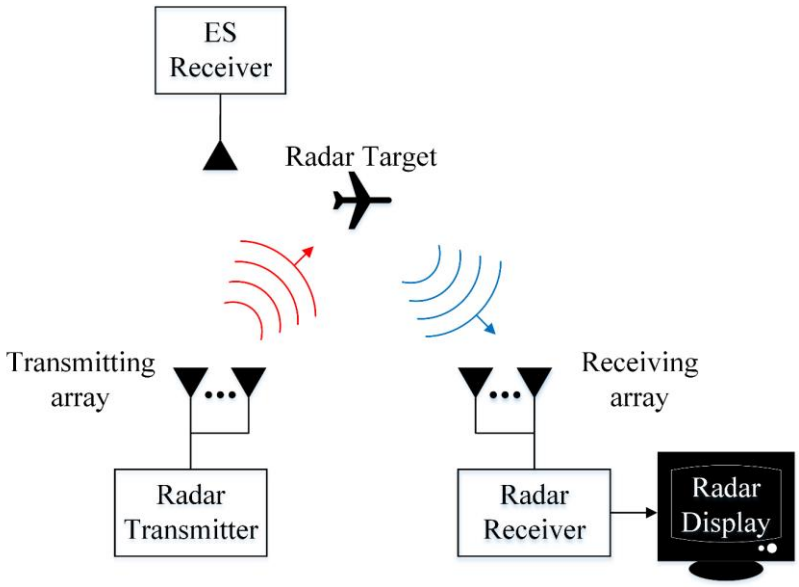


Figure 2.1: A basic radar system block diagram.

Firstly, RF signal propagation effects such as the theory of plane wave propagation and the near and far-field are presented, followed by the narrowband signal approximation. Antenna arrays, phased arrays and MIMO arrays are then introduced and a narrowband signal model for phased arrays and MIMO arrays is presented. The process of generating MIMO array signals is then discussed. Finally, ES devices including the CVR and the superhet and the ZIFR are introduced, followed by the presentation of signal models for the receivers.

2.1 Radar Signals

Radar signal properties and concepts relevant to the development of the phased array and MIMO array models are presented in the following subsections. These signal properties and concepts include: propagating plane waves, far-field signals, and the narrowband approximation.

2.1.1 Propagating Plane Waves

Propagating plane waves can be represented in the elemental complex exponential form given by

$$e(\mathbf{r}, t) = \alpha e^{j(\omega t - \mathbf{k}^T \mathbf{r})}, \tag{2.1}$$

where ω is the temporal frequency in radians per second, t is time in seconds, $\mathbf{k}$ is the wave-number, $\mathbf{r}$ is the position vector in meters and α is the collective field-strength parameters [12]. This investigation will focus on the signal-to-noise ratio (SNR) of the radar signals received by the ES receiver. The SNR can be manipulated by varying either α or the noise power. This investigation involves co-located linear arrays and thus $\mathbf{r}$ is defined as a two-dimensional position vector, in the x-y plane. The wave-number represents the spatial frequency (the number of waves per unit distance) and thus, for the two-dimensional case is given by

$$\mathbf{k} = k(\sin\theta \quad \cos\theta)^T, \tag{2.2}$$

where θ, the direction of arrival (DOA) in radians, is the angle at which the propagating wave arrives at the receiver. The angle $\theta = 0°$ is defined as the direction perpendicular to an antenna array, also referred to as "broadside". The magnitude of $\mathbf{k}$ can be expressed as

$$|\mathbf{k}| = k = 2\pi/\lambda = 2\pi f/c, \tag{2.3}$$

where λ is the wavelength in meters and c is the speed of wave propagation in m/s [13].

2.1.2 Far-Field

The three distinct regions that can be identified in electromagnetic transmission are: the near-field, Fresnel and the Fraunhofer regions. These regions are classified by the distance between the source and the point of interest in space, the wavelength and the aperture of the receiver. Consider an omnidirectional point source transmitting spherical waves. In the near-field and Fresnel regions, the wave-fronts are spherical. The Fraunhofer region, also

known as the far-field region, denotes the region in which the wave-fronts can be approximated by plane waves. Due to the nature and operation of radars, the region of interest is usually the far-field region. The development of the far-field criterion by Mahafza [14] is summarised below, supplemented by Figure 2.2.

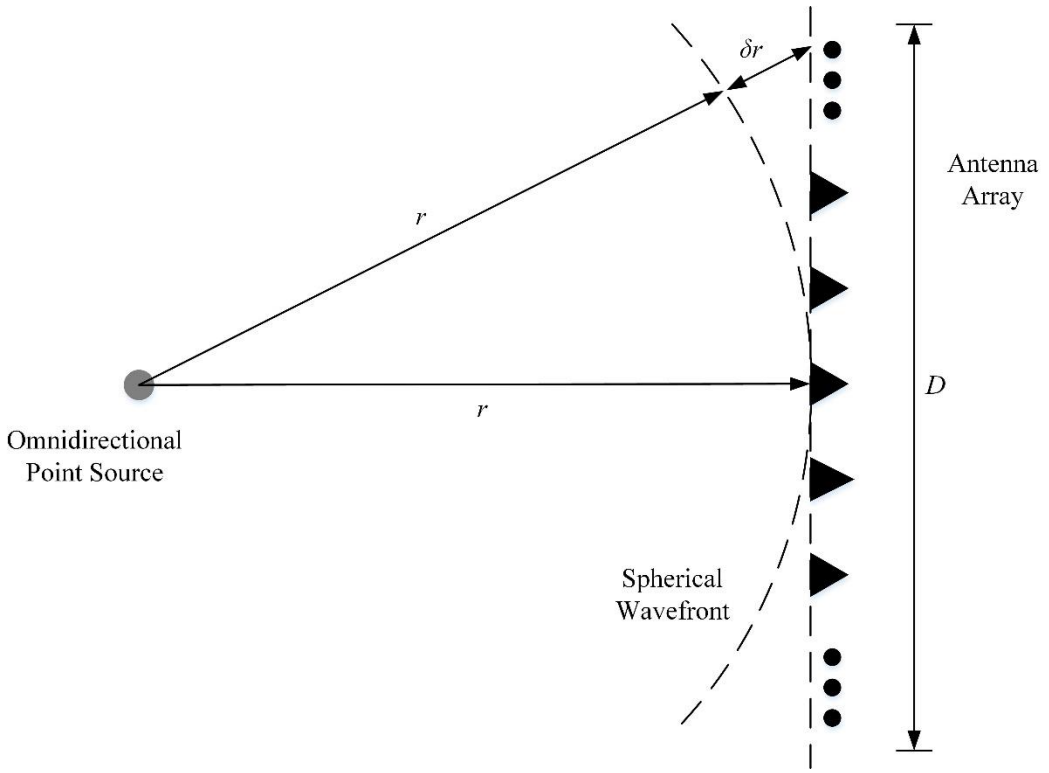


Figure 2.2: Antenna array receiving a signal transmitted by an omnidirectional point source.

The distance δr is given by

$$\delta r = \sqrt{r^2 + \left(\frac{D}{2}\right)^2} - r, \tag{2.4}$$

where $D \ll r$ due to the far field assumption. The binomial expansion is given by

$$\sqrt{1+x} = 1 + \frac{1}{2}x - \frac{1}{8}x^2 + \frac{1}{16}x^3 - \frac{5}{128}x^4 + \cdots . \tag{2.5}$$

The first two terms in the binomial expansion can be used to approximate δr as

$$\begin{aligned} \delta r &= r\left(\sqrt{1+\left(\frac{D}{2r}\right)^2}-1\right) \\ &\approx r\left(1+\frac{1}{2}\left(\frac{D}{2r}\right)^2-1\right) \\ &= \frac{D^2}{8r}. \end{aligned} \tag{2.6}$$

The criterion for a receiver to be considered in the far field is if the distance δr is less than one sixteenth of a wavelength (or $22.5°$) [14] such that

$$\delta r \approx \frac{D^2}{8r} \leq \frac{\lambda}{16}. \tag{2.7}$$

The far field criterion can then be reduced to

$$r \geq \frac{2D^2}{\lambda}. \tag{2.8}$$

2.1.3 Narrowband Signal Approximation

The narrowband approximation can be explained both temporally and spatially. Temporally, a theoretical narrowband signal satisfies [15]

$$B < 2f_c\,, \tag{2.9}$$

where B is the bandwidth in hertz and f_c is the carrier frequency in hertz. The boundary specified by (2.9) is the upper limit of the bandwidth which a signal can span and can still be written in its complex envelope form $I(t) + jQ(t)$ [15].

However, in practice, the radar bandwidth should be much smaller for the signal to be considered narrowband, for example a factor of 10 times less than the carrier frequency [16]

$$B \leq 0.1f_c\,. \tag{2.10}$$

Furthermore, according to the IEEE Standard Radar Definitions [17], radars operating at a bandwidth which is a factor of a million times less than the carrier frequency are classified as ultra-narrowband radars,

$$B \leq 0.000001f_c\,. \tag{2.11}$$

Spatially, a signal being transmitted or received by an n-element receiving antenna array needs to be considered. At a single instance in time, the signal received by each element in the array will differ. The array is therefore sampling the signal spatially. The extent by which the signals differ from each other at the different elements can be quantified by using the modulation coherence distance, given by c/B. The spatial narrowband criterion can be satisfied by ensuring the modulation coherence distance to be much greater than the aperture length in the direction of propagation [18]

$$\Delta \ll \frac{c}{B}, \tag{2.12}$$

where Δ is the antenna length in meters and B is the modulation bandwidth in hertz.

One of the main advantages of working within the narrowband criterion is that the time delay between elements can be approximated by a phase shift of the signal. This simplification is illustrated by Hudson [18] and summarised as follows. A transmitting antenna is excited with the current function

$$i(t) = m(t)e^{j\omega t}, \tag{2.13}$$

where $m(t)$ is the complex baseband modulation function. The resulting electric field has the following form

$$E(\mathbf{r}_i, t) = G(\theta)\frac{1}{|\mathbf{r}_i|}m\left(t - \frac{\mathbf{k}^T\mathbf{r}_i}{\omega}\right)e^{j(\omega t - \mathbf{k}^T\mathbf{r}_i)}, \tag{2.14}$$

where $G(\theta)$ is the antenna gain (dependent on factors such as antenna directivity) and $1/|\mathbf{r}_i|$ is the field attenuation (dependent on distance between transmitter and receiver). The narrowband criterion results in the modulation function $m\left(t - \frac{\mathbf{k}^T\mathbf{r}_i}{\omega}\right)$ being approximately constant across all the elements of the receiving antenna array at any single time instance. Therefore, it is assumed that

$$m\left(t - \frac{\mathbf{k}^T\mathbf{r}_i}{\omega}\right) = m(t - \bar{\tau}), \tag{2.15}$$

where $\bar{\tau}$, the average propagation time delay in seconds, describes the time delay between the transmitter and receiver. The resulting electric field form is

$$E(\mathbf{r}_i, t) = G(\theta)\frac{1}{|\mathbf{r}_i|}m(t - \bar{T})e^{j(\omega t - \mathbf{k}^T\mathbf{r}_i)}. \tag{2.16}$$

The error arising from the approximation of a time delay by a phase shift can be derived by considering the expression for a delayed version of the signal:

$$\begin{aligned} s(t) &= \sin(2\pi f_c(t-\tau)) && (2.17)\\ &= \sin(2\pi f_c t - 2\pi f_c \tau) && (2.18)\\ &= \sin(2\pi f_c t - \theta(f)) && (2.19) \end{aligned}$$

where f is the instantaneous frequency of the signal, and $\theta(f)$ is the frequency dependent phase. For example, a typical search radar operating at a frequency of 1 GHz with a bandwidth of 2 MHz has a frequency which ranges from 0.999 GHz to 1.001 GHz. The second term of the argument in (2.19) is the frequency dependent phase shift. This phase can be approximated as

$$\phi = 2\pi f_c \tau, \qquad (2.20)$$

where f_c is the centre frequency. The phase error due to this approximation is therefore

$$\begin{aligned} \text{error} &= \theta(f) - \phi \\ &= 2\pi f\tau - 2\pi f_c \tau \\ &= 2\pi\tau(f - f_c) \end{aligned} \qquad (2.21)$$

The narrowband approximation error for the above mentioned example search radar parameters at DOAs ranging from -60 to 60 degrees is illustrated in Figure 2.3.

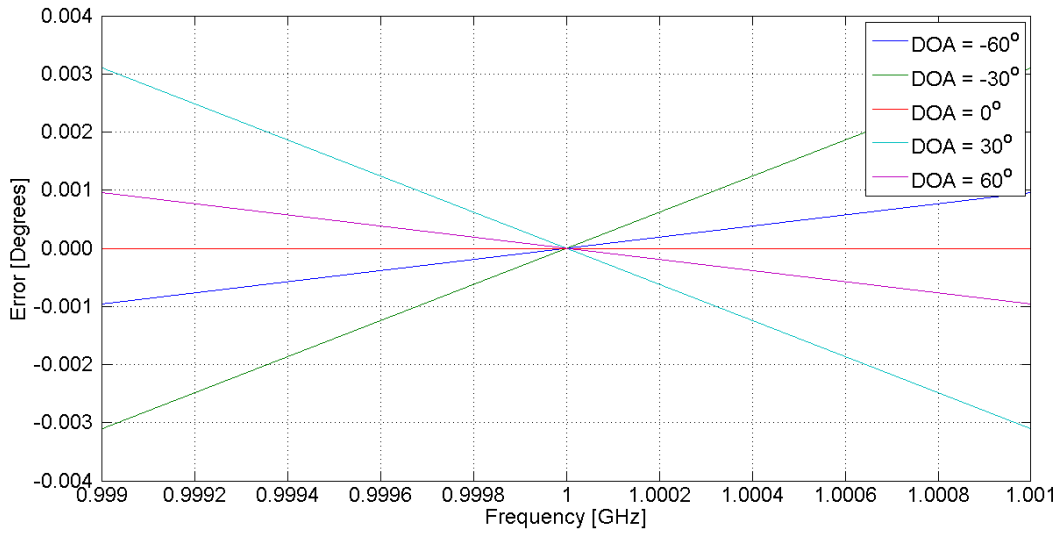


Figure 2.3: Narrowband approximation for a typical search radar operating at 1 GHz.

As mentioned in Section 2.1.1, this investigation will focus on the SNR and thus constants such as $G(\theta)$ and $\frac{1}{|\mathbf{r}_i|}$ will eventually be neglected in the model developments of the following sections.

2.2 Phased Array Model

Antennas are transducers which convert electrical signals into electromagnetic waves and vice versa. Due to reciprocity, the transmitting and receiving antenna patterns of antennas are the same. In many applications, including radar, narrow radiation patterns with high gains are necessary. These radiation patterns often may not feasibly be achieved by a single antenna [19]. A single antenna's radiation pattern can be manipulated either by varying the antenna aperture size or by controlling the antenna aperture excitation [20]. In both scenarios, the feasibility of the solution can become a concern. As the antenna's aperture is increased, the beamwidth becomes narrower and the gain increases ('focusing' the antenna in a particular direction). The null-to-null beamwidth of the antenna as a function of antenna aperture is given by [1]

$$\theta_{nn} = 2\frac{\lambda}{l}, \tag{2.22}$$

where l is the antenna aperture meters. The antenna aperture size can be increased by increasing the antenna size or using an array of antennas. The advantages and disadvantages arising from either method should be weighed for each different application. Often, the more practical solution is to use an array of antennas to create a larger combined aperture. Phased arrays also offer more agile beam operation by allowing the beam to be electronically steered [20].

Antenna arrays effectively sample signals spatially, after which the spatially sampled signals are sampled temporally. Spatial sampling is illustrated in Figure 2.4. Therefore, both temporal and spatial filtering can be performed on the received signals [21]. Spatial filtering is analogous to temporal filtering. Temporal filters are designed to pass signals of a desired frequency range, whereas spatial filters are designed to pass signals in a desired direction. In the case where a desired signal and an interfering signal occupies the same frequency band, distinguishing the two signals via temporal filtering becomes difficult. However, it is uncommon for the desired and interfering signal to originate from the same spatial direction and hence spatial filtering can be used to distinguish between the two signals. The process of performing spatial filtering is called beamforming, whereby a beam (usually the main beam) in the antenna pattern is focused in a particular desired direction.

More complex antenna pattern design can also include forming nulls in the direction of undesired signals. A typical beamformer linearly combines the spatially sampled signal from each antenna and then forms a weighted sum of these signals to obtain an output signal [21].

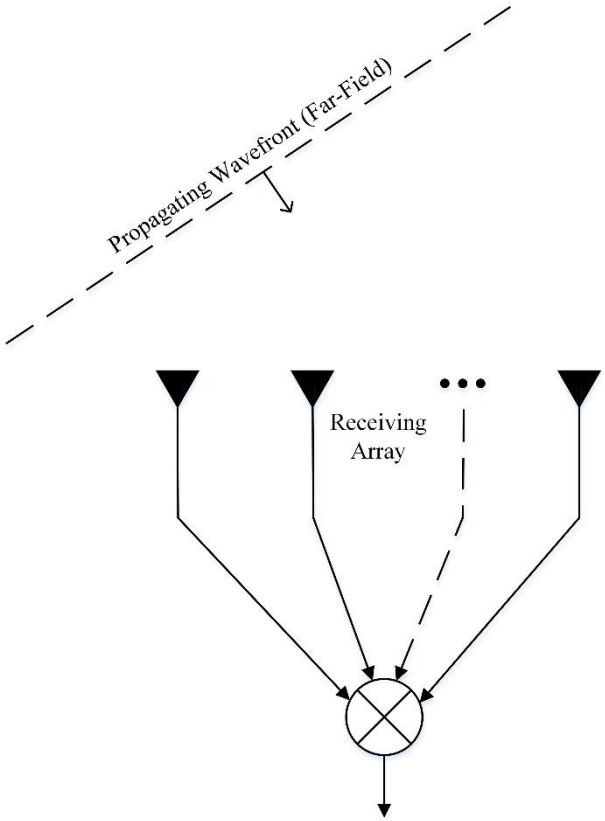


Figure 2.4: Antenna array spatially sampling a wave.

Phased arrays are antenna arrays in which the relative phase of each antenna element is manipulated such that the direction of the main beam of the antenna pattern changes. The manipulations are performed electrically via complex valued weights and allows the antenna array to receive or transmit signals in a desired direction. This allows for more agile beam operation as opposed to mechanically steering the antenna. Phased arrays also allow for graceful degradation in the event that some antenna elements fail [18]. The narrowband phased array model follows the ones described by Hudson [18], summarised by Middleton [22], and is presented in Section 2.2.1.

2.2.1 Narrowband Phased Arrays

Most practical search radars are narrowband due to technical constraints. This investigation will focus on ULAs and as a result, the model for a generic narrowband phased array can

be simplified into a narrowband phased ULA. The vector containing all of the space-dependent components in (2.16) is called the steering vector and is given by

$$\mathbf{a}(\mathbf{r}_1, \mathbf{r}_2, \dots, \mathbf{r}_N) \triangleq \begin{bmatrix} \frac{1}{|\mathbf{r}_1|} e^{j\mathbf{k}^T\mathbf{r}_1} \\ \frac{1}{|\mathbf{r}_2|} e^{j\mathbf{k}^T\mathbf{r}_2} \\ \vdots \\ \frac{1}{|\mathbf{r}_N|} e^{j\mathbf{k}^T\mathbf{r}_N} \end{bmatrix}, \tag{2.23}$$

where N is the number of elements in the array. The steering vector can be simplified as a result of logical assumptions which can be made due to the nature of radar operation and signal criteria. Recall the two dimensional assumption for ULAs in Section 2.1.1. Consider a source and a receiving ULA setup in the x-y plane as illustrated in Figure 2.5. The source is positioned at the origin and the first element of the array is positioned at a distance $|\mathbf{r}_1|$ and angle θ_1 away from the source. The elements are a distance of d apart.

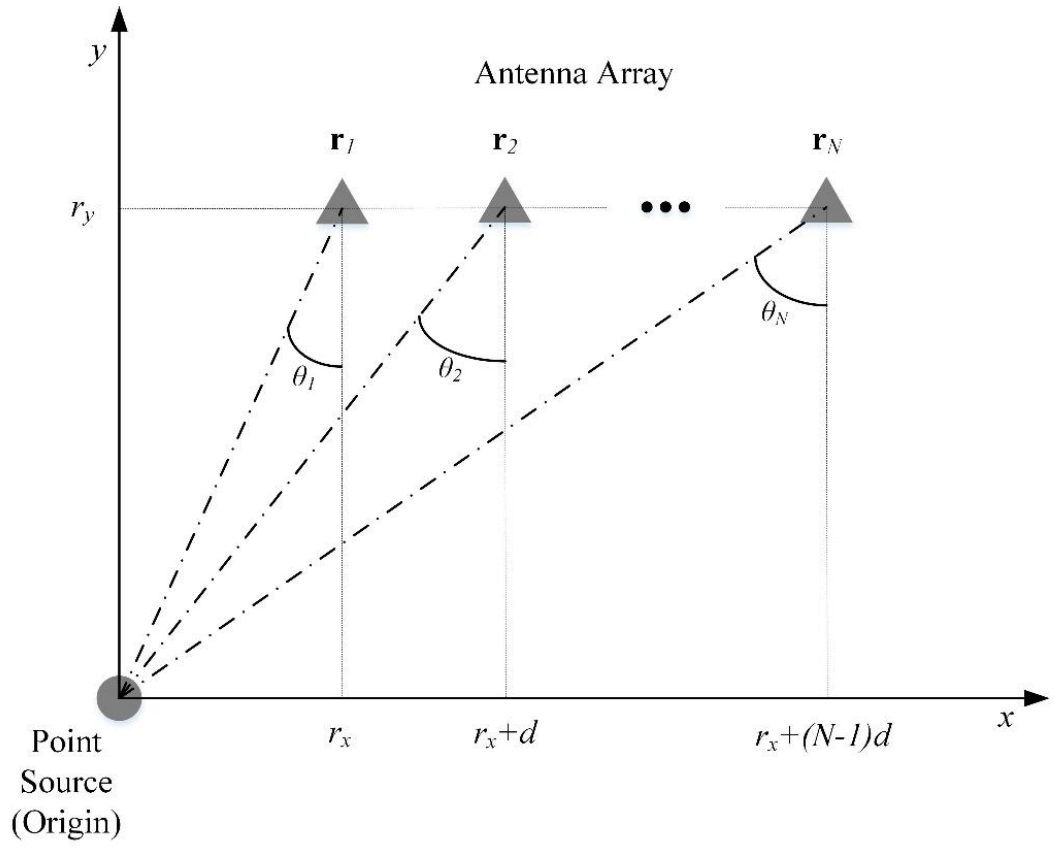


Figure 2.5: Distances and angles between a point source and antenna array elements.

The distances $|\mathbf{r}_i|$ and angles θ_i can then be expressed as

$$\mathbf{r}_i = (r_x + (i-1)d \quad r_y)^T \tag{2.24}$$

$$|\mathbf{r}_i| = \sqrt{(r_x + (i-1)d)^2 + r_y^2}\,, \tag{2.25}$$

$$\theta_i = \arctan\left(\frac{r_y}{r_x + (i-1)d}\right), \tag{2.26}$$

where $i = 1, \dots, N$. Radars generally operate in the far-field region of their own antennas, therefore $|\mathbf{r}_i| \gg d$. Hence it is assumed that the receiving array is located far enough from the source such that the difference in both distance and angle from each element to the source are negligible. In other words, $|\mathbf{r}_i| \approx r$ and $\theta_i \approx \theta$. Using (2.2) and (2.28), the product $\mathbf{k}^T\mathbf{r}_i$ is therefore expressed as

$$\mathbf{k}^T\mathbf{r}_i = k(r_x + (i-1)d)\sin\theta + kr_y\cos\theta. \tag{2.27}$$

The resulting steering vector is only dependent on the signal DOA, θ,

$$\mathbf{a}(\theta) = \frac{1}{r}e^{-jkr_x\sin\theta}e^{-jkr_y\cos\theta}\begin{bmatrix} 1 \\ e^{-jkd\sin\theta} \\ \vdots \\ e^{-jkd(N-1)\sin\theta} \end{bmatrix}, \tag{2.28}$$

where the term $kd\sin(\theta)$ is known as the electrical angle and the term $d\sin(\theta)$ is the difference in distance between the source and each subsequent receiving element. Finally, a phenomenon known as spatial aliasing needs to be accounted for. Aliasing plays the same role in the spatial domain as it does the time domain. A criterion similar to the Nyquist frequency in the time domain, known as half-wavelength spacing of the array elements is used to prevent spatial aliasing from occurring. To prevent spatial aliasing, the element spacing d should be restricted to

$$d \leq \frac{\lambda}{2}. \tag{2.29}$$

Choosing the borderline scenario of $d = \lambda/2$ and recalling that $k = 2\pi/\lambda$, the electrical angle term simplifies to $\pi\sin\theta$. Therefore, by incorporating the half-wavelength spacing and neglecting the constant terms from (2.28), the final form of the steering vector is given by

$$\mathbf{a}(\theta) = \begin{bmatrix} 1 \\ e^{-j\pi\sin\theta} \\ \vdots \\ e^{-j\pi(N-1)\sin\theta} \end{bmatrix}. \tag{2.30}$$

It should be noted that this steering vector model is only for the narrowband case. The approximation of the time delay by a phase shift discussed in Section 2.1.3 does not apply in the wideband case.

2.2.2 Received Signal Model

The received signal model, also known as the array output, presented in this section follows that of the model used by Krim and Viberg [12]. Recall that each receiving element has a gain, G. The array output is given by

$$x_i(t) = G_i(\theta)a_i(\theta)s(t), \tag{2.31}$$

where $i = 1, \ldots, N$, x_i is the signal at the ith receiving element and a_i is the ith steering element of the steering vector. Assuming that all receiving elements have the same gain $G_1 = G_2 = \cdots = G_N$, the gain constant can be neglected. The array output can also be written, in vector notation, as

$$\mathbf{x}(t) = \mathbf{a}(\theta)s(t). \tag{2.32}$$

The array output can be generalised for multiple signal sources using the principle of superposition. If M signals arrive at the N element array with DOAs $\theta_1, \theta_2, \ldots, \theta_M$, the array output for multiple signal sources is given by

$$\mathbf{x}(t) = \sum_{m=1}^{M} \mathbf{a}(\theta_m)s_m(t)\,, \tag{2.33}$$

where $s_m(t)$ is the mth signal. A steering matrix $\mathbf{A}(\theta)$ (N by M matrix) which combines the steering vectors of the M signal sources, and a vector of incoming signals $\mathbf{s}(t)$, which combines the M incoming signals can be defined as

$$\mathbf{A}(\theta) = [\mathbf{a}(\theta_1) \quad \mathbf{a}(\theta_2) \quad \ldots \quad \mathbf{a}(\theta_M)], \tag{2.34}$$

$$\mathbf{s}(t) = [s_1(t) \quad s_2(t) \quad \ldots \quad s_M(t)]. \tag{2.35}$$

The term $\mathbf{z}(t)$ is introduced to account for the additive noise and interference and the final array output is given by

$$\mathbf{x}(t) = \mathbf{A}(\theta)\mathbf{s}^{\boldsymbol{T}}(t) + \mathbf{z}(t). \tag{2.36}$$

The assumptions about the statistical properties of the array output are described in the following section.

2.2.3 Statistical Assumptions

Second-order statistics of the received signals are essential in evaluating beamformer performance. Power can be represented by the spatial covariance matrix, which in turn is commonly used to derive, optimise and evaluate the performance of beamformers [21]. Assumptions about the statistical properties and the development of the covariance matrices follow that of the work by Krim and Viberg [12] and is presented here.

It is assumed that the signal received by the array has zero mean. The N by N covariance matrix of the array output is given by

$$\mathbf{R}_X = E[\mathbf{x}(t)\mathbf{x}^H(t)]. \tag{2.37}$$

where $E[.]$ is the statistical expectation and $(.)^H$ is the Hermitian transpose. Using the result from (2.36), the covariance matrix becomes

$$\mathbf{R}_X = \mathbf{A}E[\mathbf{s}(t)\mathbf{s}^H(t)]\mathbf{A}^H + E[\mathbf{z}(t)\mathbf{z}^H(t)]. \tag{2.38}$$

The noise is assumed to be independent across all array elements. The source and noise covariance matrices can then be defined as

$$E[\mathbf{s}(t)\mathbf{s}^H(t)] = \mathbf{R}_S \tag{2.39}$$

$$E[\mathbf{z}(t)\mathbf{z}^H(t)] = \sigma^2\mathbf{I}, \tag{2.40}$$

where $\mathbf{I}$ is the identity matrix and $\sigma^2$is the common noise variance. The covariance matrix therefore becomes

$$\mathbf{R}_X = \mathbf{A}\mathbf{R}_S\mathbf{A}^H + \sigma^2\mathbf{I}. \tag{2.41}$$

This result can be used in the evaluation of the receiving antenna array performance.

2.2.4 Beamforming

Beamforming or spatial filtering, as its name suggests, filters signals spatially. Similar to temporal filtering where the frequency components of a signal within a desired frequency range are allowed to pass, beamforming allows a receiving array to be sensitive to signals within a desired DOA range. Beamforming is achieved by applying linear signal processing

operations to the received signals. The ideal beamformer passes signals arriving within the desired DOA whilst attenuating all signals arriving from other DOAs. In practice however, this result can only be closely approximated. A basic type of beamformer is the weighted delay-and-sum beamformer [13] [23], where the beamformer output is calculated by averaging the weighted and delayed versions of the signal of interest. The beamformer output $y(t)$ is then given by

$$y(t) = \frac{1}{N}\sum_{i=1}^{N} w_i x_i(t - \tau_i), \tag{2.42}$$

where w_i is the weight of the ith receiver element and τ_i is the relative delay of the ith receiver element. The main beam of the beamformer is steered by choosing the delays τ_i such that the spatial filter's passband is in a particular orientation. Therefore, to pass a plane wave propagating in direction $\mathbf{k}_0$, the beamforming delays must be chosen as [13]

$$\tau_i = -\frac{\mathbf{k}_0^T \mathbf{r}_i}{\omega}. \tag{2.43}$$

2.2.5 Array Antenna Pattern

The array antenna pattern is defined as the magnitude squared of the array response [21]. The development of the array response follows the work by Dudgeon and Mersereau [13]. Consider a receiving array steered in the direction $\mathbf{k}_0$ and a plane wave propagating in a different direction $\mathbf{k}$. Recall the propagating plane wave given by (2.1), the plane wave is given by

$$x(\mathbf{r}, t) = e\left(t - \frac{\mathbf{k}^T \mathbf{r}_i}{\omega}\right). \tag{2.44}$$

The beamformer output is then given by

$$\begin{aligned} y(t) &= \frac{1}{N}\sum_{i=1}^{N} w_i x_i(t - \tau_i) \\ &= \frac{1}{N}\sum_{i=1}^{N} w_i e^{j\omega\left(t - \frac{\mathbf{k}^T \mathbf{r}_i}{\omega} + \frac{\mathbf{k}_0^T \mathbf{r}_i}{\omega}\right)} \\ &= \frac{1}{N}\sum_{i=1}^{N} w_i e^{-j(\mathbf{k}-\mathbf{k}_0)^T \mathbf{r}_i} e^{j\omega t} \\ &= b_f(\mathbf{k} - \mathbf{k}_0) e^{j\omega t}, \end{aligned} \tag{2.45}$$

where $b_f(\mathbf{k})$ is defined as the time-independent array response. The array response is therefore a complex coefficient and can be described as the attenuation of a plane wave

propagating in the direction $\mathbf{k}$ when received by a beamformer steered in the direction $\mathbf{k}_0$. The array response is described by

$$b_f(\mathbf{k}) = \frac{1}{N}\sum_{i=1}^{N} w_i e^{-j\omega \mathbf{k}^T \mathbf{r}_i}. \tag{2.46}$$

It should be noted that $b_f(\mathbf{k})$ represents the Fourier transform of the set of weights w_i applied in the beamformer [22]. Recall the simplifications as a result of a ULA in Section 2.1.3 and (2.43). The array response can be simplified to

$$\begin{aligned} b_f(\mathbf{k}-\mathbf{k}_0) &= \frac{1}{N}\sum_{i=1}^{N} w_i e^{j\omega \mathbf{k}_0^T \mathbf{r}_i} e^{-j\omega \mathbf{k}^T \mathbf{r}_i} \\ &= \frac{1}{N}\sum_{i=1}^{N} w_i e^{j\omega\tau_i} e^{-j\pi(i-1)\sin\theta}. \end{aligned} \tag{2.47}$$

Finally, the array response can be simplified into vector form

$$b_f(\theta) = \mathbf{w}^T \mathbf{a}(\theta), \tag{2.48}$$

where $\mathbf{a}(\theta)$ is the steering vector for a ULA and $\mathbf{w}$ is the complex weight vector with i^{th} element $w_i e^{j\omega\tau_i}$. The antenna pattern can therefore be given as

$$\begin{aligned} P(\theta) &= b(\theta) b^H(\theta) \\ &= \mathbf{a}^T(\theta)\mathbf{w}\mathbf{w}^H\mathbf{a}^*(\theta), \end{aligned} \tag{2.49}$$

where $(.)^*$ is complex conjugation. The antenna pattern defines the gain of the array as a function of DOA. The antenna pattern can be plotted to offer a clear visual understanding of the antenna array.

2.2.6 Phased Array Beamforming Techniques

This investigation primarily focusses on the phased array's transmitted signal. For completeness, a brief overview of phased array receive techniques is provided. Many phased array beamforming techniques exist and their practical use depends on the requirements of specific applications. The aim of these techniques is generally to maximise the SNR in a desired DOA. The different techniques presented by Middleton [22] are briefly mentioned below and serves to provide an idea of actual beamforming techniques. The derivation and discussion of these techniques will therefore not be presented.

The simplest techniques fall under the Data Independent Beamformer (DIB) classification. As the classification name suggests, DIBs operate independent of the received signal data. For these techniques to be practical, information about the received signal, such as the DOA, is assumed to be known a-priori. Weights for a desired DOA can therefore be chosen accordingly [21]. An example of a DIB is the conventional beamformer.

The more complex techniques fall under the Statistically Optimum Beamformer (SOB) classification, which subsequently falls into the field of adaptive array techniques. SOBs vary the weights according to received signal statistics with the aim to optimise the reception of signals, thus maximising the desired signal contributions whilst minimising the noise interference [21]. Examples of SOBs include: the multiple side lobe canceller; the use of a reference signal; the maximisation of SNR; Capon; and linearly constrained minimum variance.

Due to the reciprocity of the radiation pattern of antennas, the radiation pattern is identical for both transmission and reception [19]. Therefore, the concept behind the beamforming techniques apply for both transmission and reception.

2.3 MIMO Arrays

Each antenna element in a MIMO radar array transmits a signal from a set of linearly independent signals as opposed to phased arrays where each antenna element transmits the same signal scaled by a complex weight. Phased arrays can be considered as a special case of MIMO array where all transmitted signals are chosen to be the same, hence MIMO arrays are a generalisation of phased arrays. MIMO array antenna patterns can be designed by selecting waveforms which combine to give the desired antenna pattern [7] [22]. The MIMO radar architecture, where each element transmits a mutually orthogonal signal, is illustrated in Figure 2.6.

The main advantage of MIMO arrays are the extra degrees of freedom, as a result of each antenna element transmitting a different signal member from a linearly independent set. The extra degrees of freedom offered by the diverse set of signals enable the use of a wider variety of parametric estimation techniques. Similar to the phased array, the MIMO array architecture offers an increased effective array aperture through spatial convolution of the element positions, which results in a virtual array. If the array elements were spaced equally, spatial convolution results in the over-representation of certain antenna array elements in the virtual array as demonstrated in Figure 2.7 (a). The over-representation can be remedied by sparsely distributing the transmitting or receiving antenna array elements which results

in an effective full virtual array, as demonstrated in Figure 2.7 (b) and (c) [24]. As a result, antenna arrays can be useful if physical space for the radar antenna is limited.

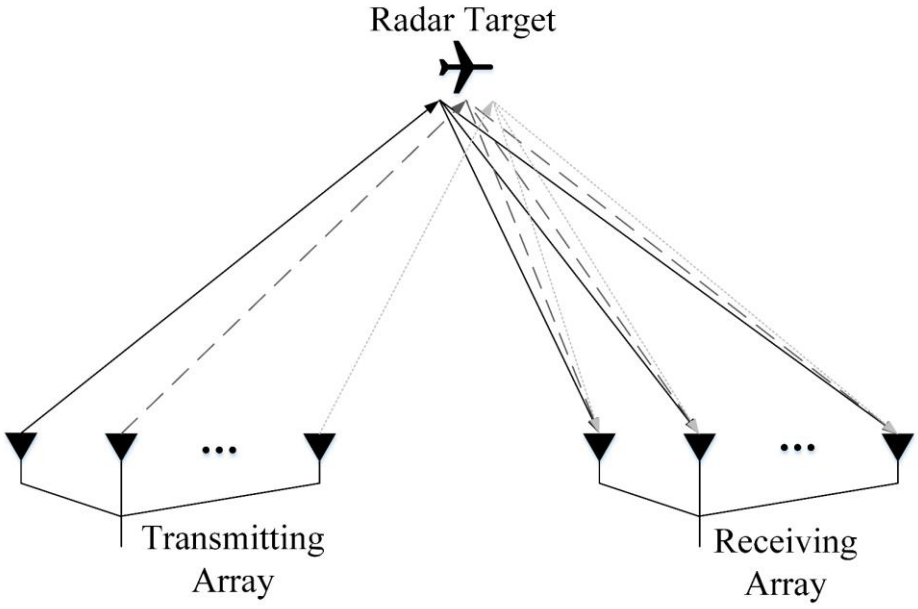
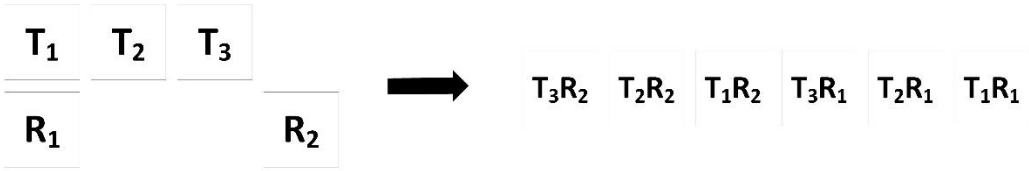


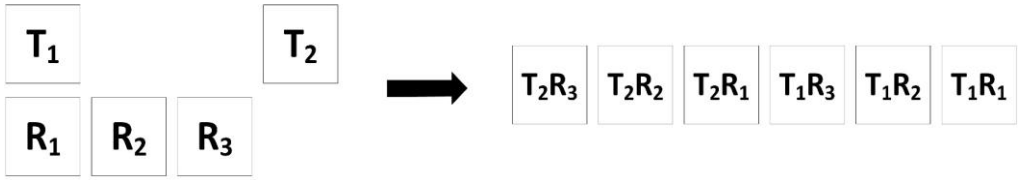
Figure 2.6: MIMO radar architecture illustration.



(a) Full transmitting and receiving arrays resulting in over-representation in the virtual array.



(b) Full transmitting and sparse receiving arrays resulting in effective virtual array.



(c) Sparse transmitting and full receiving arrays resulting in effective virtual array [25].

Figure 2.7: MIMO array spatial convolution effect.

Due to the nature of signals in MIMO radar, more complex processing is required than its phased array counterpart. There is an on-going debate as to whether or not MIMO radar implementation is actually feasible when its phased array counterpart can achieve similar if not better results with less complexity [6].

The narrowband MIMO array is a generalisation of the narrowband phased array, therefore the model is similar to the phased array model previously derived in Section 2.2. The key difference is that multiple signals can be transmitted in the MIMO array model. The MIMO array model follows the ones described by Li and Stoica [9], summarised by Middleton [22] and is presented in Section 2.3.1.

2.3.1 Narrowband MIMO Arrays

Consider an N element transmitting and receiving array. The transmitting array simultaneously transmits a set of linearly independent or orthogonal waveforms, given by

$$\mathbf{s} = \begin{bmatrix} s_1 \\ s_2 \\ \vdots \\ s_N \end{bmatrix}, \tag{2.50}$$

where s_i, $i = 1,2,\dots,N$, is the ith transmitted signal with a finite amount of samples. Let the angles θ_t and θ_r be the relative angle between the target and the transmitting and receiving arrays respectively. Similar to the phased array model, it is fair to assume that MIMO radars will generally operate in the far-field. The transmitting and receiving arrays are also typically either co-located or positioned near each other. As a result, the difference in angle between the different antenna elements to the target is assumed to be negligible. Therefore, the following assumption can be made

$$\theta_t \approx \theta_r = \theta. \tag{2.51}$$

The steering vector which accounts for the difference in path lengths between the target and the transmitting antenna elements is given by

$$\mathbf{a}_t(\theta) = \begin{bmatrix} e^{j\pi f_c \tau_1(\theta)} \\ e^{j\pi f_c \tau_2(\theta)} \\ \vdots \\ e^{j\pi f_c \tau_N(\theta)} \end{bmatrix}, \tag{2.52}$$

where τ_i, $i = 1,2,\dots,N$, is the time delay from the ith transmitting antenna element to the target.

The signals are then reflected by the target and received at the receiving array. The steering vector for the receiving array is therefore given by

$$\mathbf{a}_r(\theta) = \begin{bmatrix} e^{j\pi f_c \tilde{\tau}_1(\theta)} \\ e^{j\pi f_c \tilde{\tau}_2(\theta)} \\ \vdots \\ e^{j\pi f_c \tilde{\tau}_N(\theta)} \end{bmatrix}, \tag{2.53}$$

where $\tilde{\tau}_i$, $i = 1,2,\ldots,N$ is the time delay from the target to the ith receiving antenna element. Therefore, the received signal for a single target can be expressed as

$$Y = \mathbf{a}_r^*(\theta)\beta(\theta)\mathbf{a}_t^H(\theta)\mathbf{s} + \mathbf{z}, \tag{2.54}$$

where β is the complex amplitude proportional to the radar cross section of the target. In the case of M reflecting targets, the received signal can be generalised to

$$Y = \sum_{m=1}^{M} \mathbf{a}_r^*(\theta_m)\beta(\theta_m)\mathbf{a}_t^H(\theta_m)\mathbf{s} + \mathbf{z}. \tag{2.55}$$

In the case of a MIMO ULA, the steering vectors can be simplified to a form similar to that of the Phased ULA in (2.30)

$$\mathbf{a}_t(\theta) = \begin{bmatrix} e^{j\pi\left(-\frac{N-1}{2}\right)\sin\theta} \\ e^{j\pi\left(1-\frac{N-1}{2}\right)\sin\theta} \\ \vdots \\ e^{j\pi\left(N-1-\frac{N-1}{2}\right)\sin\theta} \end{bmatrix}. \tag{2.56}$$

Therefore, the steering vector which can be used to steer the MIMO signals presented in the following section.

2.4 MIMO Array Signal Generation

Recall from Section 2.3 that MIMO arrays transmit from a set of linearly independent or orthogonal set of signals. This section discusses the methodology of generating approximately orthogonal sets of signals for use in MIMO arrays.

Orthogonal vectors can be used as a basis for generating the MIMO signal sets. Many methods to generate orthogonal vectors exist, such as the Hadamard matrix, Frank-Zadoff-Chu sequences and Generalized chirp-like sequences [26] [27] [28].

The Hadamard matrix provides exactly orthogonal prime samples and will therefore be used in this investigation to generate MIMO signals. The rows from Hadamard matrices

can be used to generate the orthogonal vectors. These vectors usually consist of values chosen from the set {-1, +1}, and lack intermediate values. Practically, MIMO signals can therefore be generated by interpolating the orthogonal vectors. The Hadamard matrix and signal interpolation are presented in the following subsections.

2.4.1 Hadamard Matrix

The Hadamard matrix is named after French mathematician Jacques Hadamard. An nth order Hadamard matrix is a n by n matrix, denoted **H**, consisting of 1's and -1's such that

$$\mathbf{H}\mathbf{H}^T = n\mathbf{I}_n\,, \tag{2.57}$$

where $\mathbf{I}_n$ is an nth order identity matrix [26]. It should be noted that columns of the Hadamard matrix are mutually orthogonal. James Joseph Sylvester published the first examples of Hadamard matrices using the method

$$\begin{bmatrix}\mathbf{H} & \mathbf{H}\\ \mathbf{H} & -\mathbf{H}\end{bmatrix}, \tag{2.58}$$

which can be used for iterations increasing in orders 2^t. Hadamard later showed that the matrices are also valid for multiples of 4 [26]. The order of the Hadamard matrix is therefore limited to $n = 1{,}2$ and multiples of 4 thereafter, as illustrated below

$$\mathbf{H}(1) = [1], \mathbf{H}(2) = \begin{bmatrix}1 & 1\\ 1 & -1\end{bmatrix}, \mathbf{H}(4) = \begin{bmatrix}1 & 1 & 1 & 1\\ 1 & -1 & 1 & -1\\ 1 & 1 & -1 & -1\\ 1 & -1 & -1 & 1\end{bmatrix}, \ldots \tag{2.59}$$

2.4.2 Signal Interpolation

Interpolation is the process of digitally converting the sampling frequency of a signal to a new higher sampling rate with the aim of minimising the error between the original and the new signal. This process is summarised in the block diagram illustrated in Figure 2.8. This is as opposed to decimation, where the new signal has a lower sampling rate [29].

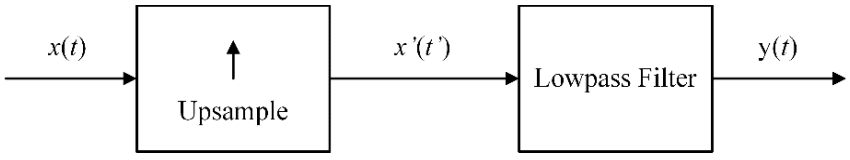


Figure 2.8: Interpolation block diagram.

There are many scenarios where sampling rate conversion is required. Consider a scenario where a system's input signal may already be pre-sampled at another sampling rate. It is

then necessary to convert the sampling rate to suit the requirements of the system. Another scenario to consider is a system which has a processing algorithm where it may be more convenient and efficient to process signals at different sampling rates in different parts of the algorithm. It is then necessary to convert the sampling rate mid-algorithm. These systems are known as multi-rate systems [29]. The process of interpolation presented below follows the work by Crochiere [29] and is illustrated graphically in Figure 2.9. Consider the sinusoid signal x with frequency f shown in Figure 2.9 (a)

$$x(t) = \sin(2\pi f t). \tag{2.60}$$

The signal is sampled at a frequency of $4f$, which meets the Nyquist sampling criterion. The signal will be interpolated by an arbitrary factor of L such that

$$\frac{T'}{T} = \frac{1}{L}, \tag{2.61}$$

where T is the original sampling period [s] and T' is the interpolated sampling period in seconds. Firstly, interpolating a signal by a factor L implies that $L - 1$ new samples (zeros) must be inserted between each sample pair of the original signal, as shown in Figure 2.9 (b). Therefore,

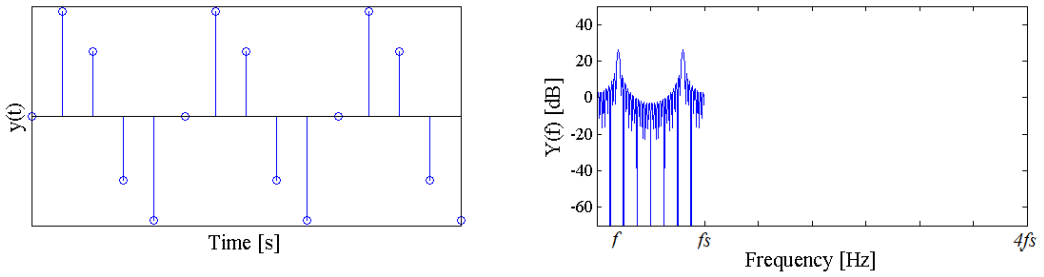
$$x'(t') = \begin{cases} x(t'/L), & t' = 0, \pm L, \pm 2L, \dots \\ 0 & \text{otherwise.} \end{cases} \tag{2.62}$$

This procedure consequently modifies the frequency spectrum of the signal. This results in the spectrum containing images of the original frequency component, centered at harmonics of the original sampling frequency. A suitable low-pass filter is then required to remove the unwanted higher frequency components, resulting in the recovery of the original frequency component as shown in Figure 2.9 (c). The transfer function of a low-pass filter to achieve this is given by

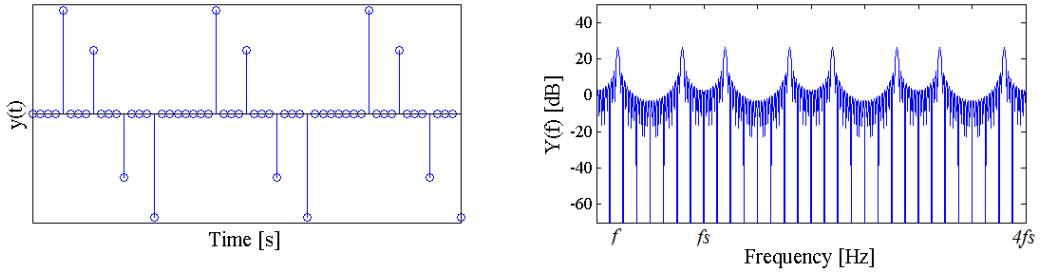
$$H(\omega) = \begin{cases} G, & |\omega| \leq \dfrac{2\pi f_s T'}{2} = \dfrac{\pi}{2} \\ 0 & \text{otherwise,} \end{cases} \tag{2.63}$$

where f_s is the sampling frequency in hertz and G is the filter gain. The gain of the filter should be chosen such that the amplitude of the interpolated signal is correct (i.e. $G = L$ in the passband). The final result is the interpolation of the original signal by a factor of L. Many different types of low-pass filters can be used for interpolation, and each filter has its own degree of accuracy. Examples of commonly used finite impulse response (FIR)

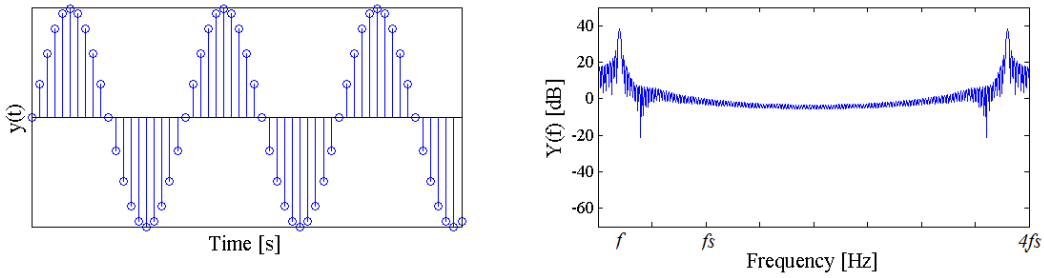
filters include the sinc filter and the raised cosine filter. Alternatively, a simple albeit more inaccurate method (depending on nature of the original samples) is linear interpolation.



(a) Original sine wave with frequency f sampled at $4f_s$.



(b) Upsampling the original signal with $L-1$ zeros between the original samples.



(c) Original signal interpolated by a factor of $L = 4$.

Figure 2.9: Numeric example of a sinusoid signal being interpolated by a factor of L.

Interpolation for complex signals is conceptually similar to interpolation of real signals, with the exception that the real and imaginary components are interpolated separately.

It should be noted that when the Hadamard sequences are interpolated by the sinc and the raised cosine filters, the sequences are no longer equal in power. The peak-to-average power ratio (PAPR) also is not constant from sequence to sequence and is greater than unity for each sequence. PAPR is defined as:

$$\text{PAPR} = \frac{P_p}{P_{avg}} \tag{2.64}$$

where P_p is the peak power, P_{avg} is the average power [30]. A radar designer would prefer to transmit signals which have a unity PAPR so that amplifiers can be driven into their saturated regions and thus deliver more transmit power. A Linear Root-of-Unity (LRU) interpolation technique addresses the abovementioned restrictions, and is presented in the following subsection.

2.4.3 Constant Envelope Linear Root-of-Unity Filtering

Constant Envelope Linear Root-of-Unity (CE-LRU) filtering interpolates successive complex signal samples on the unit circle as illustrated in Figure 2.1 [31]. Thus, signal samples are given by

$$a_k = e^{-j\phi(k)}, \tag{2.65}$$

where a_k is a complex valued sample and ϕ is the phase of the sample in radians [31]. The Hadamard matrix consist of 1's and -1's, which correspond to $\phi = 0$ and $\phi = \pi$ respectively. If all of the original signal samples are on the unit circle, which is the case with a Hadamard sequence, the resultant interpolated signal remains on the unit circle as well. The implementation of the CE-LRU technique is illustrated in Figure 2.11.

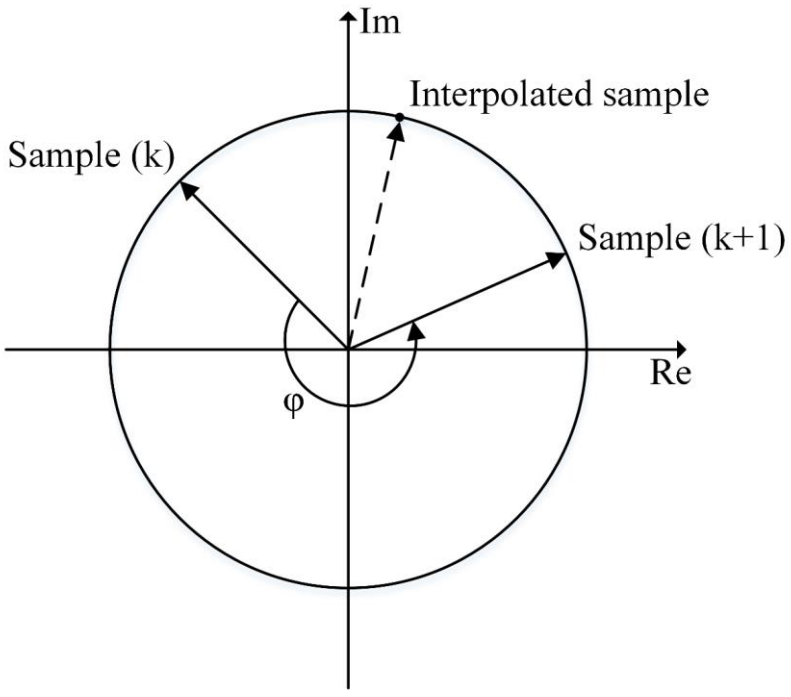


Figure 2.10: CE-LRU filtering *[32]*.

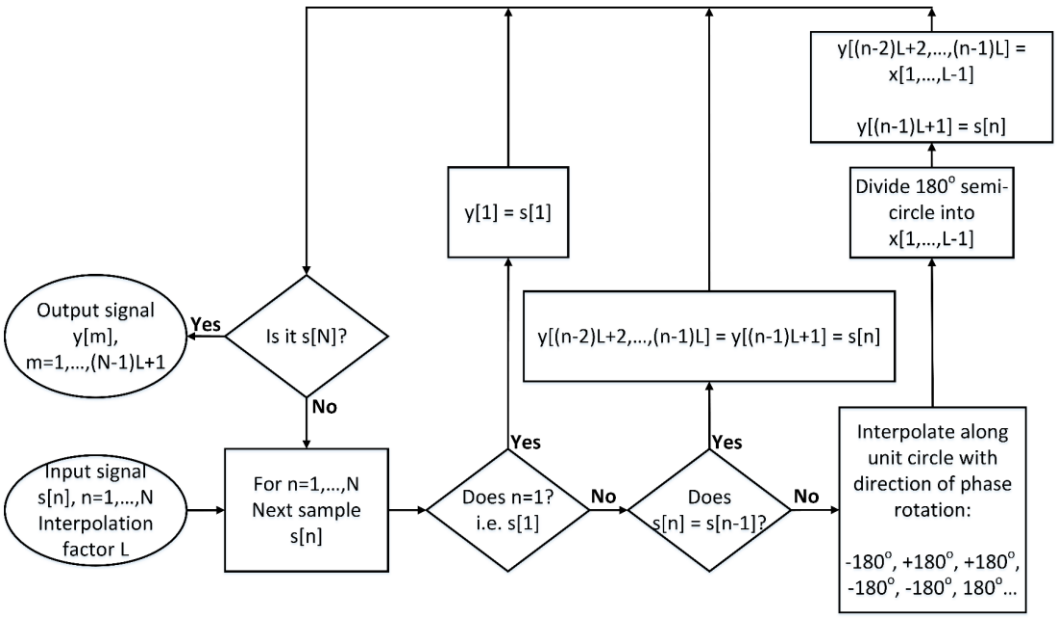


Figure 2.11: CE-LRU block diagram.

The interpolated signal has unity PAPR and the resulting average power of the signal is 1 watt. This result agrees with the simulation constraints discussed in Section 3.

2.5 ES Receivers

ES, more specifically radar intercept receivers, usually consists of a passive receiving device which is used to detect whether radars are transmitting, and if so what types of radar are currently being deployed in the device's neighbourhood. Radars can be classified by their signal transmission characteristics such as: amplitude modulation, DOA, time of arrival, pulse repetition interval (PRI), pulse length and transmit frequency. More complex characteristics such as PRI modulation characteristics and inter/intra-pulse frequency and phase modulation can also be measured by advanced ES equipment [33]. It should be noted that this is not a comprehensive list of characteristics.

Traditionally, the intercept receivers had no difficulties detecting the radars as the radars needed to transmit enough power to ensure that the signals are detectable even after reflecting off objects of interest. This is as opposed to the intercept receiver receiving the signal at a significantly shorter distance than the radar receiver. A comparison of the detection ranges of phased array radar and MIMO radar to that of the CVR and the ZIFR is discussed and illustrated in Section 4.2. The development of low probability of intercept (LPI) radars has given radar a means to avoid absolute detection. An increase in signal

processing gain allows radars to transmit at a lower instantaneous power level (assuming that intercept receivers do not have identical processing gains to the radars, which would imply perfect knowledge of the radar's signal) [34].

The ES receivers that will be discussed are the CVR and the ZIFR. The receiver models are developed and discussed in the following subsections.

2.5.1 Crystal Video Receiver (CVR)

The CVR is an ES receiver in its simplest form is illustrated in Figure 2.12, and the detection model is derived in Section 2.6.1. It is a cost-effective device which is able to detect signals over a wide frequency range. However, the CVR's performance degrades in an environment with multiple simultaneous (time overlapping) signals. In its simplest form, the CVR consists of a crystal diode detector and a video amplifier. In addition, a pre-amplifier can be used to increase the sensitivity of the CVR. Typically, a bandpass filter is also used to restrict the received signal to a particular frequency band of interest [2] [35].

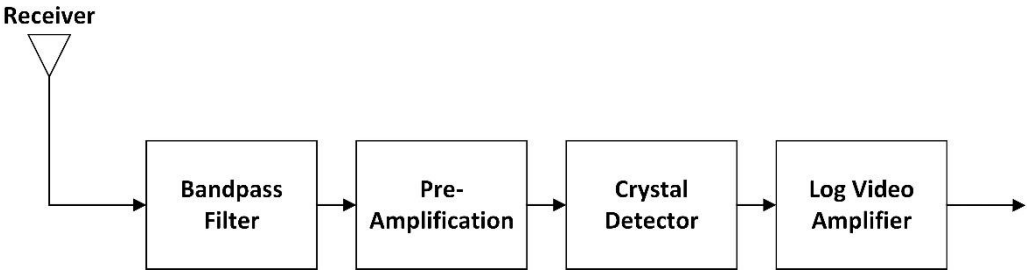


Figure 2.12: CVR system overview.

The CVR essentially performs a full-wave rectifying action on the received signal, which consequently distorts the signal's original frequency characteristics. A low-pass filter is therefore required after the crystal detector to remove any undesired higher frequency components. The typical CVR's sensitivity ranges between -40 dBm to -50 dBm without pre-amplification and between -65 dBm and -80 dBm with pre-amplification [2] [33] [36].

2.5.2 Superheterodyne Receiver

The superhet is a commonly and diversely used receiver. As its name suggests, the superhet "heterodynes" or shifts a portion of the signal's frequency components to a fixed intermediate frequency (IF) using a tune-able local oscillator. The IF amplifier, filter and detector can then simply operate at a fixed band of frequencies. As a result, amplifier characteristics such as gain and bandwidth can be precisely controlled [2] [35]. The superhet is illustrated in Figure 2.13.

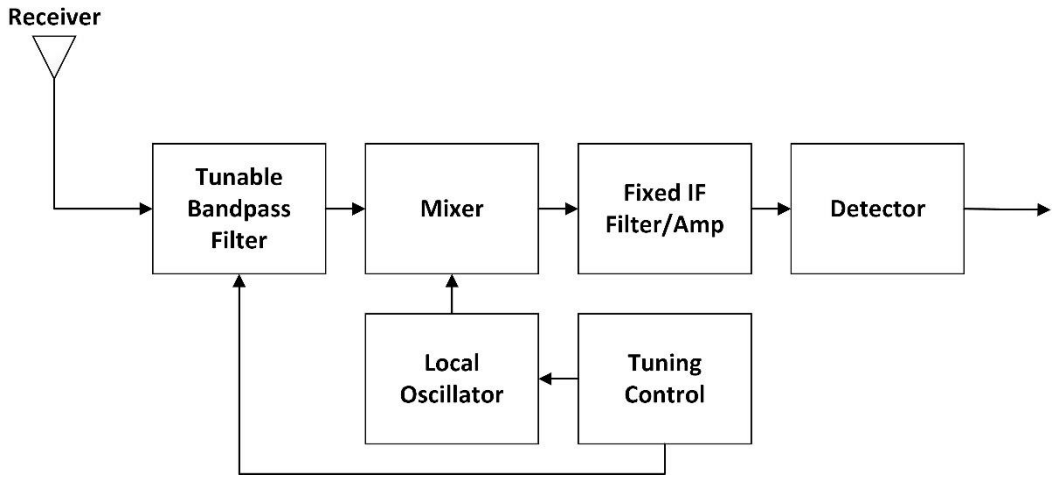


Figure 2.13: Superhet system overview.

Firstly, a tuneable bandpass filter is used to ensure that the received signal is within the desired frequency range. The received signal is then mixed with an internally produced signal at the local oscillator frequency. The mixing of the signals results in a signal with two frequency components, one at the frequency of the sum of the input frequencies and the other at the difference of the input frequencies. A low-pass filter is then used to filter out the double frequency components. The resulting signal with just the lower frequency component, which is known as the IF signal, can therefore be amplified and detected. To cover a wide range of frequencies, the superhet has a tuning mechanism which adjusts the bandpass filter and local oscillator accordingly.

The superhet is more sensitive than the CVR, but suffers from a probability of intercept performance loss, unless the frequency of the radar to be intercepted is known a-priori. The typical range for a narrowband superhet's sensitivity is approximately -90 dBm for a 1 MHz bandwidth [33]. For the purposes of this investigation, a specific type of superhet known as the zero IF receiver (ZIFR) is used. Henceforth, all instances of "superhet" specifically refer to the ZIFR, which is discussed in the following subsection.

2.5.2.1 Zero IF Receiver

This investigation will focus on a specific type of superhet, the ZIFR. The ZIFR tunes the local oscillator to the centre frequency of the signal being received. This is as opposed to the standard superhet where the zero IF is only accomplished after converting to an intermediate frequency. Compared to the envelope detector, the phase information of the signal is retained using the zero-IF technique [35]. The ZIFR is illustrated in Figure 2.14.

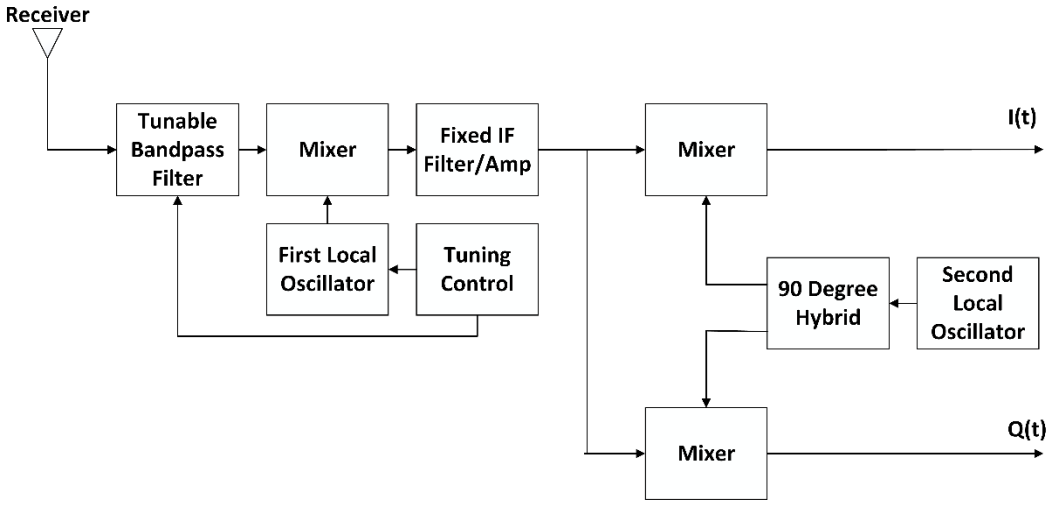


Figure 2.14: ZIFR system overview *[35]*.

The ZIFR allows the signal to be represented in this form:

$$s(t) = (I + jQ)e^{-j2\pi f_c t}. \tag{2.66}$$

The detection model of the ZIFR is derived in Section 2.6.2.

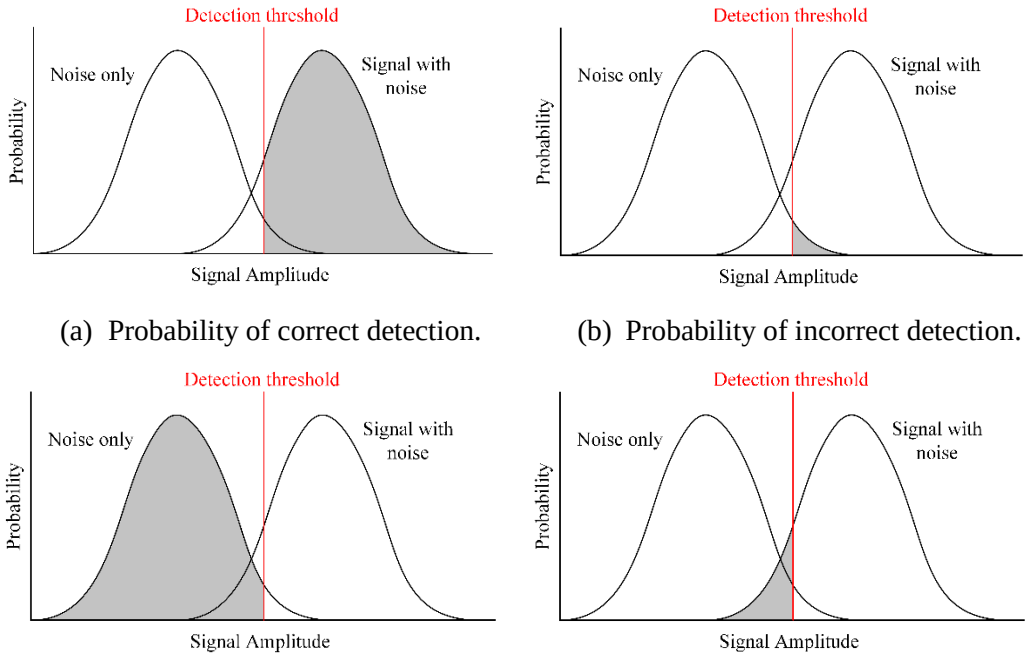
2.6 Signal Detection in ES receivers

Signal detection is the function of detecting the desired signal in the presence of uncertainty. Uncertainty in signal detection exists as a result of internal and external noise in addition to the signal [37]. Internal noise is generated from the equipment itself as opposed to external noise which originates from the environment. As previously stated, the propagation environment is neglected in this study. Therefore, only the internal noise is considered. Internal noise consists primarily of thermal noise, and can be characterised as white, Gaussian noise. The terms white and Gaussian refers to a signal's uniform spectral density over the band of interest and its Probability Distribution Function (PDF) respectively [38].

Consider detecting a signal in background noise. The signal has an arbitrary mean μ in the presence of white, zero-mean, Gaussian noise. A signal amplitude threshold E_t must be chosen such that if this threshold is crossed, a detection occurs. Signal plus noise results in the random fluctuation of the signal amplitude and can result in signal detection errors. Signal fluctuations as a result of noise only can result in a false alarm. Signal plus noise (negative amplitude) can also fall short of the detection threshold and go undetected. There are four possible outcomes [15] as illustrated in Figure 2.15:

- correct detection - a signal is present and a detection occurs;
- incorrect detection (false alarm) - a signal is not present and a detection occurs;
- correct rejection - a signal is not present and no detection occurs; and
- incorrect rejection (missed detection) - a signal is present and no detection occurs.

Correct detections and correct rejections are the desired outcomes. Therefore, a high probability of the desired outcomes is preferable. It should be noted that the probability of false alarm (PFA), denoted by P_{fa}, cannot be reduced to zero. The detection threshold must thus be chosen with an acceptable PFA in mind.



(a) Probability of correct detection. (b) Probability of incorrect detection.

(c) Probability of correct rejection. (d) Probability of incorrect rejection.

Figure 2.15: Four possible signal detection outcomes.

The signal detection models for the CVR and ZIFR are developed and presented in Sections 2.6.1 and 2.6.2 respectively. The signal models of the ES receivers involve mathematical operations applied to the signal plus noise. Therefore, the signal detection models are based heavily on the transformation of random variables.

2.6.1 CVR Detection Model

The CVR model is developed under the following simplifying assumptions:

- the received signal is assumed to be in the frequency band of interest so that the bandpass filter can be neglected; and
- the amplifiers can be neglected as SNR is a more useful unit of measure which scales with amplitude.

The CVR model is therefore developed with the primary focus on the crystal detector and the low-pass filter. Consider a MIMO transmitting array and a CVR in the far-field region. The CVR has a single antenna and is positioned in a location in which the radar is expected to be transmitting. The signal received by the ES receiver is dependent on the instantaneous combination of time-shifted versions of the orthogonal codes transmitted by each element of the MIMO transmit array. Given that the transmit antennas of the MIMO radar can be spaced by multiple wavelengths, the received signal at the ES receiver is thus dependent on the relative angle between the radar antenna and the ES receiver. Recall (2.50) and (2.56), which are the orthogonal set of signals and the MIMO array receiving steering vector respectively. The output of the crystal detector is therefore given by

$$\mathbf{x} = |\mathbf{a}_r^H(\theta_{ES})\mathbf{s}|, \tag{2.67}$$

where θ_{ES} is the relative angle between the radar and the ES receiver. The low-pass filter can be implemented digitally by making use of a moving average approximation which is matched to the radar's pulse length. Other alternatives such as a sinc filter also exist, but lead to a more complex implementation and a loss in SNR performance of the detector against conventional radar signals. The low-pass filter coefficients can to be chosen for unity noise gain [39]. Therefore, the filter coefficients h are given by

$$h = \sqrt{1/n} \tag{2.68}$$

$$\mathbf{h} = [h \quad h \quad \ldots \quad h], \tag{2.69}$$

where n is the number of filter coefficients and $\mathbf{h}$ is the vector of elements each equal to h. The CVR output $\mathbf{y}$ is given by

$$\mathbf{y} = \mathbf{x} * \mathbf{h}, \tag{2.70}$$

where $*$ is the discrete convolution operation.

The CVR receives real signals, and is consequently only affected by real noise. Consider the real, white, Gaussian noise with mean μ, variance σ^2 and standard deviation σ given by

$$f(x;\mu,\sigma) = \frac{1}{\sigma\sqrt{2\pi}} e^{-(-x-\mu)^2/2\sigma^2}. \tag{2.71}$$

The Cumulative Distribution Function (CDF) for the standard normal distribution is

$$F(y;\mu,\sigma) = \int_{-\infty}^{y} \frac{1}{\sigma\sqrt{2\pi}} e^{-(-x-\mu)^2/2\sigma^2} dx. \tag{2.72}$$

An alternate form of the CDF, which can be calculated numerically, is given by

$$F(y;\mu,\sigma) = \frac{1}{2}\left[1 + \text{erf}\left(\frac{y-\mu}{\sigma\sqrt{2}}\right)\right], \tag{2.73}$$

where $\text{erf}(.)$ is the error function defined as

$$\text{erf}(x) = \frac{1}{\sqrt{\pi}}\int_{-x}^{x} e^{-t^2}\, dt = \frac{2}{\sqrt{\pi}}\int_{0}^{x} e^{-t^2}\, dt. \tag{2.74}$$

Note that there is no universal definition for the error function. Therefore, it can be presented in many forms [15]. Recall the full-wave rectification as a result of the crystal diode in (2.67). The rectification was modelled by taking the absolute value of the signal. The result is the transformation of the normal distribution into the folded normal distribution. Graphically, the folded normal distribution is the standard normal distribution folded along the vertical axis such that the negative values are all converted into positive values whilst maintaining the same amplitude. The mean and standard deviation will consequently change. The folded normal distribution is given by

$$f_{FN}(x;\mu_{FN},\sigma_{FN}) = \frac{1}{\sigma_{FN}\sqrt{2\pi}} e^{-(-x-\mu_{FN})^2/2\sigma_{FN}^2} + \frac{1}{\sigma_{FN}\sqrt{2\pi}} e^{-(x-\mu_{FN})^2/2\sigma_{FN}^2}, \tag{2.75}$$

where $x \in [0,\infty)$. The corresponding CDF and its alternate form is given respectively by

$$\begin{aligned} F_{FN}(y;\mu_{FN},\sigma_{FN}) \quad = \quad & \int_{-\infty}^{y} \frac{1}{\sigma_{FN}\sqrt{2\pi}} e^{-(-x-\mu_{FN})^2/2\sigma_{FN}^2} dx \\ & + \int_{-\infty}^{y} \frac{1}{\sigma_{FN}\sqrt{2\pi}} e^{-(x-\mu_{FN})^2/2\sigma_{FN}^2} dx \end{aligned} \tag{2.76}$$

$$F_{FN}(y;\mu_{FN},\sigma_{FN}) = \frac{1}{2}\left[\operatorname{erf}\left(\frac{y+\mu_{FN}}{\sigma_{FN}\sqrt{2}}\right) + \operatorname{erf}\left(\frac{y-\mu_{FN}}{\sigma_{FN}\sqrt{2}}\right)\right], \tag{2.77}$$

where μ_{FN} and σ_{FN}^2 are the mean and the variance of the folded normal distribution respectively. These parameters are given by

$$\mu_{FN} = \sigma\sqrt{\frac{2}{\pi}}e^{(-\mu^2/2\sigma^2)} + \mu\left[1 - 2F\left(\frac{-\mu}{\sigma}\right)\right], \tag{2.78}$$

$$\sigma_{FN}^2 = \mu^2 + \sigma^2 - \left[\sigma\sqrt{\frac{2}{\pi}}e^{(-\mu^2/2\sigma^2)} + \mu\left[1 - 2F\left(\frac{-\mu}{\sigma}\right)\right]\right]^2, \tag{2.79}$$

where μ, σ^2 and F are the mean, variance and CDF of a standard normal distribution. White noise has a zero-mean ($\mu = 0$). Therefore, the mean and variance for the folded normal distribution can be simplified to

$$\mu_{FN} = \sigma\sqrt{\frac{2}{\pi}}, \tag{2.80}$$

$$\sigma_{FN}^2 = \sigma^2 - \left[\sigma\sqrt{\frac{2}{\pi}}\right]^2 = \sigma^2\left(1 - \frac{2}{\pi}\right). \tag{2.81}$$

Recall the low-pass filter required in the CVR from (2.77). The first-order approximation of the low-pass filter is implemented by averaging over n samples, using a FIR filter with coefficients of h. The effect of the filter on the mean and variance is given by

$$\begin{aligned} \mu_f &= nh\mu_{FN} \\ &= nh\sigma\sqrt{\frac{2}{\pi}}, \end{aligned} \tag{2.82}$$

$$\begin{aligned} \sigma_f^2 &= nh^2\sigma_{FN}^2 \\ &= nh^2\sigma^2\left(1 - \frac{2}{\pi}\right). \end{aligned} \tag{2.83}$$

The resulting mean μ_f and variance σ_f^2 can then be used in (2.77), and the CDF can then be used to determine the approximate detection amplitude threshold E_t for a desired PFA

$$F_{FN}(y;\mu,\sigma)=\frac{1}{2}\left[erf\left(\frac{y+nh\sigma\sqrt{\frac{2}{\pi}}}{\sqrt{2nh^2\sigma^2\left(1-\frac{2}{\pi}\right)}}\right)+erf\left(\frac{y-nh\sigma\sqrt{\frac{2}{\pi}}}{\sqrt{2nh^2\sigma^2\left(1-\frac{2}{\pi}\right)}}\right)\right]. \quad (2.84)$$

The threshold is then used to determine the Probability of Detection (PD) of MIMO radar signals. The detailed algebraic manipulation of (2.84) to determine the detection threshold is presented in Section 3.4.

2.6.2 ZIFR Detection Model

The ZIFR model is developed under the following simplifying assumptions:

- The specific type of superhet being modelled is the ZIFR, which retains the phase information of the signals.
- Signal modulation and demodulation can be neglected as the result should not differ theoretically [40] [41].
- The received signal is assumed to be in the frequency band of interest so that the bandpass filter can be neglected.
- The amplifiers can be neglected as SNR is a more useful unit of measure which scales with amplitude.

The ZIFR model is developed with the primary focus on the complex envelope and the low pass filter. The ZIFR is therefore modelled similarly to the CVR, with the exception of the ZIFR being a quadrature receiver. Consequently, the signal noise takes on complex values. Recall (2.70):

$$\mathbf{y}=\mathbf{x}*\mathbf{h}. \quad (2.85)$$

Consider the complex Gaussian noise whereby both real and complex components are normally distributed with mean $\mu=0$ and variance σ^2. The complex envelope in (2.67) is given by

$$|.|=\sqrt{I^2+Q^2}, \quad (2.86)$$

where I and Q are the real and complex components respectively. The output of the complex envelope is therefore Rayleigh distributed [38], with PDF defined by

$$f_R(x;\sigma_R)=\frac{x}{\sigma_R^2}e^{\left(-x^2/2\sigma_R^2\right)},\ \ x\geq 0. \quad (2.87)$$

The CDF of the Rayleigh distribution is given by

$$F_R(y;\sigma_R) = \int_y^{\infty} \frac{x}{\sigma_R^2} e^{\left(-x^2/2\sigma_R^2\right)} dx. \tag{2.88}$$

The low-pass filter with n filter taps effectively sums multiple Rayleigh distributed random variables. For a large n, the result can be approximated by a normal distribution, with PDF and CDF given by (2.71) and (2.73). The mean μ_R and variance σ_R of the Rayleigh distribution, in terms of the input normal distribution's parameters, are given by

$$\mu_R = \sigma\sqrt{\frac{\pi}{2}}, \tag{2.89}$$

$$\sigma_R^2 = \frac{4-\pi}{2}\sigma^2. \tag{2.90}$$

The effect of the low-pass filter on the mean and variance is given by

$$\begin{aligned} \mu_f &= nh\mu_R \\ &= nh\sigma\sqrt{\frac{\pi}{2}}, \end{aligned} \tag{2.91}$$

$$\begin{aligned} \sigma_f^2 &= nh^2\sigma_R^2 \\ &= nh^2\sigma^2\left(\frac{4-\pi}{2}\right). \end{aligned} \tag{2.92}$$

The resulting mean μ_f and variance σ_f^2 can then be used in (2.73) to determine the approximate detection amplitude threshold E_t for a desired PFA

$$F(y;\mu,\sigma) = \frac{1}{2}\left[1 + \operatorname{erf}\left(\frac{y - nh\sigma\sqrt{\frac{\pi}{2}}}{\sqrt{nh^2\sigma^2\left(\frac{4-\pi}{2}\right)}}\right)\right]. \tag{2.93}$$

The threshold is then used to determine the PD of MIMO radar signals. The algebraic manipulation to determine the detection threshold from (2.93) is presented in Section 3.5.

2.7 Conclusion

This chapter has presented the fundamental theory and assumptions necessary to develop the required mathematical models. Mathematical models for the narrowband phased array and the narrowband MIMO array were developed, along with the signal generation process for each respective model. Mathematical models for the CVR and ZIFR were then presented. The simulation setup designed to carry out this investigation is presented in the following chapter.

3 Simulation Setup

This chapter presents the simulation setup for this investigation. To provide context for the detectability of MIMO radar signals, a conventional phased array radar reference case is required as a basis for comparison. The investigation will be conducted on a variety of co-located antenna array setups by varying the number of antenna elements and the inter-element spacing. Both ideal omnidirectional antennas and theoretical patch antennas will be implemented and the results compared. A semicircle (180°) range in azimuth, as illustrated in Figure 3.1, will be considered for each setup in this investigation.

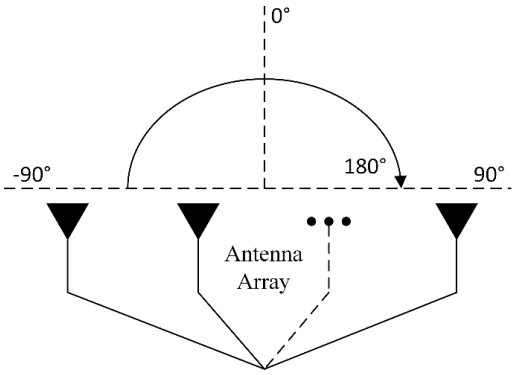


Figure 3.1: Semicircle (180°) range.

For each setup, the ES receiver will effectively be scanned over the 180-degree arc, and the detectability of the transmitted signals will be assessed at each position. It is difficult to fairly compare phased arrays and MIMO arrays [6]. The following constraints will be used in attempt to create a fair platform for comparison between the two cases:

- The same number of antenna elements is used for each phased array and corresponding MIMO array setup.
- The same inter-element spacing is used for each phased array and corresponding MIMO array setup.
- The PAPR should be unity for all transmitted signals in both phased array and MIMO array setups. As a result, each antenna element will transmit the same amount of power (1 watt) for both the phased array and the MIMO array.
- The SNR is determined by assuming the maximum potential combined signal power as determined by the total number of elements in the array for both phased array and MIMO array setups.
- The phased array and MIMO signals should have approximately equal bandwidths.

The antenna array setups for both the phased array and the MIMO array to be investigated will consist of 4, 8 and 16 antenna elements. For each setup, the inter-antenna element spacing to be considered is 0.5λ, λ, 2λ and 4λ. Due to the MIMO signal generation process, which is presented in Section 3.2, there are 16 possible signals to choose from. For the 4-element case, 4 out of 16 signals are chosen. Similarly, for the 8-element case, 8 out of 16 signals are chosen. For computational practicality, not all potential combinations will be simulated. The simulations to be performed per ES receiver are summarised in Table 1 and Table 2. A total of 56 setups will be simulated for the MIMO case and 24 setups will be simulated for the phased array case.

It is noted that array spacing larger than 0.5λ may be less common in practice. However, this investigation does fall within the research domain and therefore does extend to cases which may not be common in practice. It is further noted that array spacing larger than 0.5λ are considered in literature, for example the thin/full and full/thin arrays presented by Brookner [25].

Table 1. Simulation setup for phased arrays by varying number of antenna elements and inter-element spacing.

Number of antenna elements	**Number of sets of signals**	**Inter-element spacing**
4	1	0.5λ, λ, 2λ, 4λ
8	1	0.5λ, λ, 2λ, 4λ
16	1	0.5λ, λ, 2λ, 4λ

Table 2. Simulation setup for MIMO arrays by varying number of antenna elements and inter-element spacing.

Number of antenna elements	**Number of sets of signals**	**Inter-element spacing**
4	4	0.5λ, λ, 2λ, 4λ
8	2	0.5λ, λ, 2λ, 4λ
16	1	0.5λ, λ, 2λ, 4λ

The detection model for both ES receivers will assume that the receiver's low-pass filters are matched to the radar pulse length. It is noted that although matched filters are theoretical possible, the author is not aware of any such implementation for ES receivers in practice.

However, for computational practicality, this investigation will focus on the best case detection scenario, by assuming the pulse length is known a-priori.

The radar parameters of a typical search radar system are given in Table 3 [1]. The parameters for the simulation of the radar are given in Table 4. The simulation parameters are used in the signal generation process for both the phased array and the MIMO array. Note that both ES receivers will be simulated with $P_{fa} = 10^{-4}$.

Table 3: Typical example of search radar parameters.

Parameter	**Values**
Carrier frequency	1 GHz
Sampling frequency	10 MHz
Sampling time	0.1 μs
Pulse length	10-20 μs
Number of samples per signal	100-200

Table 4: Parameters for simulation of the radar.

Parameter	**Values**
Carrier frequency	2.5 MHz
Sampling frequency	10 MHz
Sampling time	0.1 μs
Pulse length	12.1 μs
Number of samples per signal	121

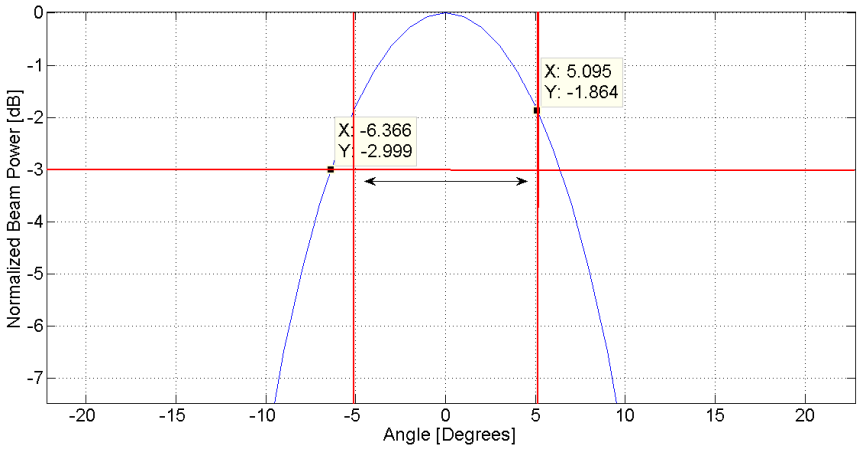
The following subsections first introduce the phased array signal generation and the MIMO signal generation. Constraints such as the PAPR and bandwidth are highlighted for both types of signals. The implementation of the CVR and the ZIFR are then presented. Finally, the effective antenna patterns for each simulation setup are compared to provide insight into the simulation results.

3.1 Phased Array Signal Generation

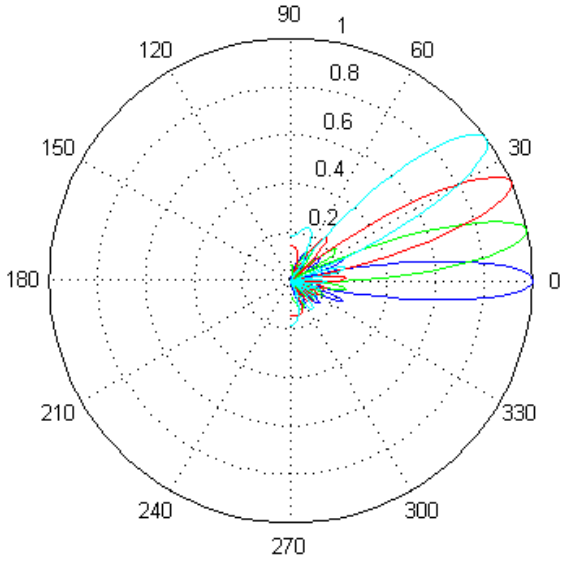
Recall the narrowband phased array model presented in Section 2.2. Beamforming allows the phased array to transmit or receive signals in a particular direction. In phased array radars, signals are transmitted with a high gain in a particular direction by steering the antenna pattern of the transmitting array in said direction. The probability of receiving a

returning echo of the transmitted signal is highest when the receiving array is steered in the same direction.

Therefore, phased array radar operates by electronically stepping the main beam across a range of DOAs, typically in intervals, depending on the beamwidth [1], as illustrated in Figure 3.2. The DOA intervals that a typical phased array radar would perform is determined by overlapping the beams at 80 % of the main beam's 3 dB beamwidth points [5].



(a) Illustration of 80 % of the main beam's 3 dB beamwidth.



(b) Polar illustration of stepping of main beam for typical search radar operation.

Figure 3.2: Example of phased array radar beam stepping operation.

This overlapping of the beams results in a 1.86 dB loss at the DOA of the overlap, and the radar designer may consider stepping back into this DOA on a subsequent scan.

In the phased array reference case, the main beam will be electrically steered from -60 to 60 degrees. At angles below -60 degrees and above 60 degrees, the beam will remain steered to -60 and 60 degrees respectively due to the fact that it is uncommon for linear arrays steer past this point in practice. This mimics a practical phased array radar's angle scanning operation. The resulting detectability of the phased array radar signals will be at its highest when the main beam is at the same angle as the position of the ES receiver. Figure 3.3 demonstrates that the phased array transmit signal is significantly more detectable in the main beam region of the antenna pattern than in the sidelobe region. The difference is approximately 15 dB. Therefore, the engineering approximation will be made that the main beam of the phased array is steered directly at the ES receiver.

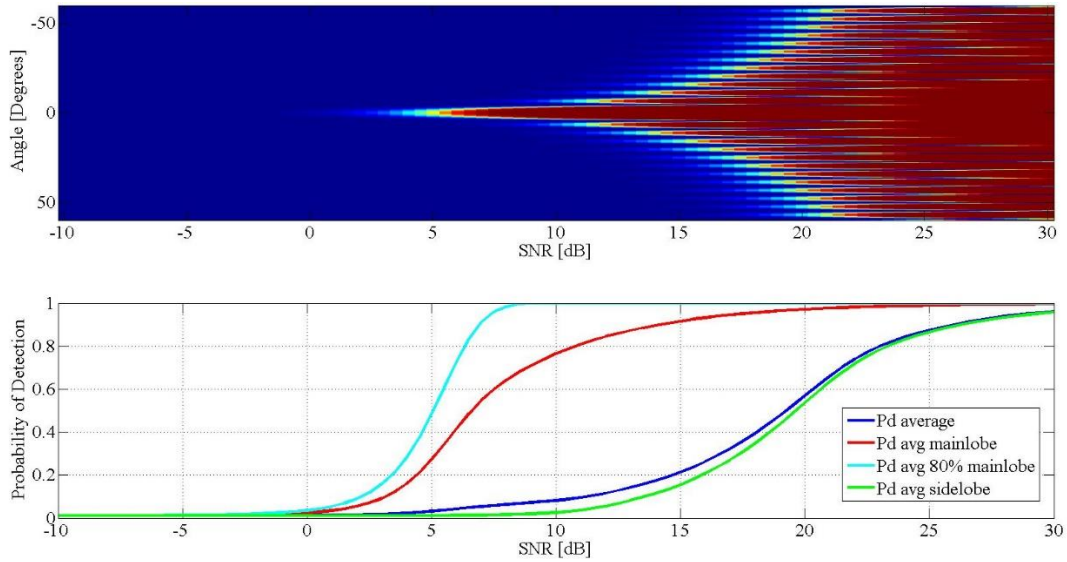
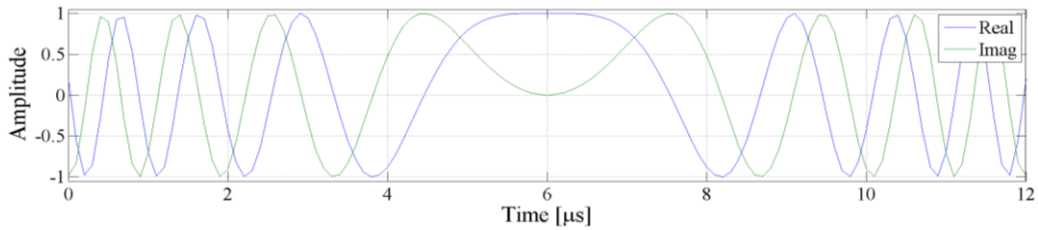


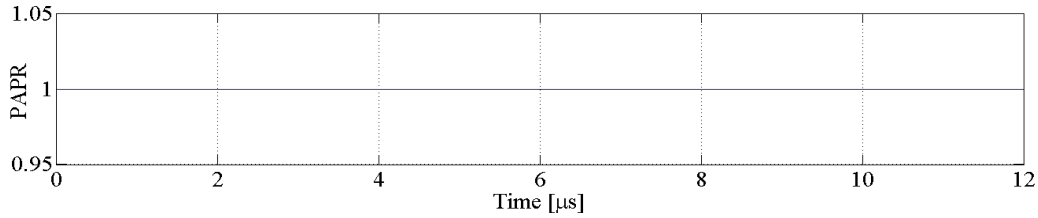
Figure 3.3: PD comparison of phased array main beam versus side lobes, for the case of 4-element array.

To perform a fair comparison between the phased array radar and MIMO radar, the case of the typical operation of each radar is considered. The detectability of the phased array radar when its main beam is steered in the direction of the ES receiver will therefore be compared to that of the MIMO radar, where the signals are transmitted in the entire 180-degree space. This is comparable due to the fact that the phased array's main beam will eventually cover the full scanning angular space and consequently risk the radar being detected by a ES receiver. The typical operation of each radar does present the worst case scenario in terms of detectability by an ES receiver. However, this worst case scenario is also the most likely case for each radar's target detection functionality.

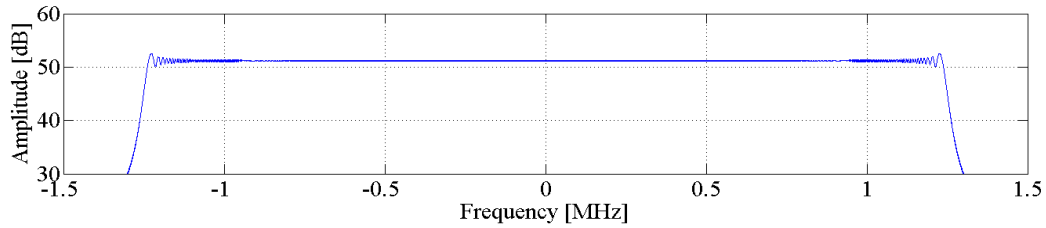
Each phased array antenna element transmits the same signal, multiplied by a complex weight. The transmitted signal is a complex linear chirp signal as illustrated in Figure 3.4.



(a) Complex chirp example.



(b) PAPR of the complex chirp.



(c) Frequency spectrum of the complex chirp with the signal length extended for illustration purposes.

Figure 3.4: Complex chirp signal example.

As illustrated, the signal satisfies the 1 watt transmit power constraint and the unity peak-to-average constraint. This complex chirp is used for all phased array simulations.

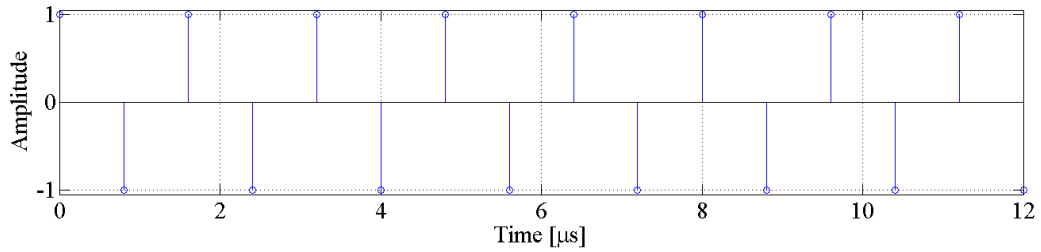
3.2 MIMO Array Signal Generation

The MIMO array model and the generation of MIMO radar signals was presented in Section 2.3 and 2.4 respectively. The Hadamard matrix is used as a basis for generating the set of orthogonal signals for the MIMO radar. Coinciding with the simulation setups where the largest number of antenna elements in an array is 16, a 16^{th} order Hadamard matrix, given by (3.1), is used for the signal generation.

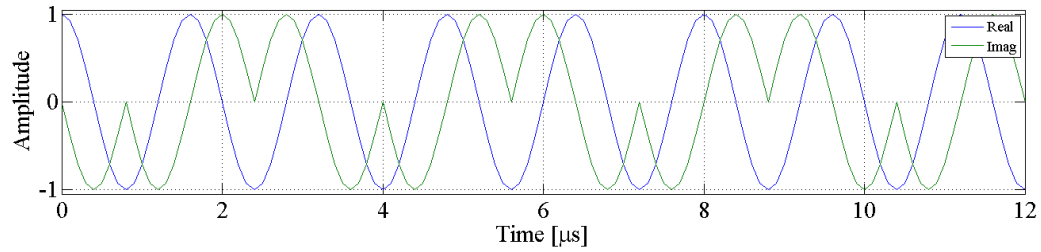
$$\mathbf{H}(16) = \begin{bmatrix} 1 & 1 & 1 & 1 & 1 & 1 & 1 & 1 & 1 & 1 & 1 & 1 & 1 & 1 & 1 & 1 \\ 1 & -1 & 1 & -1 & 1 & -1 & 1 & -1 & 1 & -1 & 1 & -1 & 1 & -1 & 1 & -1 \\ 1 & 1 & -1 & -1 & 1 & 1 & -1 & -1 & 1 & 1 & -1 & -1 & 1 & 1 & -1 & -1 \\ 1 & -1 & -1 & 1 & 1 & -1 & -1 & 1 & 1 & -1 & -1 & 1 & 1 & -1 & -1 & 1 \\ 1 & 1 & 1 & 1 & -1 & -1 & -1 & -1 & 1 & 1 & 1 & 1 & -1 & -1 & -1 & -1 \\ 1 & -1 & 1 & -1 & -1 & 1 & -1 & 1 & 1 & -1 & 1 & -1 & -1 & 1 & -1 & 1 \\ 1 & 1 & -1 & -1 & -1 & -1 & 1 & 1 & 1 & 1 & -1 & -1 & -1 & -1 & 1 & 1 \\ 1 & -1 & -1 & 1 & -1 & 1 & 1 & -1 & 1 & -1 & -1 & 1 & -1 & 1 & 1 & -1 \\ 1 & 1 & 1 & 1 & 1 & 1 & 1 & 1 & -1 & -1 & -1 & -1 & -1 & -1 & -1 & -1 \\ 1 & -1 & 1 & -1 & 1 & -1 & 1 & -1 & -1 & 1 & -1 & 1 & -1 & 1 & -1 & 1 \\ 1 & 1 & -1 & -1 & 1 & 1 & -1 & -1 & -1 & -1 & 1 & 1 & -1 & -1 & 1 & 1 \\ 1 & -1 & -1 & 1 & 1 & -1 & -1 & 1 & -1 & 1 & 1 & -1 & -1 & 1 & 1 & -1 \\ 1 & 1 & 1 & 1 & -1 & -1 & -1 & -1 & -1 & -1 & -1 & -1 & 1 & 1 & 1 & 1 \\ 1 & -1 & 1 & -1 & -1 & 1 & -1 & 1 & -1 & 1 & -1 & 1 & 1 & -1 & 1 & -1 \\ 1 & 1 & -1 & -1 & -1 & -1 & 1 & 1 & -1 & -1 & 1 & 1 & 1 & 1 & -1 & -1 \\ 1 & -1 & -1 & 1 & -1 & 1 & 1 & -1 & -1 & 1 & 1 & -1 & 1 & -1 & -1 & 1 \end{bmatrix} \quad (3.1)$$

Different interpolation filters, such as the sinc filter and the raised cosine filter, were implemented. However, these filters did not satisfy the unity PAPR constraint or the 1 watt transmit power constraint. Therefore, the CE-LRU filter is used to interpolate the Hadamard sequences by a factor of 8. The results of interpolating the second row (randomly chosen for illustration purposes) of the matrix given by (3.1) are illustrated in Figure 3.5. It is noted that the output of CE-LRU implementation contains $L - 1$ samples compared to expected output, where L is the interpolation factor. For example, a 16-sample input with an interpolation factor of $L = 8$ results in an output of 121 samples instead of 128 samples. The complex chirps generated for the phased array case were adjusted accordingly to 121 samples as well.

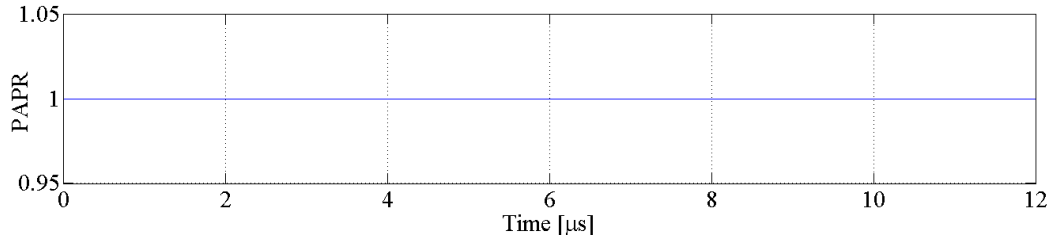
As illustrated, the signal satisfies the 1 watt transmit power constraint. This applies to all 16 possible signals. In Figure 3.5 (d), the sequence length was extended to properly illustrate the frequency spectrum. In a shorter sequence, peaks would have been more evident in the frequency spectrum. Each interpolated element of the code is a complex sinusoid at a fixed frequency, and thus causes a peak in the spectrum. For longer sequences, this effect should average out. Unlike the phased array case, the MIMO array will not be steered as it operates by transmitting energy in all directions, and then forms transmit beams after reception. The signal bandwidth constraint also holds as the bandwidth of the MIMO signals and the phased array's complex chirp are similar. As illustrated in Figure 3.6 (b), 90% of the signal power for both signals is captured at approximately 1.1 MHz.



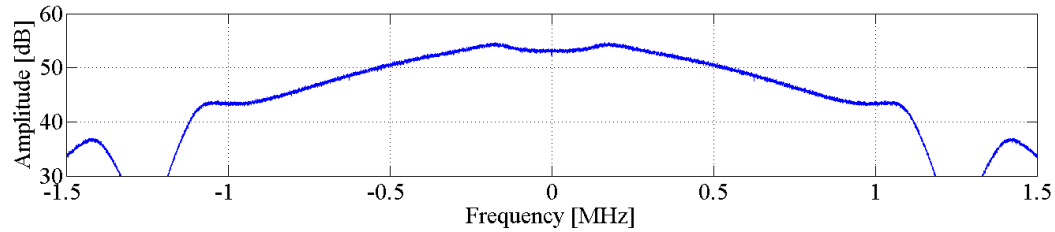
(a) Example of Hadamard sequence.



(b) Example of resulting MIMO signal.

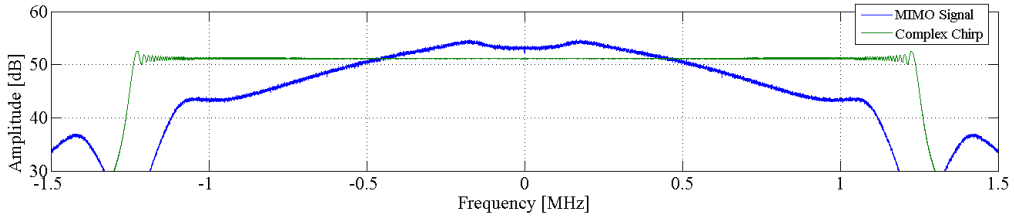


(c) PAPR of the MIMO signal.

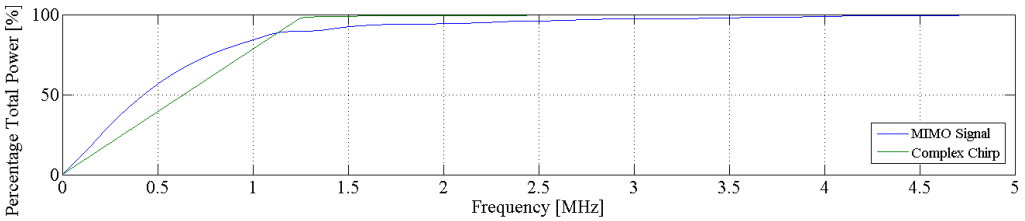


(d) Frequency spectrum of the MIMO signal with the signal length extended for illustration purposes.

Figure 3.5: MIMO signal generation example.



(a) Frequency spectrum of the MIMO signal compared to the complex chirp.



(b) Percentage captured power of the MIMO signal compared to the complex chirp.

Figure 3.6: Bandwidth comparison between the MIMO signal and the complex chirp.

3.3 Theoretical Patch Antenna Implementation

The theoretical antenna pattern for a typical patch antenna is given by [42]

$$b(\theta) = \cos\theta \frac{\sin\left(\frac{\beta W}{2}\sin\theta\right)}{\frac{\beta W}{2}\sin\theta}, \tag{3.2}$$

where $\beta = 2\pi/\lambda$ and $W = \lambda/2$. The resulting antenna pattern is illustrated in Figure 3.7.

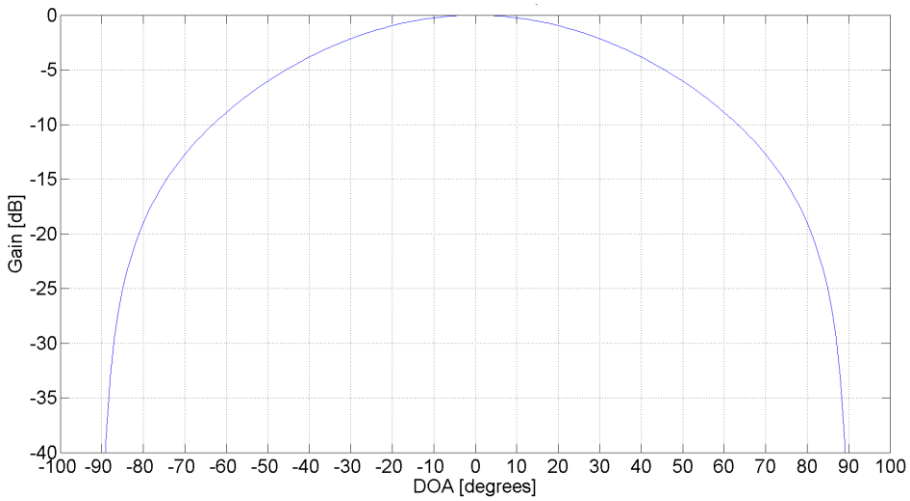


Figure 3.7: Theoretical patch antenna pattern.

This result can be directly applied to the ideal omnidirectional antenna pattern, which effectively results in the antenna pattern of an array of patch antennas [19]. For the sake of

comparison, the theoretical patch antenna will be used in the simulation setups listed in Table 5.

Table 5: Patch antenna simulation setups.

Array Type	Number of antenna elements	Number of sets of signals	Inter-element spacing
MIMO & Phased	4	1	0.5λ, 4λ
MIMO & Phased	8	1	0.5λ, 4λ
MIMO & Phased	16	1	0.5λ, 4λ

3.4 CVR Implementation

An overview of the CVR signal detection implementation is illustrated in Figure 3.8. The implementation includes the signal generation, the signal transmission and the signal detection by the ES receiver.

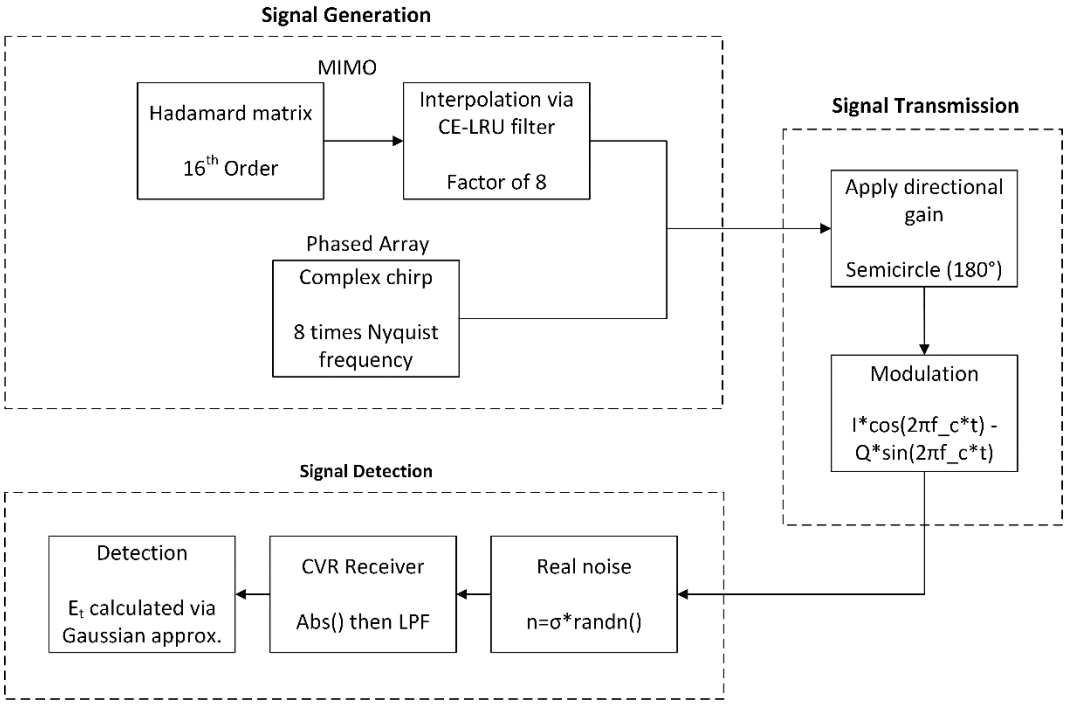


Figure 3.8: Overview of CVR implementation.

The signal generation of the phased array and the MIMO array and the steering of the signals was discussed in Sections 3.1 and 3.2 respectively. The signal pulse length is 12.1μs,

sampled at 10MHz. The CVR only considers the instantaneous amplitude of signals. Consider the signal given by

$$s(t) = I(t) + jQ(t), \tag{3.3}$$

where $I(t)$ is the real component and $Q(t)$ is the complex component. The time dependency is neglected for simplicity. The signal is then modulated

$$\begin{aligned} s_m &= (I + jQ)e^{j2\pi f_c t} \\ &= (I + jQ)[\cos(2\pi f_c t) + j\sin(2\pi f_c t)] \\ &= [I\cos(2\pi f_c t) - Q\sin(2\pi f_c t)] + j[I\sin(2\pi f_c t) + Q\cos(2\pi f_c t)], \end{aligned} \tag{3.4}$$

where f_c is the carrier frequency. The real part of s_m is then transmitted

$$s_t = Re(s_m) = I\cos(2\pi f_c t) - Q\sin(2\pi f_c t). \tag{3.5}$$

For computational practicality, the signal is modulated onto a carrier frequency of 2.5 MHz to retain the 10 MHz sampling frequency. This reduces the number of samples that need to be processed.

Real valued white Gaussian noise is added to the transmitted signal before the detection takes place. The full-wave rectifying action of the diode is modelled by the absolute value function $|.|$ and the low-pass filter is implemented through first order approximations

$$\mathbf{x}_{FWR} = |\mathbf{s}_t + \mathbf{z}|, \tag{3.6}$$

$$\mathbf{y} = \mathbf{x}_{FRW} * \mathbf{h}, \tag{3.7}$$

where $\mathbf{z}$ is the additive noise and $\mathbf{h}$ is the filter coefficients. Recall the assumption from Section 3, where it is assumed that the low-pass filter for the CVR is matched to the radar pulse length. For a large number of filter taps, the output of the filter is approximately Gaussian distributed. The CDF of the Gaussian distribution is algebraically manipulated to calculate the detection threshold E_t for $P_{fa} = 10^{-4}$. The variance σ_{FN}^2 and mean μ_{FN} of a folded normal distribution are given by

$$\begin{aligned} \sigma_{FN}^2 &= \sigma^2 - \left[\sigma\sqrt{\frac{2}{\pi}}\right]^2 \\ &= \sigma^2\left[1 - \frac{2}{\pi}\right] \end{aligned} \tag{3.8}$$

$$\mu_{FN} = \sigma\sqrt{\frac{2}{\pi}}, \tag{3.9}$$

where σ is the standard deviation of a normal distribution. The low-pass filter sums n of these random variables with filter coefficient $h = 1$

$$\sigma_f^2 = nh^2\sigma_{FN}^2 = n\sigma^2\left[1 - \frac{2}{\pi}\right], \tag{3.10}$$

$$\mu_f = nh\mu_{FN} = n\sigma\sqrt{\frac{2}{\pi}}. \tag{3.11}$$

Assuming n is large enough that the filter's output is approximately Gaussian, the PD can be approximated by the CDF of a Gaussian distribution at the threshold E_{t0}

$$P_d(E_{t0}) = \frac{1}{2}\left[1 + \text{erf}\left(\frac{E_{t0}}{\sigma_f\sqrt{2}}\right)\right]. \tag{3.12}$$

Using the identity

$$\begin{aligned} \text{erfc}(x) &= 1 - \text{erf}(x), \\ \text{erf}(x) &= 1 - \text{erfc}(x), \end{aligned} \tag{3.13}$$

the PD becomes

$$P_d(E_{t0}) = \frac{1}{2}\left[1 + 1 - \text{erfc}\left(\frac{E_{t0}}{\sigma_f\sqrt{2}}\right)\right]. \tag{3.14}$$

Solving for the detection threshold Et for a chosen P_{fa}

$$\begin{aligned} P_{fa} &= 1 - P_d(E_{t0}) \\ &= 1 - \frac{1}{2}\left[1 + 1 - \text{erfc}\left(\frac{E_{t0}}{\sigma_f\sqrt{2}}\right)\right] \\ &= 1 - 1 + \frac{1}{2}\text{erfc}\left(\frac{E_{t0}}{\sigma_f\sqrt{2}}\right) \\ P_{fa} &= \frac{1}{2}\text{erfc}\left(\frac{E_{t0}}{\sigma_f\sqrt{2}}\right) \\ \text{erfc}^{-1}(2P_{fa}) &= \frac{E_{t0}}{\sigma_f\sqrt{2}} \\ E_{t0} &= \sigma_f\sqrt{2}\text{erfc}^{-1}(2P_{fa}). \end{aligned} \tag{3.15}$$

The final threshold is given by the mean μ_f plus the zero-mean threshold E_{t0}

$$\begin{aligned} E_t &= \mu_f + E_{t0} \\ &= n\sigma\sqrt{\frac{2}{\pi}} + \sqrt{n\sigma^2\left(1-\frac{2}{\pi}\right)}\,\sqrt{2}\text{erfcinv}(2P_{fa}) \\ &= n\sigma\sqrt{\frac{2}{\pi}} + \sigma\sqrt{2n\left(1-\frac{2}{\pi}\right)}\,\text{erfcinv}(2P_{fa}). \end{aligned} \tag{3.16}$$

The resulting detection threshold is

$$E_t(\sigma) = 121.2045\sigma. \tag{3.17}$$

The Gaussian distribution assumption at the output of the filter resulted in an error of approximately 11% in the PFA for the calculated detection threshold

$$P_{fa} = 1.111 \times 10^{-4}. \tag{3.18}$$

The detection threshold value was varied slightly around (3.17). For each value, 10^9 iterations of random noise were used to determine the actual PFA. The results were interpolated to determine the actual threshold value corresponding to $P_{fa} = 10^{-4}$. The error compensation is illustrated in Figure 3.9.

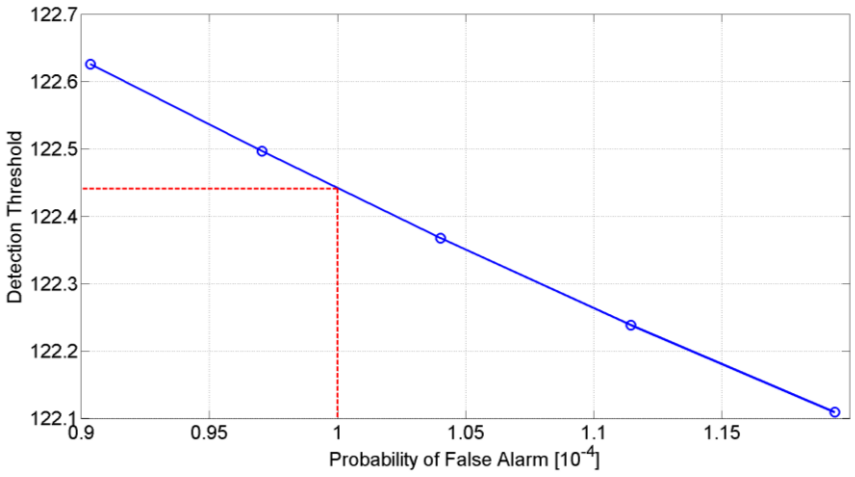


Figure 3.9: CVR detection threshold error correction for P_{fa}=10^{-4}.

The correct detection threshold was found to be

$$E_t(\sigma) = 122.4411\sigma. \tag{3.19}$$

The detection threshold is then used determine the detectability of the phased array and MIMO signals using the CVR.

3.5 ZIFR Implementation

An overview of the ZIFR signal detection implementation is illustrated in Figure 3.10. Recall from Section 2.5.2 that the ZIFR being implemented is the ZIFR, which retains the phase information of the signals. The implementation includes the signal generation, the signal transmission and the signal detection by the ES receiver.

The signal generation for the phased array and the MIMO array and the steering of the signals was discussed in Sections 3.1 and 3.2 respectively. The ZIFR receives complex signals and as a result is simpler to implement than the CVR implementation because modulation can be neglected as the original signal is recovered.

The implementation of the ZIFR signal detection is similar to that of the CVR, with the exception of adding complex valued noise as opposed to real valued noise. The complex envelope is obtained through the absolute function, $|.|$, for complex values and the low-pass filter is implemented by convolution with the filter coefficients **h**. Similar to the CVR implementation, the low-pass filter is matched to the radar pulse length, so the pulse length is assumed to be known a-priori. This also allows fair comparison of the detection performance between the CVR and ZIFR receivers.

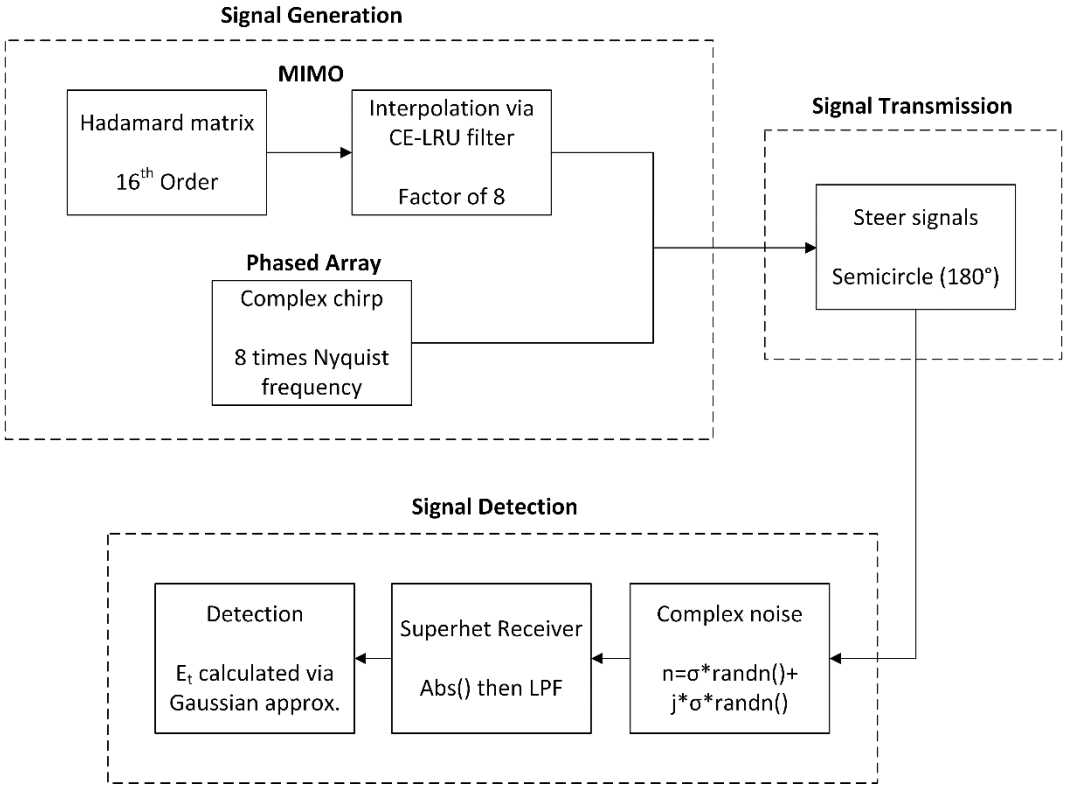


Figure 3.10: Overview of the ZIFR implementation.

The CDF of the Gaussian distribution is algebraically manipulated to calculate the detection threshold E_t for $P_{fa} = 10^{-4}$. The variance σ_R^2 and mean μ_R of a Rayleigh distributed random variable are given by [38]

$$\sigma_R^2 = \sigma^2\left(\frac{4-\pi}{2}\right), \tag{3.20}$$

$$\mu_R = \sigma\sqrt{\frac{\pi}{2}}. \tag{3.21}$$

The low-pass filter sums n of these random variables with filter coefficient $h = 1$

$$\sigma_f^2 = nh^2\sigma_R^2 = n\sigma^2\left(\frac{4-\pi}{2}\right), \tag{3.22}$$

$$\mu_f = nh\mu_R = n\sigma\sqrt{\frac{\pi}{2}}. \tag{3.23}$$

Assuming n is large enough that the filter's output is approximately Gaussian, the zero-mean P_d can be approximated by the CDF of a zero mean Gaussian distribution at zero-mean threshold of E_{t0}

$$P_d(E_{t0}) = \frac{1}{2}\left[1 + \text{erf}\left(\frac{E_{t0}}{\sigma_f\sqrt{2}}\right)\right]. \tag{3.24}$$

Using the identity

$$\begin{aligned} \text{erfc}(x) &= 1 - \text{erf}(x), \\ \text{erf}(x) &= 1 - \text{erfc}(x), \end{aligned} \tag{3.25}$$

the PD becomes

$$P_d(E_{t0}) = \frac{1}{2}\left[1 + 1 - \text{erfc}\left(\frac{E_{t0}}{\sigma_f\sqrt{2}}\right)\right]. \tag{3.26}$$

Solving for the detection threshold Et for a chosen P_{fa}

$$\begin{aligned} P_{fa} &= 1 - P_d(E_{t0}) \\ &= 1 - 1 + \frac{1}{2}\text{erfc}\left(\frac{E_{t0}}{\sigma_f\sqrt{2}}\right) \\ P_{fa} &= \frac{1}{2}\text{erfc}\left(\frac{E_{t0}}{\sigma_f\sqrt{2}}\right) \\ E_{t0} &= \sigma_f\sqrt{2}\text{erfcinv}(2P_{fa}). \end{aligned} \tag{3.27}$$

The final threshold is given by the mean μ_f plus the zero-mean threshold E_{t0}

$$\begin{aligned} E_t &= \mu_f + E_{t0} \\ &= n\sigma\sqrt{\frac{\pi}{2}} + \sqrt{n\sigma^2\left(\frac{4-\pi}{2}\right)}\,\sqrt{2}\text{erfcinv}(2P_{fa}) \\ E_t &= n\sigma\sqrt{\frac{\pi}{2}} + \sigma\sqrt{n(4-\pi)}\,\text{erfcinv}\left(2P_{fa}\right). \end{aligned} \tag{3.28}$$

Similar to the CVR case, the error made due to the approximations in the derivation is corrected by running 10^9 iterations of random noise to determine the actual PFA. The result is shown in Figure 3.11.

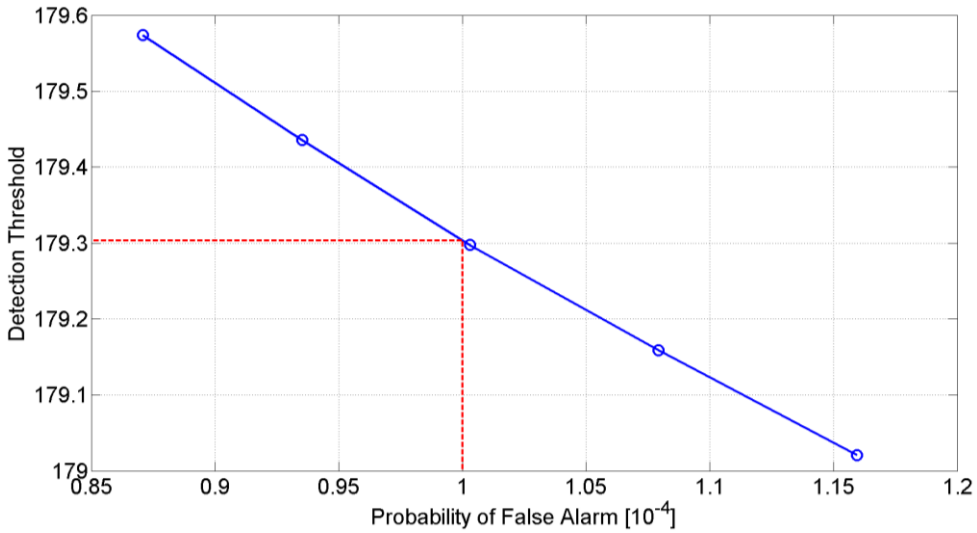


Figure 3.11: ZIFR detection threshold error correction for P_{fa}=10^{-4}.

The corrected detection threshold was determined to be

$$E_t(\sigma) = 179.3033\sigma. \tag{3.29}$$

The detection threshold is then used determine the detectability of the phased array and MIMO signals using the ZIFR.

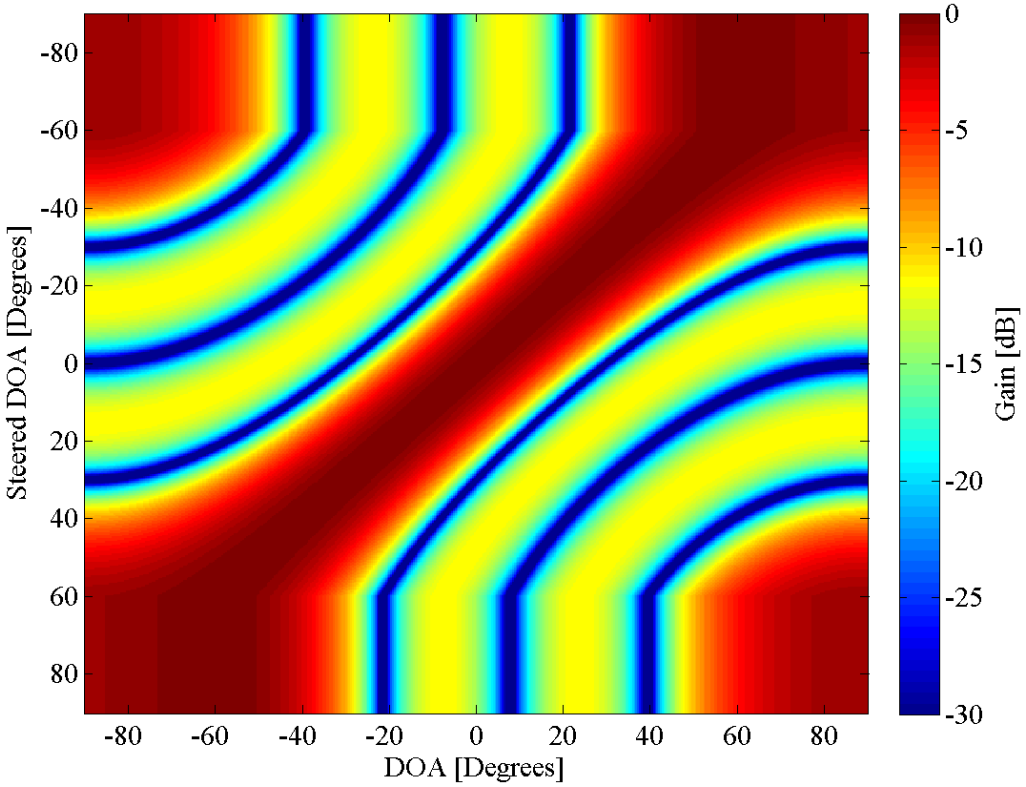
3.6 Simulation Setup for Antenna Pattern Comparison

The phased array and MIMO array setups, described in Table 1 and Table 2 respectively, all have unique antenna patterns. As a result, the detectability of transmitted signals in each case are expected to differ. It should be noted that grating lobes are more evident in the main angles of interest (-60 to 60 degrees) when using ideal omnidirectional antennas as opposed to a theoretical patch antenna.

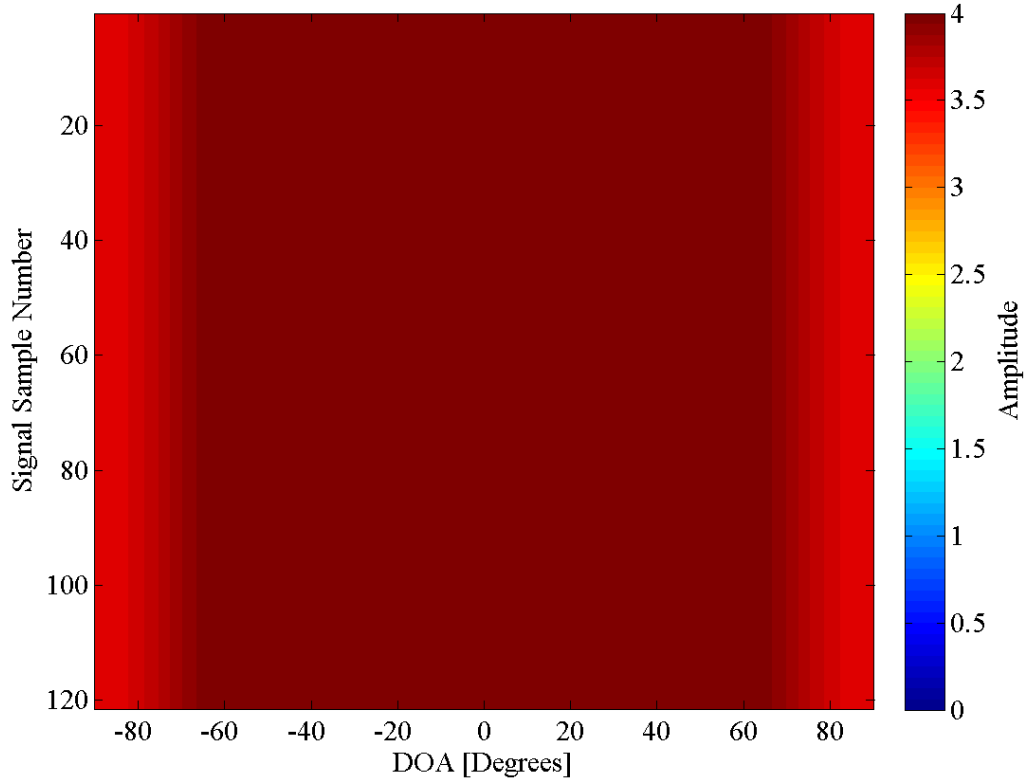
The simulated antenna patterns are presented in the following subsections. Owing to the large number of simulation setups, the first two graphs of each subsection are intentionally enlarged so that the axis labels are easily legible. Thereafter, the remainder of the graphs from each subsection are included for the sake of completeness. The axis labels are identical with the exception of the scale for the transmitted signal amplitude, which scales according to the number of antenna elements in the array.

3.6.1 Ideal Omnidirectional Phased Array Antenna Patterns

The antenna patterns of the phased array setups using ideal omnidirectional antenna elements are illustrated in Figure 3.12 through to Figure 3.23. Alongside the antenna pattern is the transmitted signal's amplitude for all DOAs. Each horizontal line in the antenna pattern figures is the antenna pattern steered to a particular direction as indicated by the vertical axis. The antenna patterns confirm that the phased array is steered from -60 to 60 degrees, which is characterised by the peak gain moving across from the bottom left corner to the top right corner of each plot. Furthermore, it is evident that at angles below -60 and above 60, the beam will remain steered at -60 and 60 degrees respectively. This is shown by the unchanging horizontal lines below -60 and above 60 degrees on the vertical axis. This area is effectively the remaining portion of the antenna pattern when the pattern has been steered to its limit at -60 or 60 degrees. The transmitted signal amplitudes are scaled by the antenna pattern's gain in each DOA. It illustrates the peak values of the transmitted signals, where detection of the signals by the ES receiver is more likely.

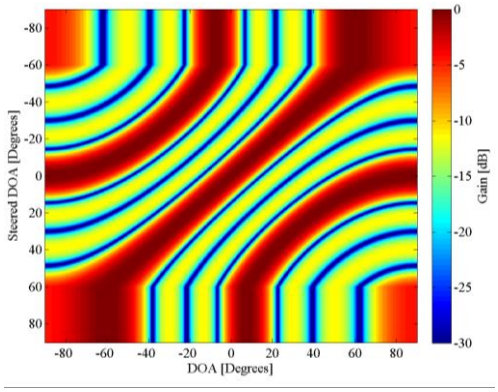


(a) Logarithmic antenna pattern for all DOAs.

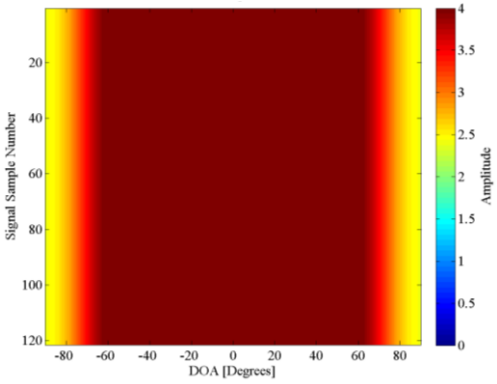


(b) Transmitted signal amplitude versus DOA.

Figure 3.12: Four-antenna element phased array 0.5λ inter-element spacing.

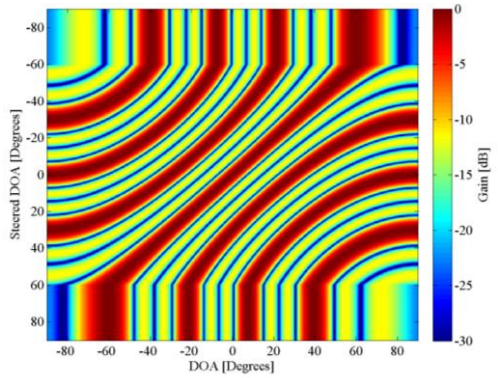


(a) Logarithmic antenna pattern for DOAs.

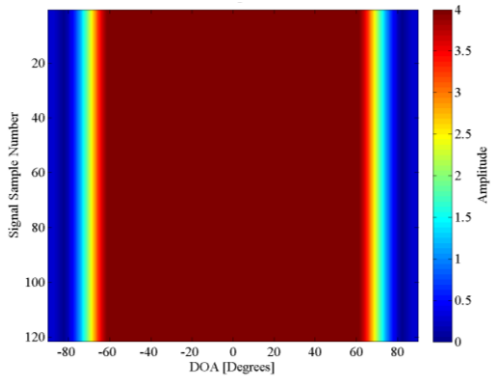


(b) Transmitted signal amplitude versus DOA.

Figure 3.13: Four-antenna element phased array with 1.0λ inter-element spacing.

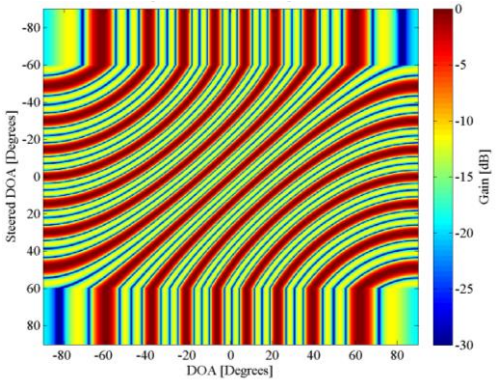


(a) Logarithmic antenna pattern for DOAs.

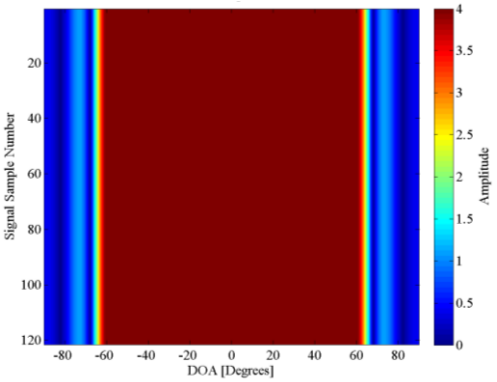


(b) Transmitted signal amplitude versus DOA.

Figure 3.14: Four-antenna element phased array with 2.0λ inter-element spacing.

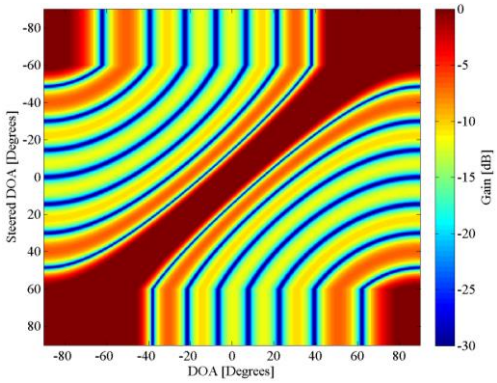


(a) Logarithmic antenna pattern for DOAs.

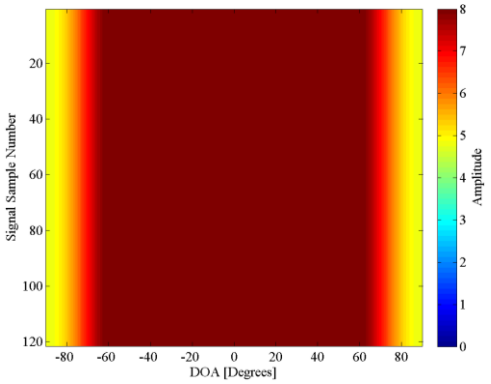


(b) Transmitted signal amplitude versus DOA.

Figure 3.15: Four-antenna element phased array with 4. 0λ inter-element spacing.

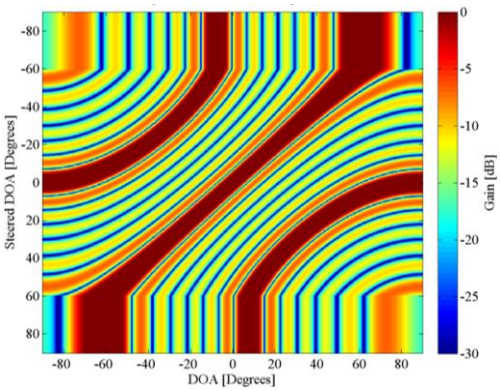


(a) Logarithmic antenna pattern for DOAs.

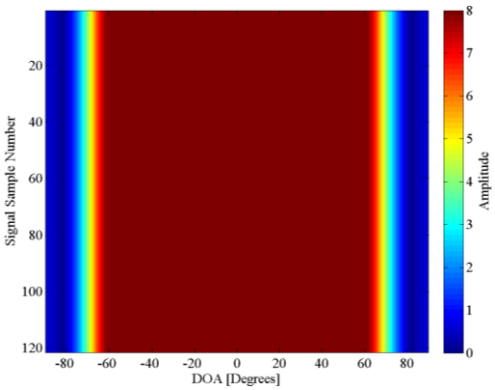


(b) Transmitted signal amplitude versus DOA.

Figure 3.16: Eight-antenna element phased array with 0.5λ inter-element spacing.

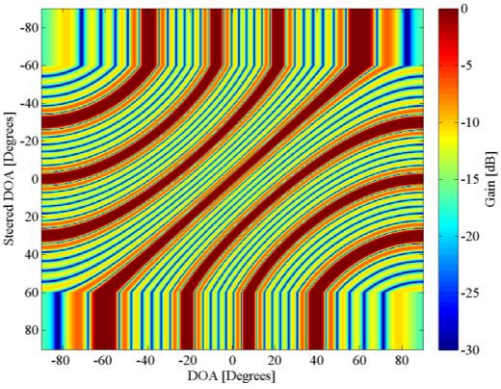


(a) Logarithmic antenna pattern for DOAs.

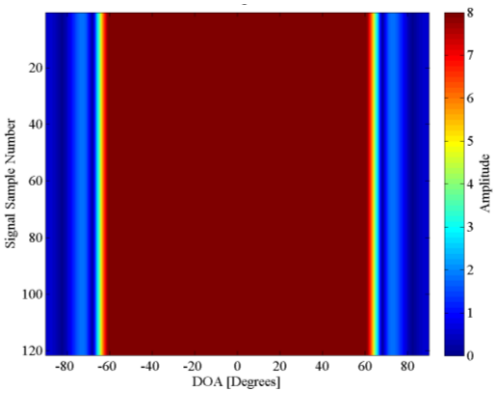


(b) Transmitted signal amplitude versus DOA.

Figure 3.17: Eight-antenna element phased array with 1.0λ inter-element spacing.

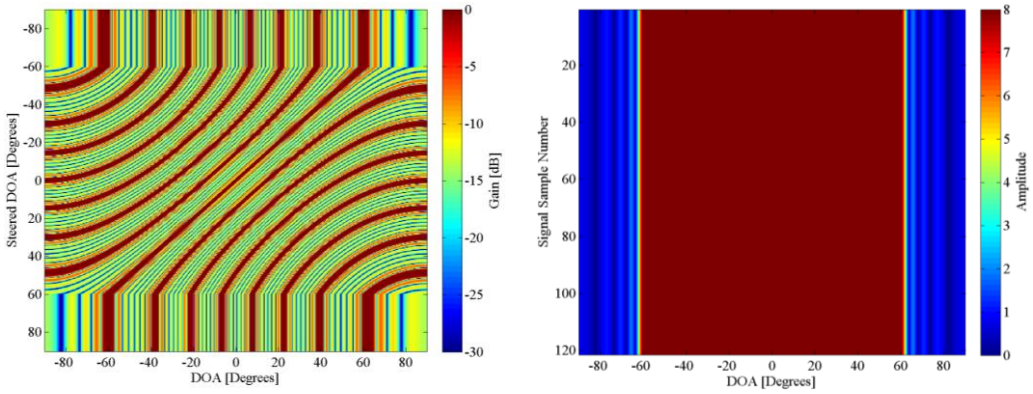


(a) Logarithmic antenna pattern for DOAs.



(b) Transmitted signal amplitude versus DOA.

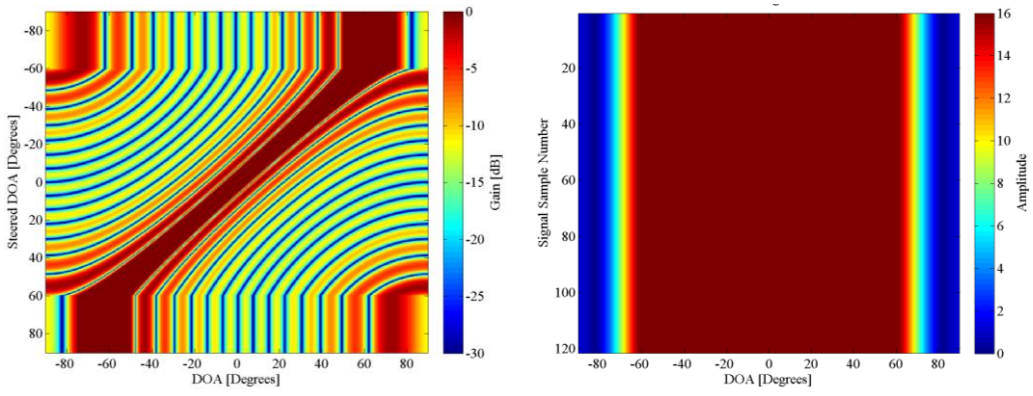
Figure 3.18: Eight-antenna element phased array with 2.0λ inter-element spacing.



(a) Logarithmic antenna pattern for DOAs.

(b) Transmitted signal amplitude versus DOA.

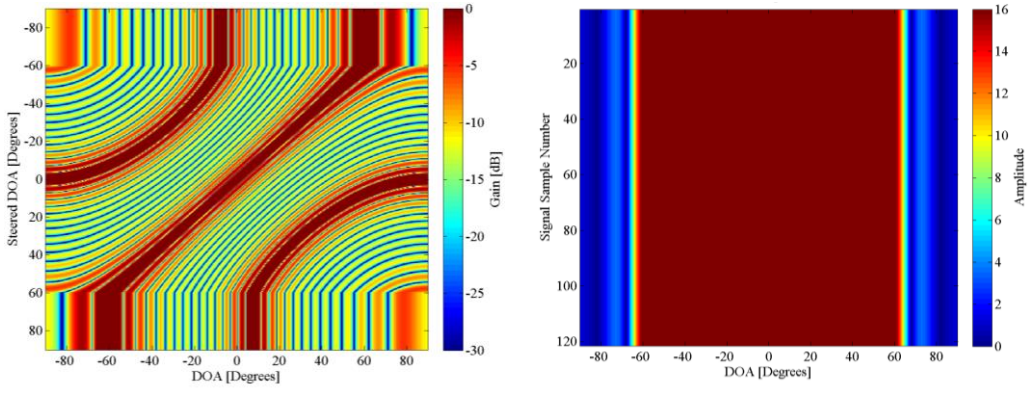
Figure 3.19: Eight-antenna element phased array with 4.0λ inter-element spacing.



(a) Logarithmic antenna pattern for DOAs.

(b) Transmitted signal amplitude versus DOA.

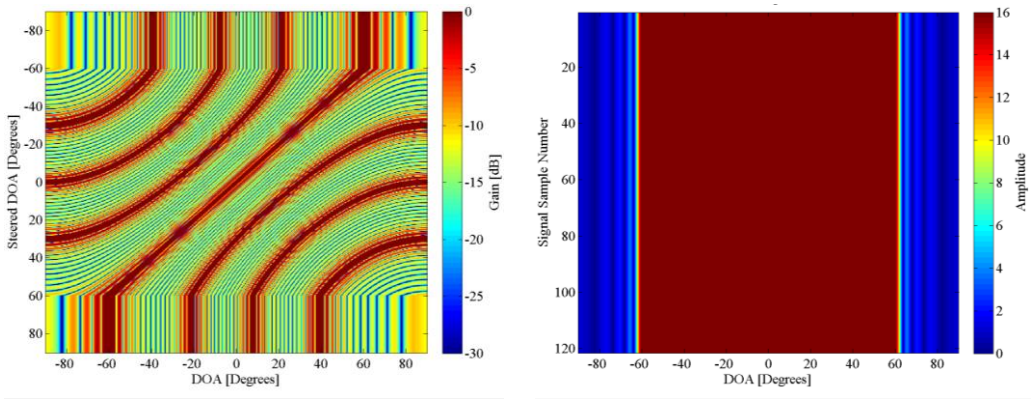
Figure 3.20: Sixteen-antenna element phased array with 0.5λ inter-element spacing.



(a) Logarithmic antenna pattern for DOAs.

(b) Transmitted signal amplitude versus DOA.

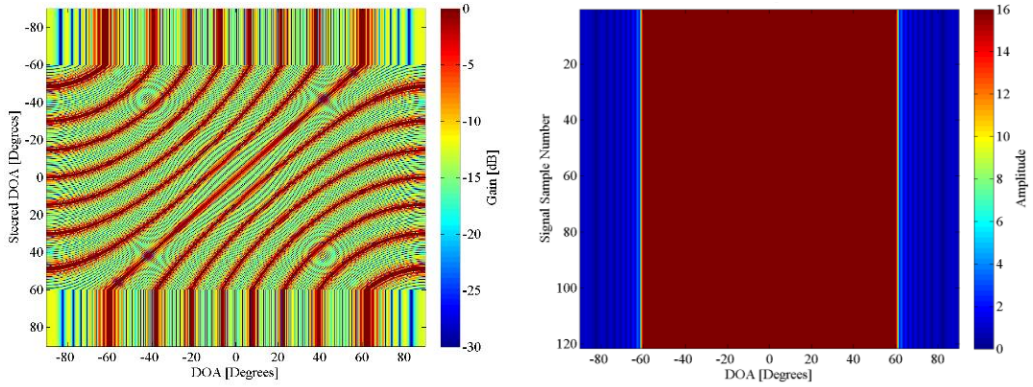
Figure 3.21: Sixteen-antenna element phased array with 1.0λ inter-element spacing.



(a) Logarithmic antenna pattern for DOAs.

(b) Transmitted signal amplitude versus DOA.

Figure 3.22: Sixteen-antenna element phased array with 2.0λ inter-element spacing.



(a) Logarithmic antenna pattern for DOAs.

(b) Transmitted signal amplitude versus DOA.

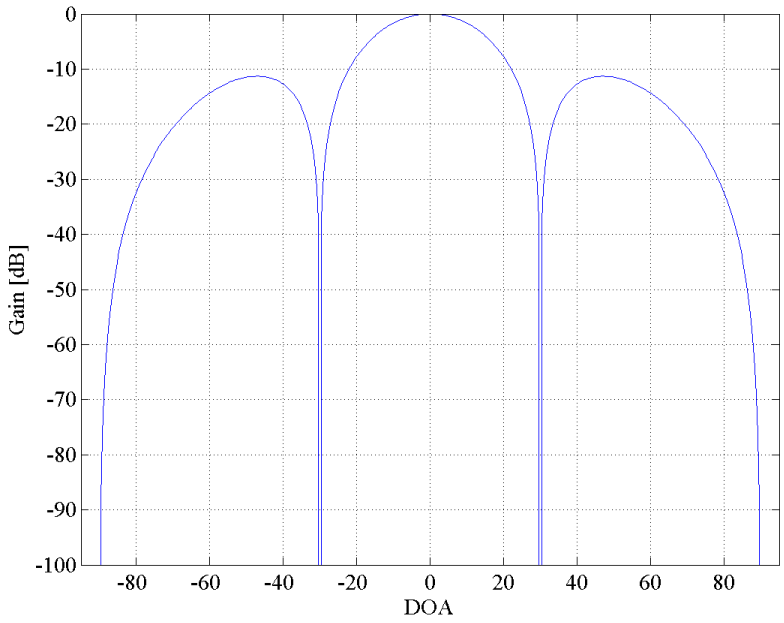
Figure 3.23: Sixteen-antenna element phased array with 4.0λ inter-element spacing.

3.6.2 Ideal Omnidirectional MIMO Array Antenna Patterns

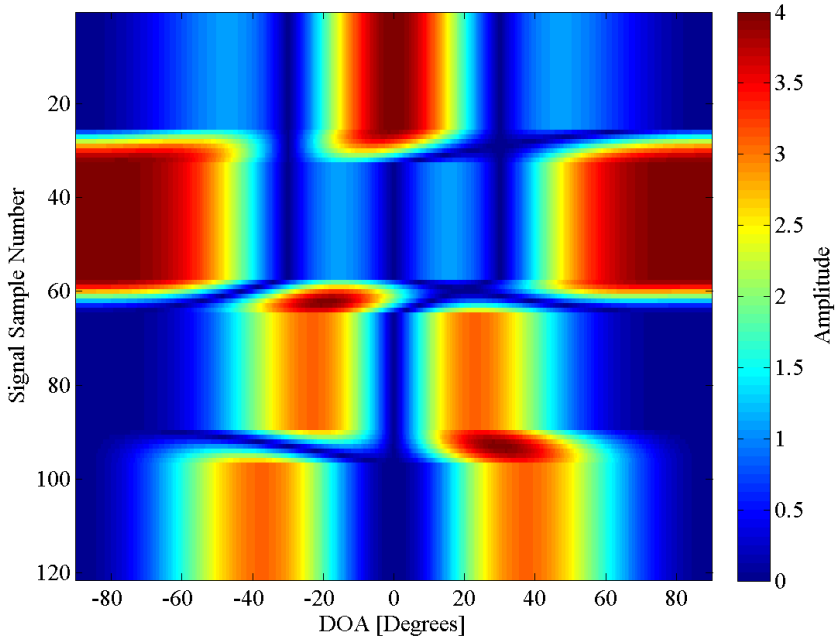
The antenna patterns of the MIMO array setups using ideal omnidirectional antenna elements are illustrated in Figure 3.24 through to Figure 3.35. Unlike the phased array radar, the transmit antenna pattern of the MIMO radar is not steered. The effect of the antenna array transmission is similar to that of a broadside antenna pattern. The transmitted signals combine unpredictably as a result of the combination of the approximately orthogonal set of signals. As discussed, multiple unique sets of signals are used in the different MIMO setups. Only one example of a set of signals for each MIMO array setup is presented. The details of the presented setups are given in Table 6.

Table 6: MIMO array illustrated transmitted signals.

Number of antenna elements	Set of signals (Rows of Hadamard matrix)
4	1,5,9,13
8	2,4,6,8,10,12,14,16
16	All 16

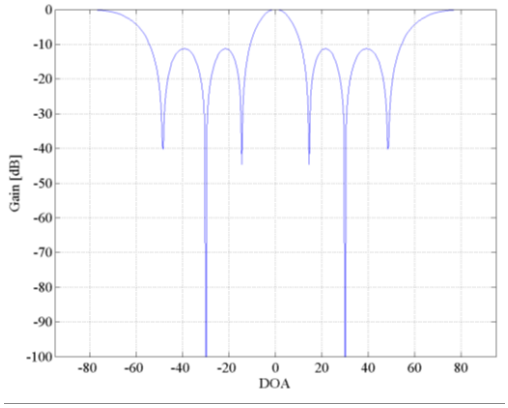


(a) Logarithmic antenna pattern for DOAs.

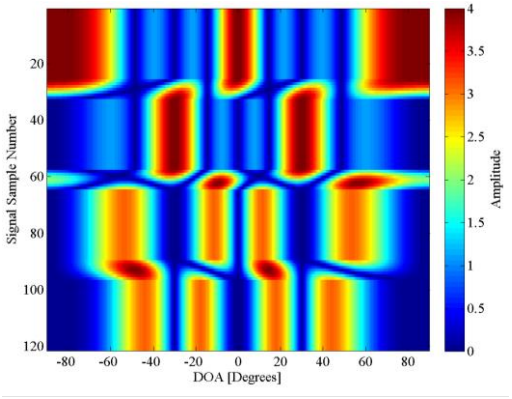


(b) Transmitted signal amplitude versus DOA.

Figure 3.24: Four-antenna element MIMO array with 0.5λ inter-element spacing.

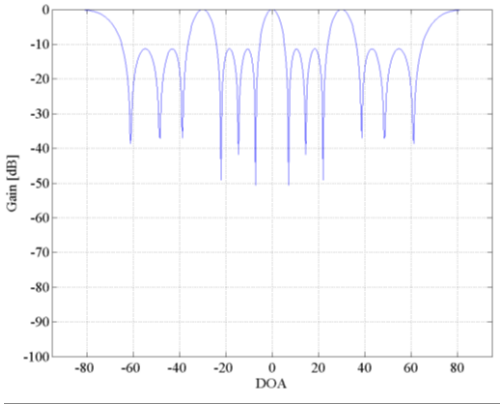


(a) Logarithmic antenna pattern for DOAs.

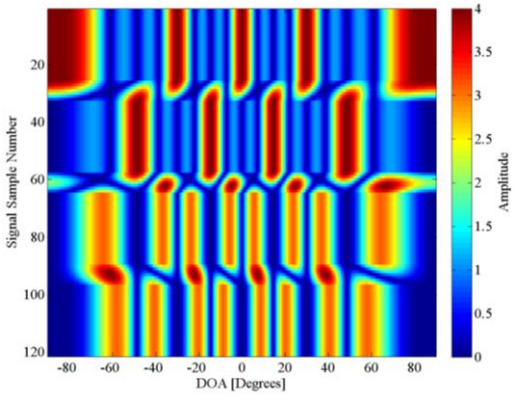


(b) Transmitted signal amplitude versus DOA.

Figure 3.25: Four-antenna element MIMO array with 1.0λ inter-element spacing.

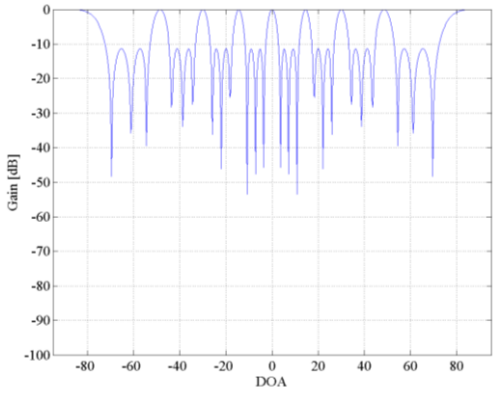


(a) Logarithmic antenna pattern for DOAs.

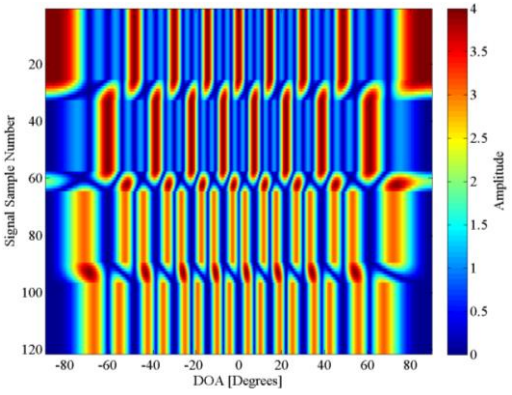


(b) Transmitted signal amplitude versus DOA.

Figure 3.26: Four-antenna element MIMO array with 2.0λ inter-element spacing.

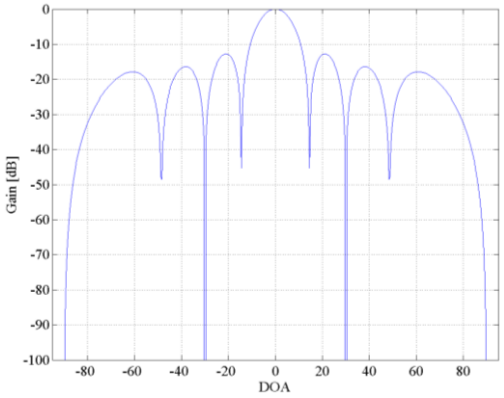


(a) Logarithmic antenna pattern for DOAs.

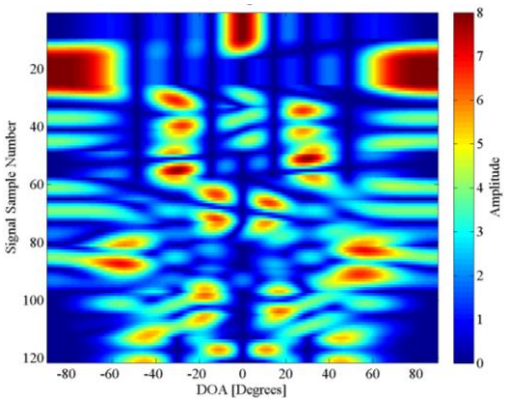


(b) Transmitted signal amplitude versus DOA.

Figure 3.27: Four-antenna element MIMO array with 4.0λ inter-element spacing.

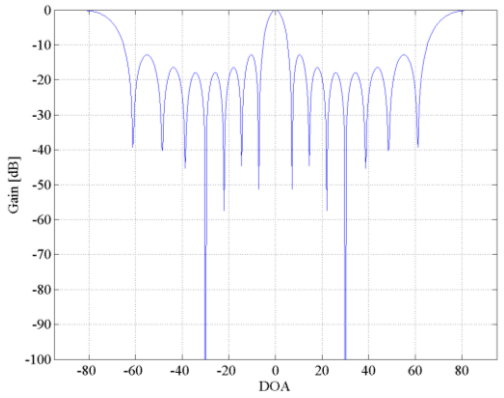


(a) Logarithmic antenna pattern for DOAs.

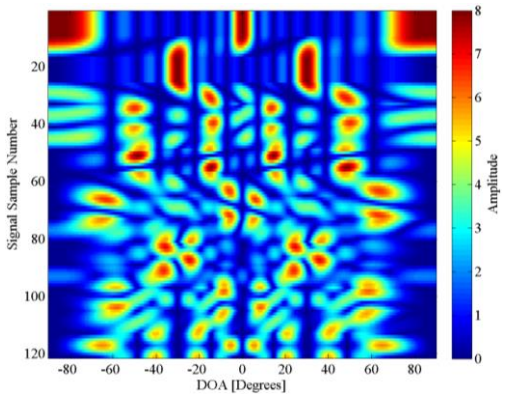


(b) Transmitted signal amplitude versus DOA.

Figure 3.28: Eight-antenna element MIMO array with 0.5λ inter-element spacing.

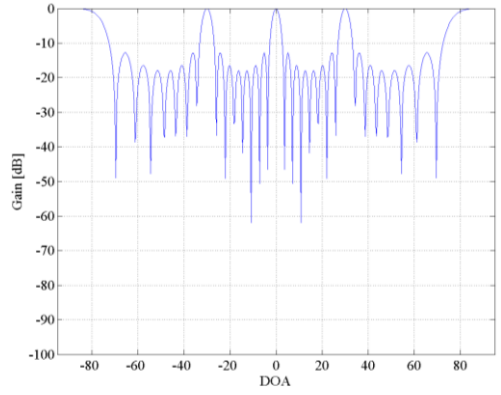


(a) Logarithmic antenna pattern for DOAs.

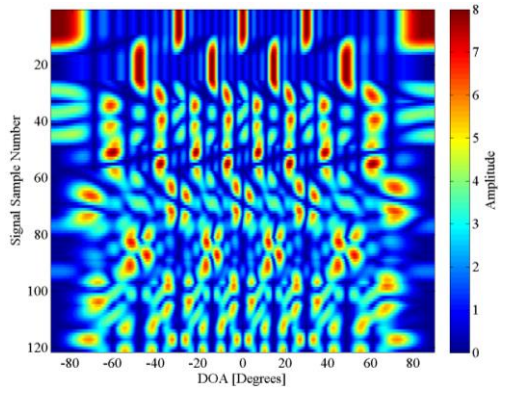


(b) Transmitted signal amplitude versus DOA.

Figure 3.29: Eight-antenna element MIMO array with 1.0λ inter-element spacing.

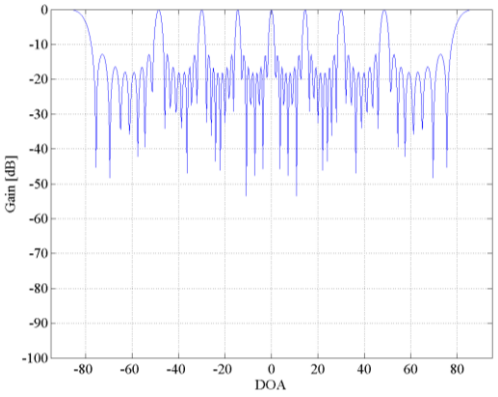


(a) Logarithmic antenna pattern for DOAs.

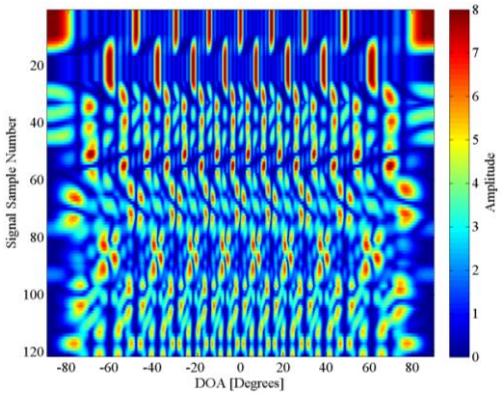


(b) Transmitted signal amplitude versus DOA.

Figure 3.30: Eight-antenna element MIMO array with 2. 0λ inter-element spacing.

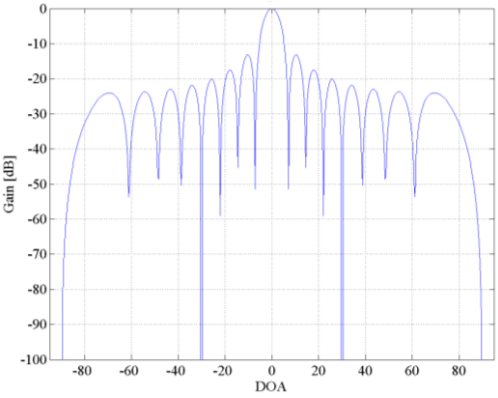


(a) Logarithmic antenna pattern for DOAs.

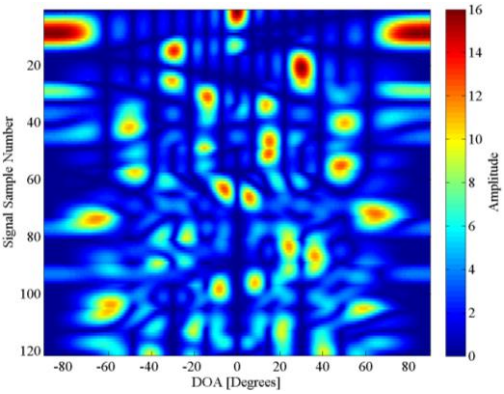


(b) Transmitted signal amplitude versus DOA.

Figure 3.31: Eight-antenna element MIMO array with 4.0λ inter-element spacing.

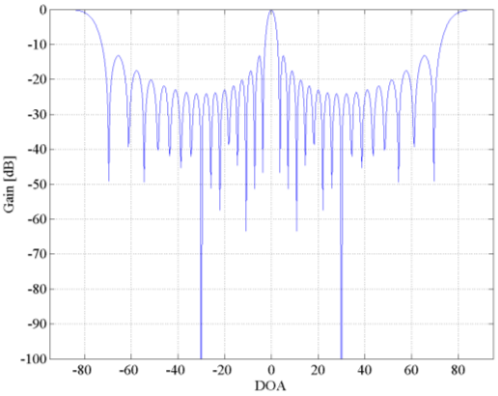


(a) Logarithmic antenna pattern for DOAs.

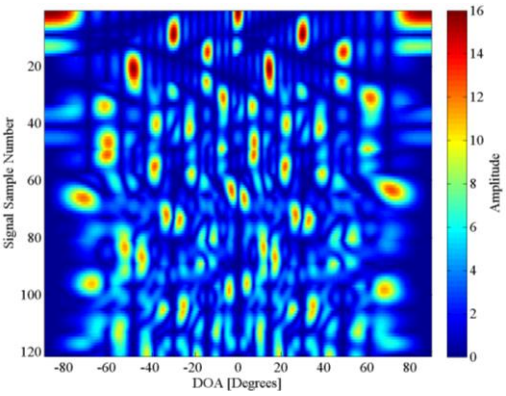


(b) Transmitted signal amplitude versus DOA.

Figure 3.32: Sixteen-antenna element MIMO array with 0.5λ inter-element spacing.

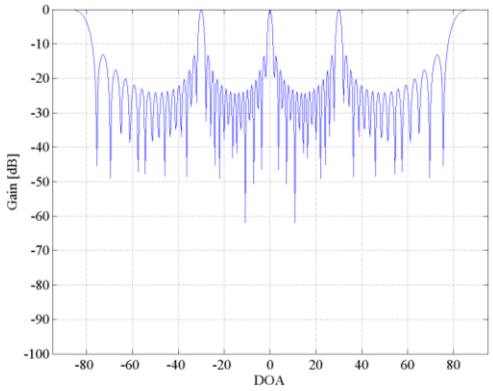


(a) Logarithmic antenna pattern for DOAs.

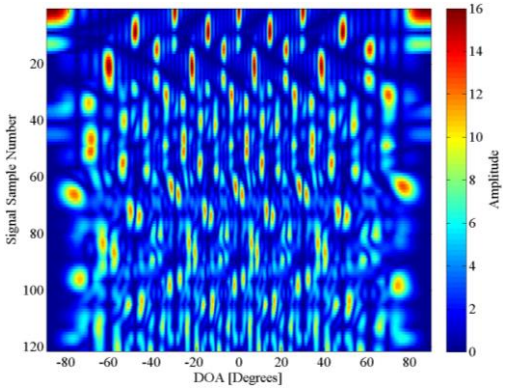


(b) Transmitted signal amplitude versus DOA.

Figure 3.33: Sixteen-antenna element MIMO array with 1.0λ inter-element spacing.

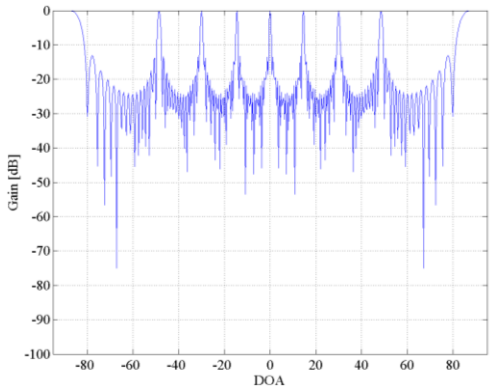


(a) Logarithmic antenna pattern for DOAs.

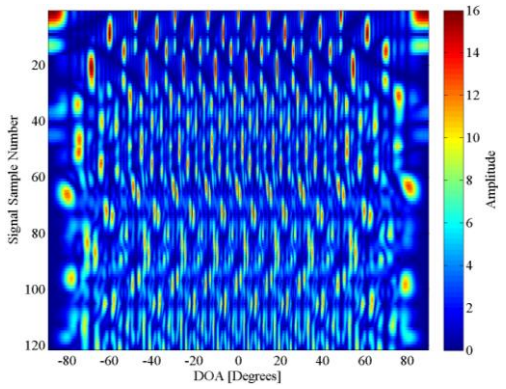


(b) Transmitted signal amplitude versus DOA.

Figure 3.34: Sixteen-antenna element MIMO array with 2.0λ inter-element spacing.



(a) Logarithmic antenna pattern for DOAs.

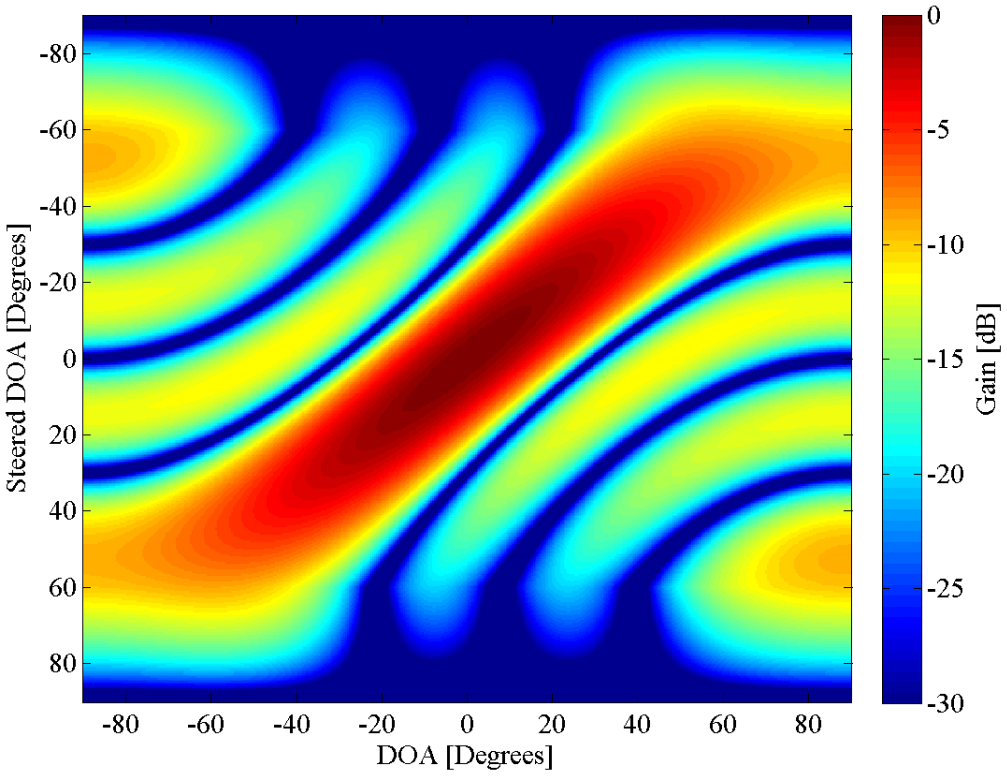


(b) Transmitted signal amplitude versus DOA.

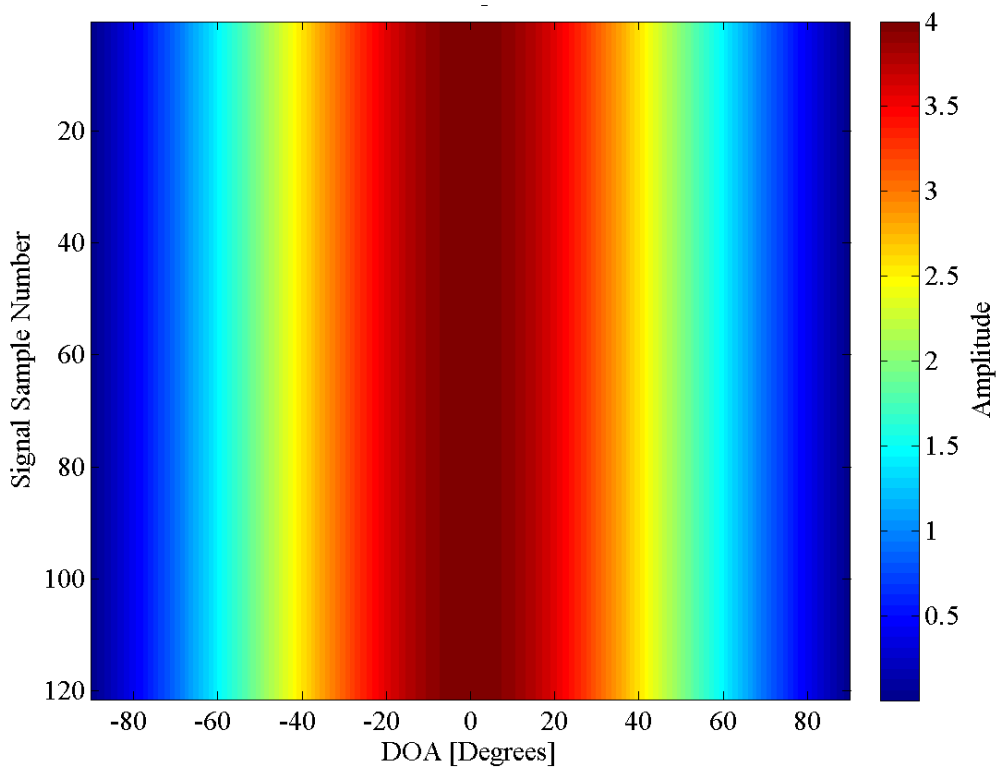
Figure 3.35: Sixteen-antenna element MIMO array with 4.0λ inter-element spacing.

3.6.3 Theoretical Patch Phased Array Antenna Patterns

The antenna patterns of the phased array setups using theoretical patch antenna elements are illustrated in Figure 3.36 through to Figure 3.41. As discussed in Section 3.3, the theoretical patch antenna pattern is applied directly to the ideal omnidirectional antenna pattern. This effectively results in the antenna pattern of an array of patch antennas.

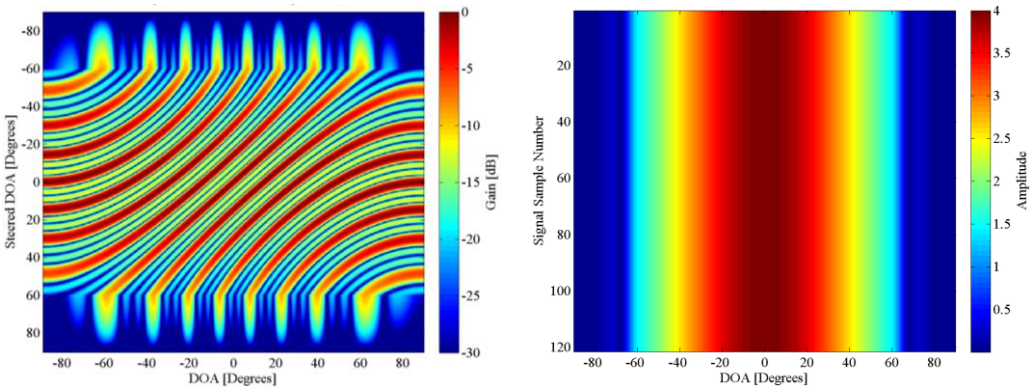


(a) Logarithmic antenna pattern for DOAs.



(b) Transmitted signal amplitude versus DOA.

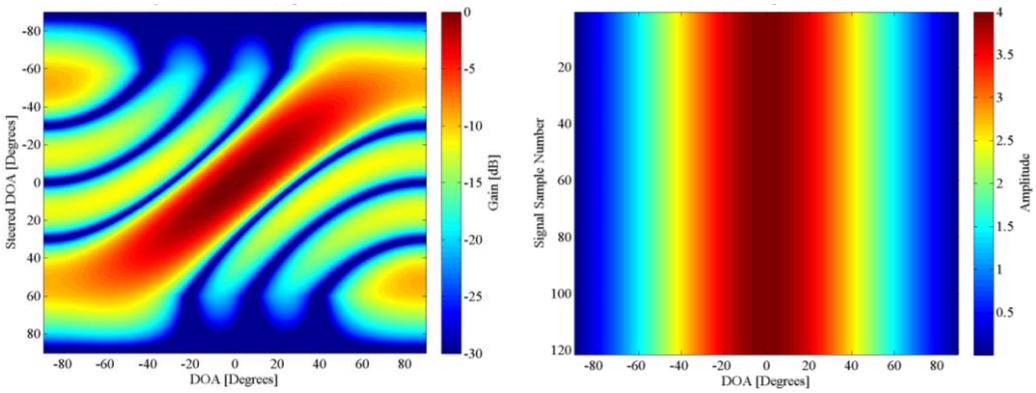
Figure 3.36: Four patch antenna element phased array with 0.5λ inter-element spacing.



(a) Logarithmic antenna pattern for DOAs.

(b) Transmitted signal amplitude versus DOA.

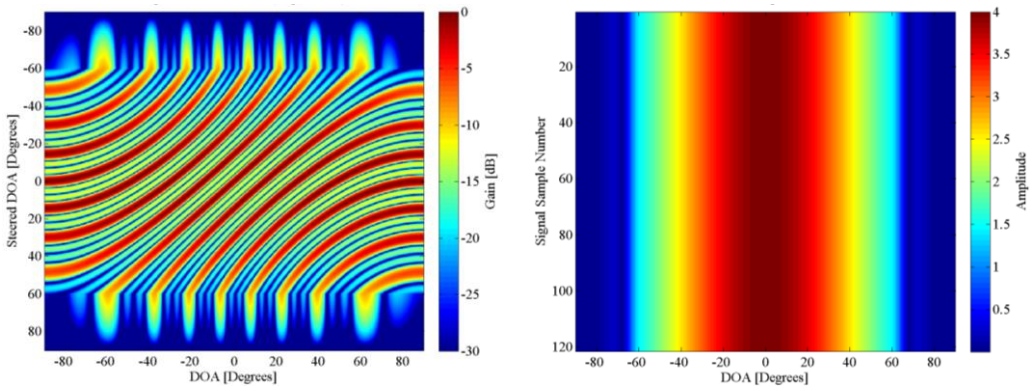
Figure 3.37: Four patch antenna element phased array with 4.0λ inter-element spacing.



(a) Logarithmic antenna pattern for DOAs.

(b) Transmitted signal amplitude versus DOA.

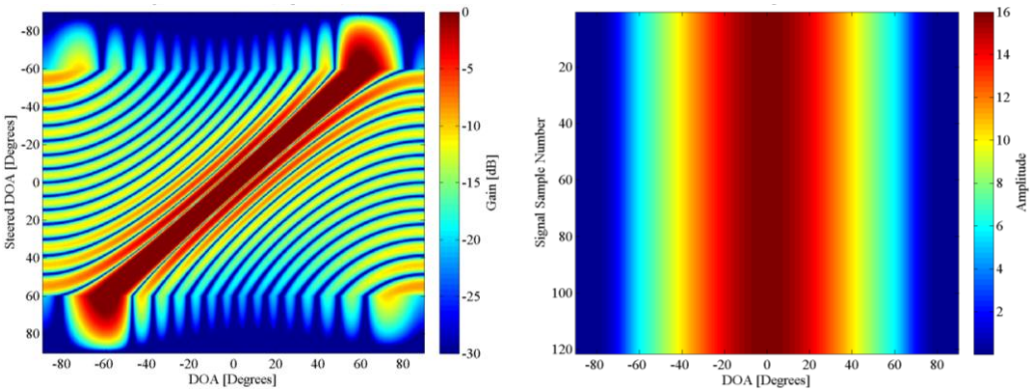
Figure 3.38: Eight patch antenna element phased array with 0.5λ inter-element spacing.



(a) Logarithmic antenna pattern for DOAs.

(b) Transmitted signal amplitude versus DOA.

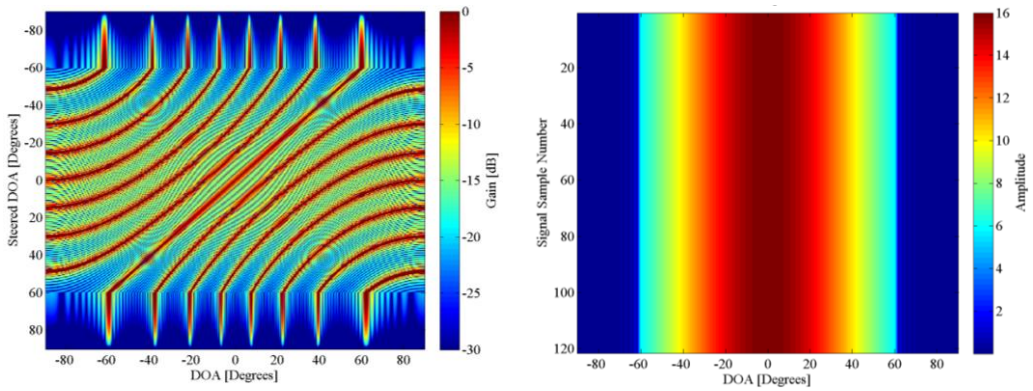
Figure 3.39: Eight patch antenna element phased array with 4.0λ inter-element spacing.



(a) Logarithmic antenna pattern for DOAs.

(b) Transmitted signal amplitude versus DOA.

Figure 3.40: Sixteen patch antenna element phased array with 0.5λ inter-element spacing.



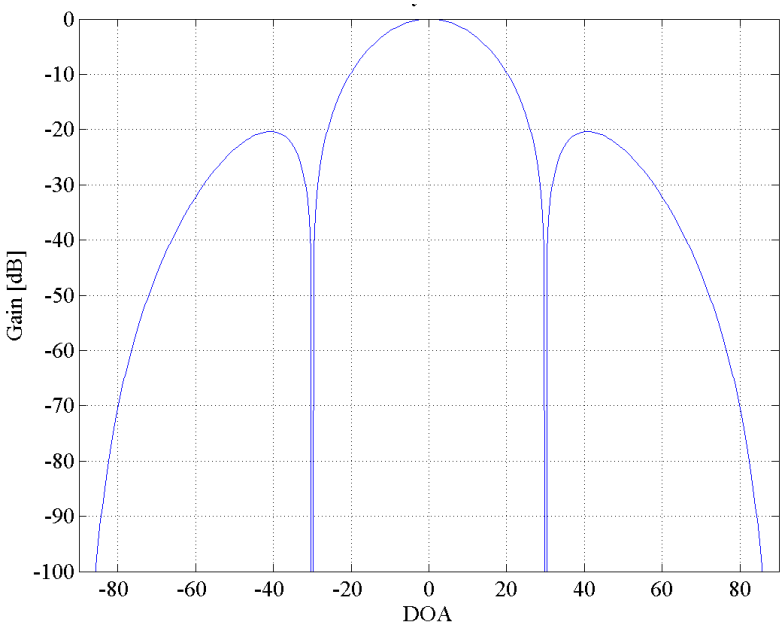
(a) Logarithmic antenna pattern for DOAs.

(b) Transmitted signal amplitude versus DOA.

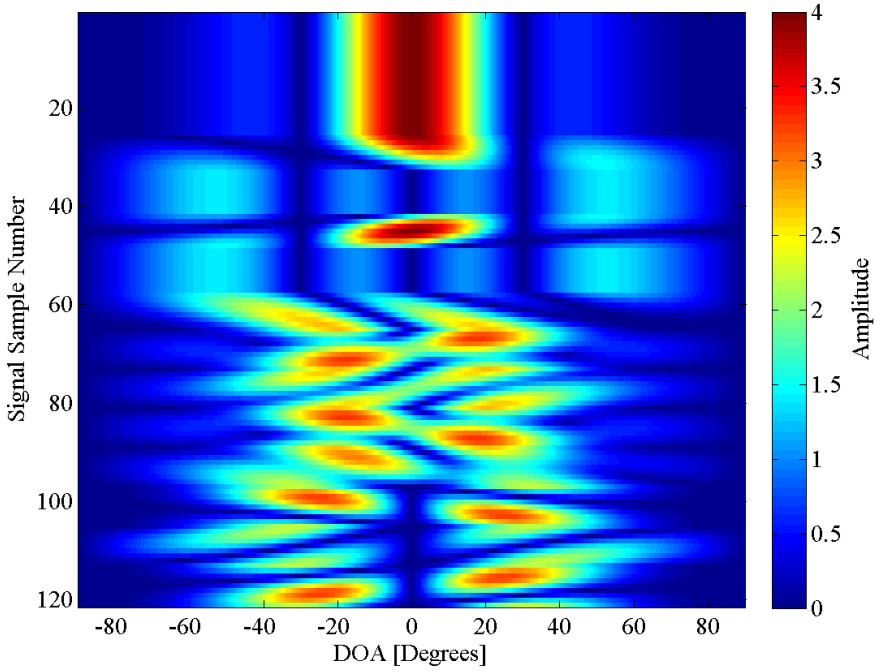
Figure 3.41: Sixteen patch antenna element phased array with 4.0λ inter-element spacing.

3.6.4 Theoretical Patch MIMO Array Antenna Patterns

The antenna patterns of the MIMO array setups using theoretical patch antenna elements are illustrated in Figure 3.42 through to Figure 3.47. Similar to the phased array case in Section 3.6.3, the theoretical patch antenna pattern is applied directly to the ideal omnidirectional antenna patterns.

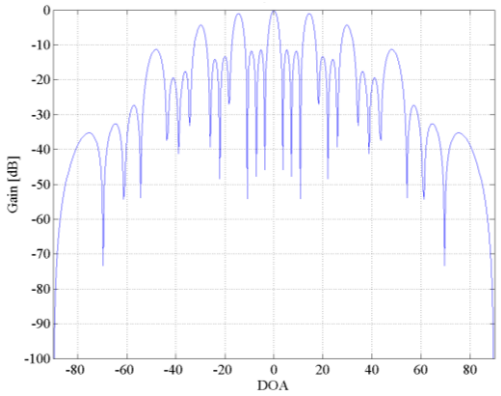


(a) Logarithmic antenna pattern for DOAs.

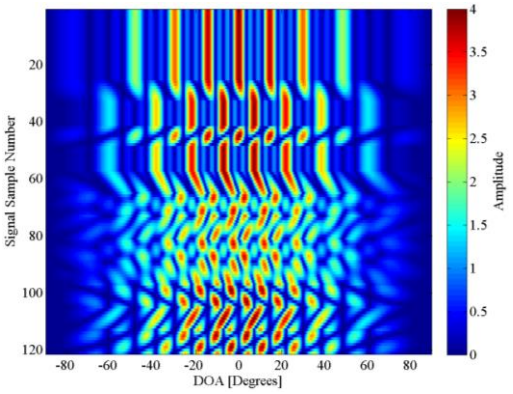


(b) Transmitted signal amplitude versus DOA.

Figure 3.42: Four patch antenna element MIMO with 0.5λ inter-element spacing.

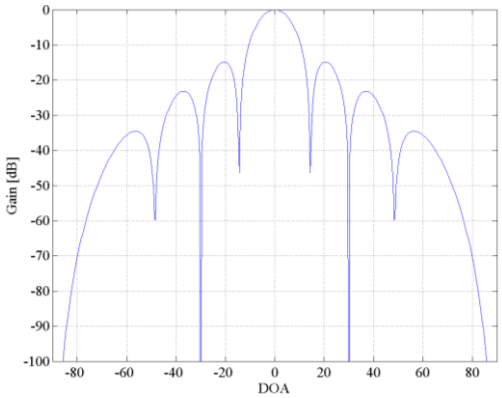


(a) Logarithmic antenna pattern for DOAs.

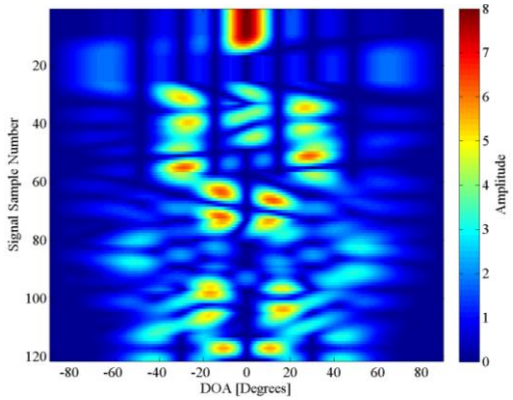


(b) Transmitted signal amplitude versus DOA.

Figure 3.43: Four patch antenna element MIMO with 4.0λ inter-element spacing.

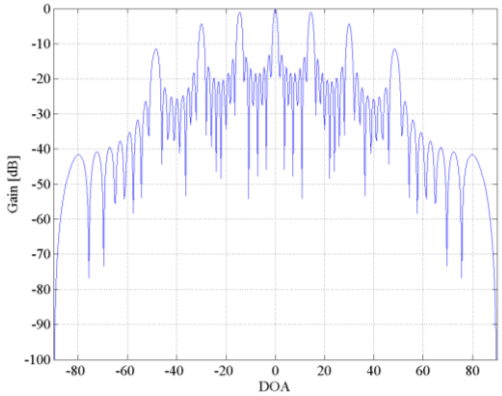


(a) Logarithmic antenna pattern for DOAs.

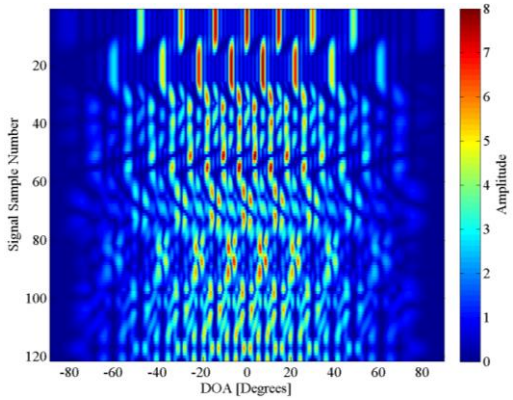


(b) Transmitted signal amplitude versus DOA.

Figure 3.44: Eight patch antenna element MIMO with 0.5λ inter-element spacing.

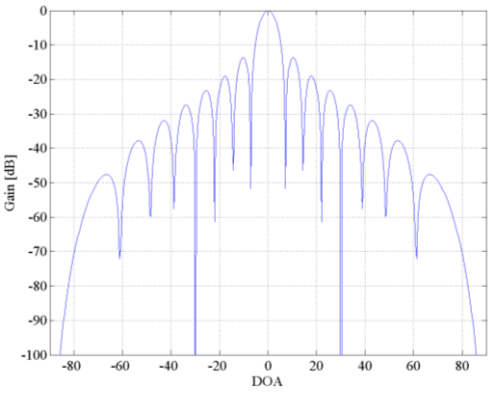


(a) Logarithmic antenna pattern for DOAs.

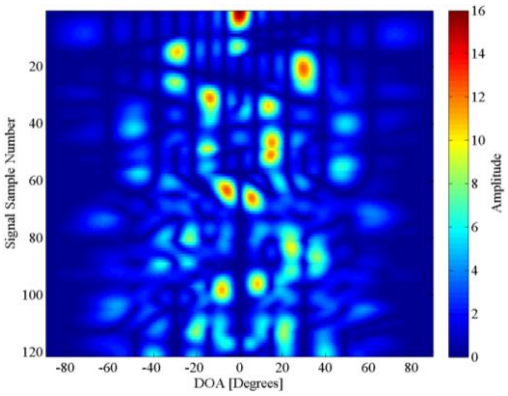


(b) Transmitted signal amplitude versus DOA.

Figure 3.45: Eight patch antenna element MIMO with 4.0λ inter-element spacing.

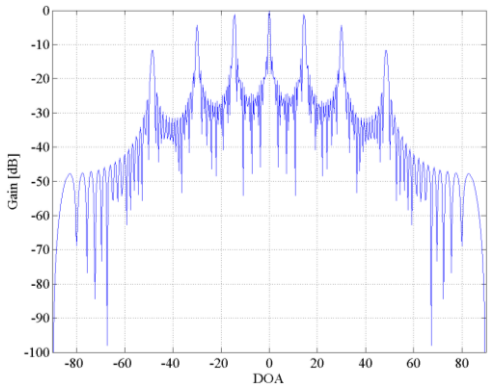


(a) Logarithmic antenna pattern for DOAs.

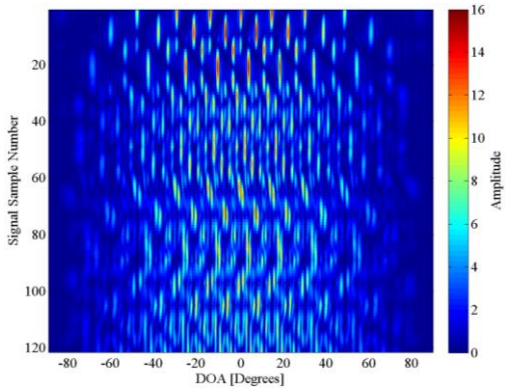


(b) Transmitted signal amplitude versus DOA.

Figure 3.46: Sixteen patch antenna element MIMO with 0.5λ inter-element spacing.



(a) Logarithmic antenna pattern for DOAs.



(b) Transmitted signal amplitude versus DOA.

Figure 3.47: Sixteen patch antenna element MIMO with 4.0λ inter-element spacing.

3.7 Conclusion

This chapter presented the simulation setup including: the simulation parameters; the signal generation for both phased array and MIMO cases; and the ES receiver implementation for both CVR and ZIFR. The resulting antenna patterns for all the simulation setups were illustrated to provide insight into the final ES receiver detection results of the phased array and MIMO radar. The detections results are presented, analysed and discussed in the following chapter.

4 Results, Analysis and Discussion

This chapter presents the ES receiver detection results from the simulation setups described in Section 3. The detection results using ideal omnidirectional antennas in the phased array and MIMO array will hereafter be referred to as the "ideal" results. The detection results using a theoretical patch antenna in the phased array and MIMO array will hereafter be referred to as the "patch" results. To make this chapter more readable, not all of the detection results will be presented. The detection results that will be presented are summarised in Table 7.

Table 7: Illustrated simulation results for the CVR.

ES Receiver	Array Type	Antenna Type	Number of Antennas	Inter-element spacing
CVR	Phased	Ideal	4	0.5λ
CVR	Phased	Ideal	4	4.0λ
CVR	Phased	Ideal	8	0.5λ
CVR	Phased	Ideal	8	4.0λ
CVR	MIMO	Ideal	4	0.5λ
CVR	MIMO	Ideal	4	4.0λ
CVR	MIMO	Ideal	8	4.0λ
CVR	Phased	Patch	4	4.0λ
CVR	MIMO	Patch	4	4.0λ

The simulation setups presented are selected intentionally to highlight the following effects:

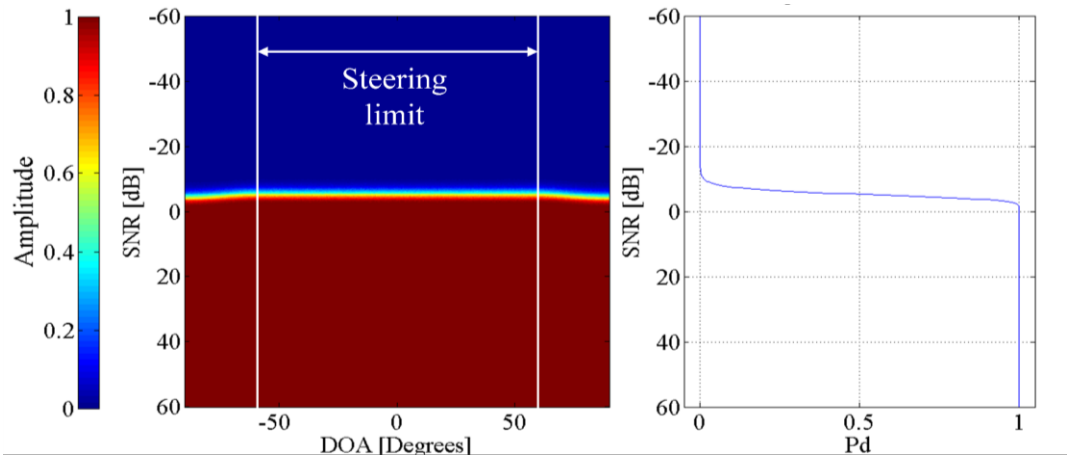
- increasing the number of antenna elements;
- increasing the inter-element spacing;
- phased array radar versus MIMO radar; and
- ideal omnidirectional antenna versus a typical patch antenna.

The same relative result applies to the ZIFR detection of the same simulation setups (excluding the difference in detection performance between the two different ES receivers). These effects are evident in the overall comparison of all the detection results, which are presented in Section 4.2. It is noted that the relative difference in findings between the 4-antenna and 8-antenna cases are comparable to the difference in findings between the 8-antenna and 16-antenna cases. The difference in findings are characterised by the doubling of the number of antenna elements. Therefore, there is no need to individually

present any of the 16 antenna cases. Each individual simulation setup result will consist of two graphs. The first graph is the PD result as a function of DOA for angles between -90 degrees and 90 degrees. The second graph averages the PD over all the DOAs to show the mean PD. This result is thus the expected value of PD if the azimuth position of the ES receiver is a uniformly distributed random variable. The detection results are analysed and discussed to highlight the various findings of this investigation.

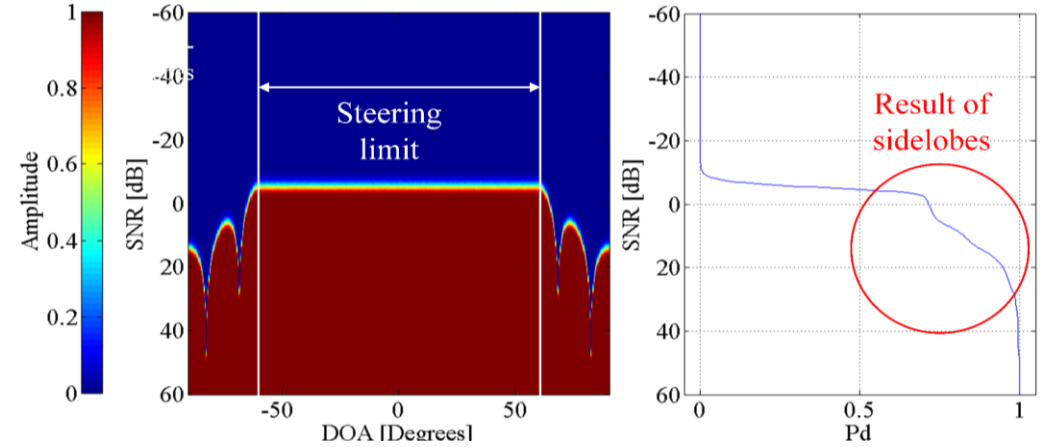
4.1 Discussion of Emphasized Detection Results

Individual simulation setups have been selected to emphasize notable regions in the detection results. For the purposes of this investigation, the detectability of the phased array radar and MIMO radar is considered at the SNR point where $P_d = 0.6$. The detectability of the ideal 4-element phased array radar using the CVR is given in Figure 4.1 and Figure 4.2.



(a) PD over all DOAs. (b) Average PD over all DOAs.

Figure 4.1: CVR detection results of a 4-element phased array at 0.5λ spacing.

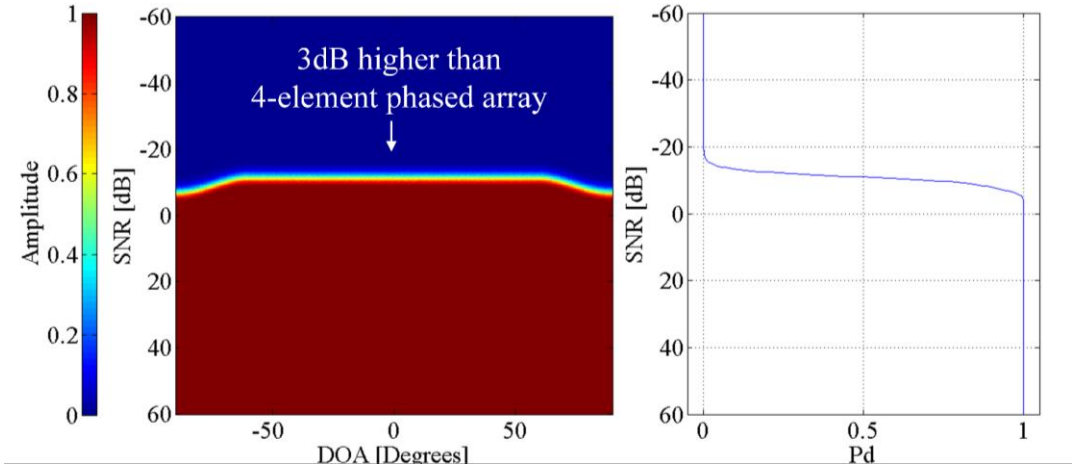


(a) PD over all DOAs. (b) Average PD over all DOAs.

Figure 4.2: CVR detection results of a 4-element phased array at 4.0λ spacing.

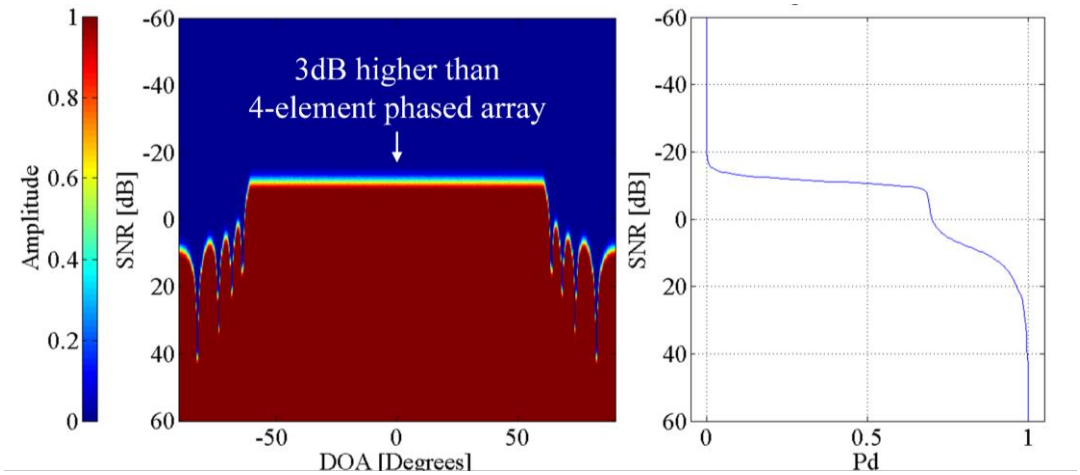
These results illustrate the effect of increasing the inter-element spacing. As discussed in Section 3.1, the beam in the phased array reference case is only scanned from -60 to 60 degrees. Beyond the angle limitation, the presence of the antenna side lobes is evident, and this region has a significant impact on the average PD over all DOAs.

The detectability of the ideal 8-element phased array radar using the CVR, given by Figure 4.3 and Figure 4.4, illustrates the effect of increasing the number of elements in the array. For the phased array radar case, the coherent combination of the signals results in an increased detectability of the signal in the presence of noise. Therefore, doubling the number of antenna elements in the array results in an increase in detectability of 3 dB as illustrated in Figure 4.5.



(a) PD over all DOAs. (b) Average PD over all DOAs.

Figure 4.3: CVR detection results of an 8-element phased array at 0.5λ spacing.



(a) PD over all DOAs. (b) Average PD over all DOAs.

Figure 4.4: CVR detection results of an 8-element phased array at 4.0λ spacing.

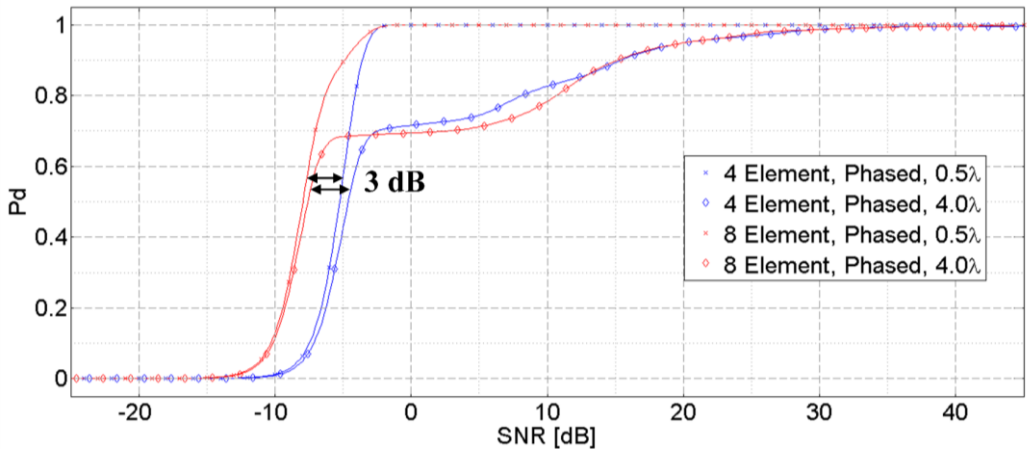
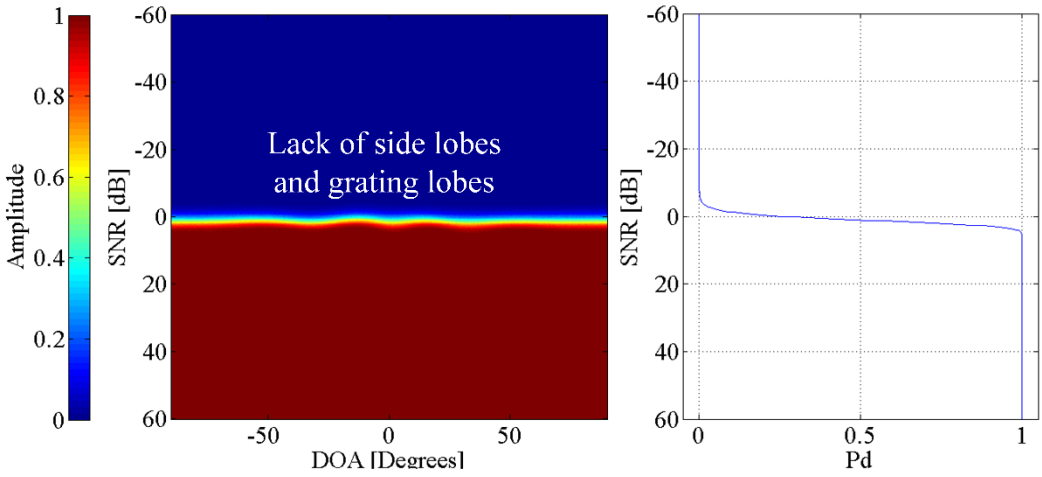


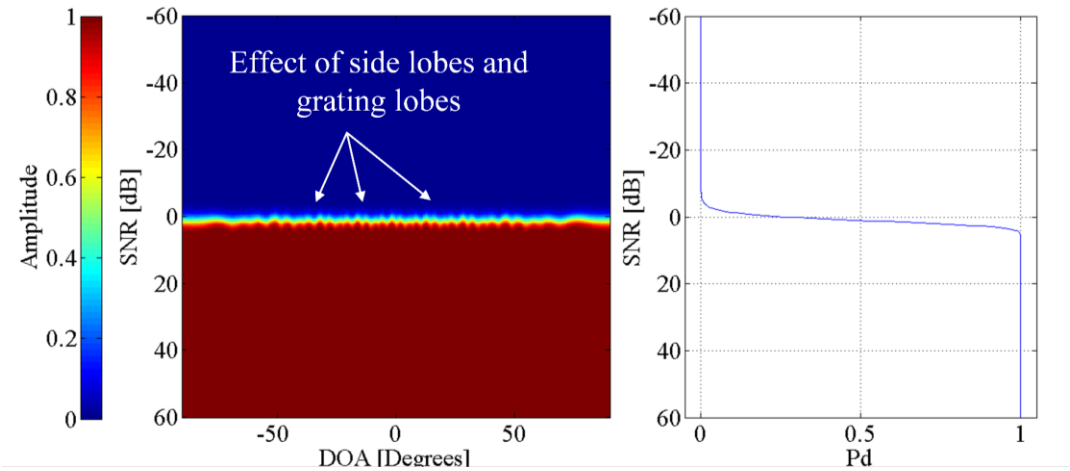
Figure 4.5: CVR detection results for 4-element versus 8-element phased arrays.

The detectability of the ideal 4-element MIMO radar using the CVR is given by Figure 4.6 and Figure 4.7. The detectability of the ideal 8-element MIMO radar is given by Figure 4.8. In comparison to the phased array radar case with the same number of antenna elements, the MIMO radar is less detectable than the phased array radar (6 dB for a 4-element phased array versus MIMO). It should also be noted that the MIMO radar's detectability is approximately the same for differing number of antenna elements in the array, as well as varying the inter-element spacing in the antenna array. This is expected due to the coherent combination of the orthogonal MIMO signals. The side lobes and grating lobes are also present in the MIMO radar results as the inter-element spacing is increased. These findings are summarised in Figure 4.9.



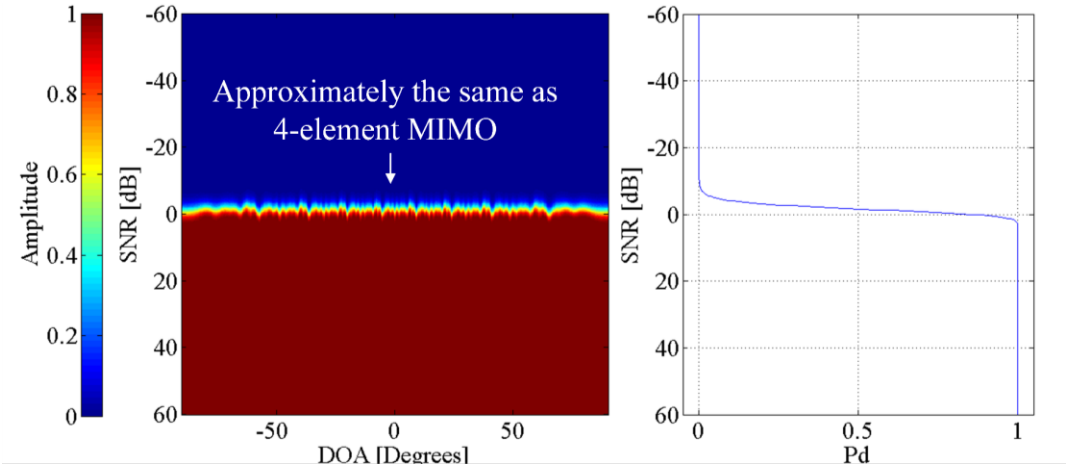
(a) PD over all DOAs. (b) Average PD over all DOAs.

Figure 4.6: CVR detection results of a 4-element MIMO array at 0.5λ spacing.



(a) PD over all DOAs. (b) Average PD over all DOAs.

Figure 4.7: CVR detection results for a 4-element MIMO array at 4.0λ spacing.



(a) PD over all DOAs. (b) Average PD over all DOAs.

Figure 4.8: CVR detection results of an 8-element MIMO array at 4.0λ spacing.

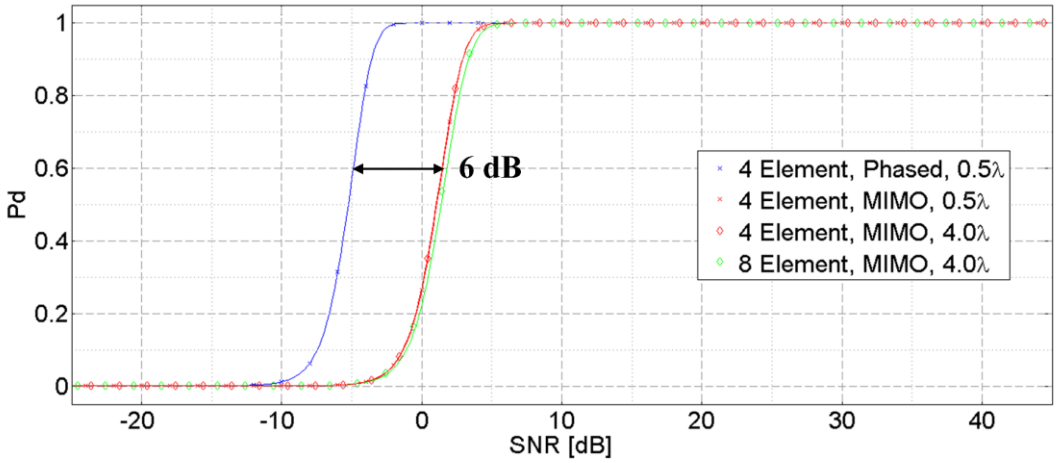
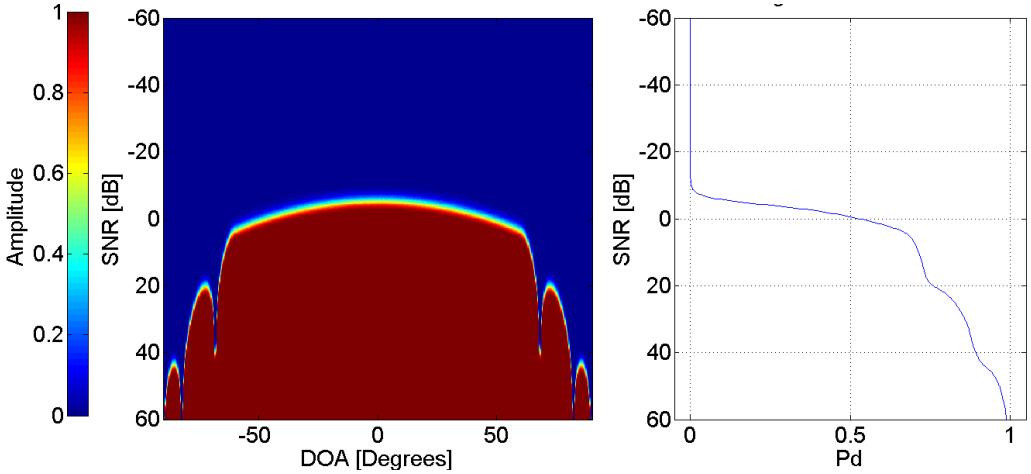


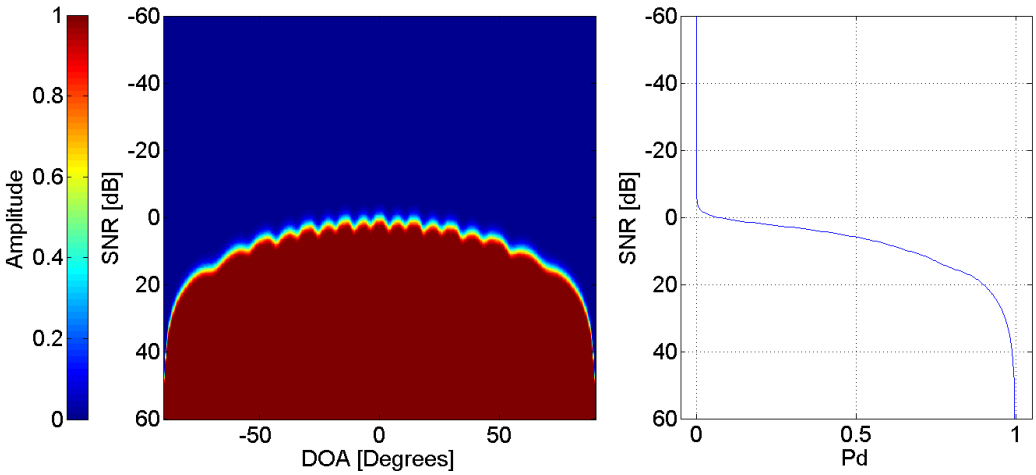
Figure 4.9: CVR detection results of a 4-element versus 8-element MIMO array.

The detectability of the patch 4-element phased array radar and MIMO radar using the CVR is given by Figure 4.10 and Figure 4.11 respectively. The effect of the patch antenna pattern is evident, reducing the side lobes significantly due to the nulls at -90 and 90 degrees. The 4-element antenna comparison between the phased array radar and the MIMO radar still differs by approximately 6 dB as illustrated in Figure 4.12.



(a) PD over all DOAs. (b) Average PD over all DOAs.

Figure 4.10: CVR detection results of a 4-element patch antenna phased array at 4.0λ spacing.



(a) PD over all DOAs. (b) Average PD over all DOAs.

Figure 4.11: CVR detection results of a 4-element patch antenna MIMO array at 4.0λ spacing.

MIMO radar was found to be more detectable at high PDs. This is as a result of the -60 and 60 degree steering limit on the phased array radar. The average PD of the phased array radar therefore drops significantly when the side lobes and grating lobes are included.

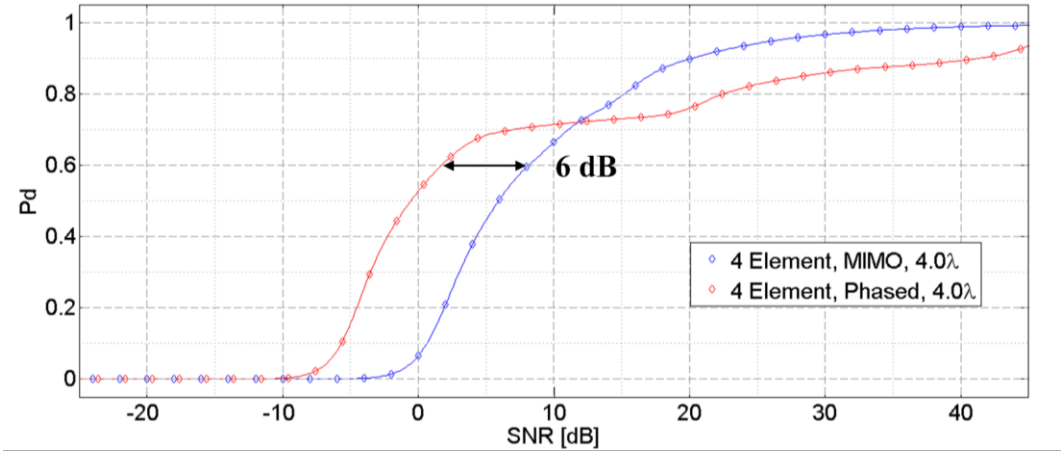


Figure 4.12: CVR detection results of 4-element phased array versus the 4-element MIMO array using patch antennas.

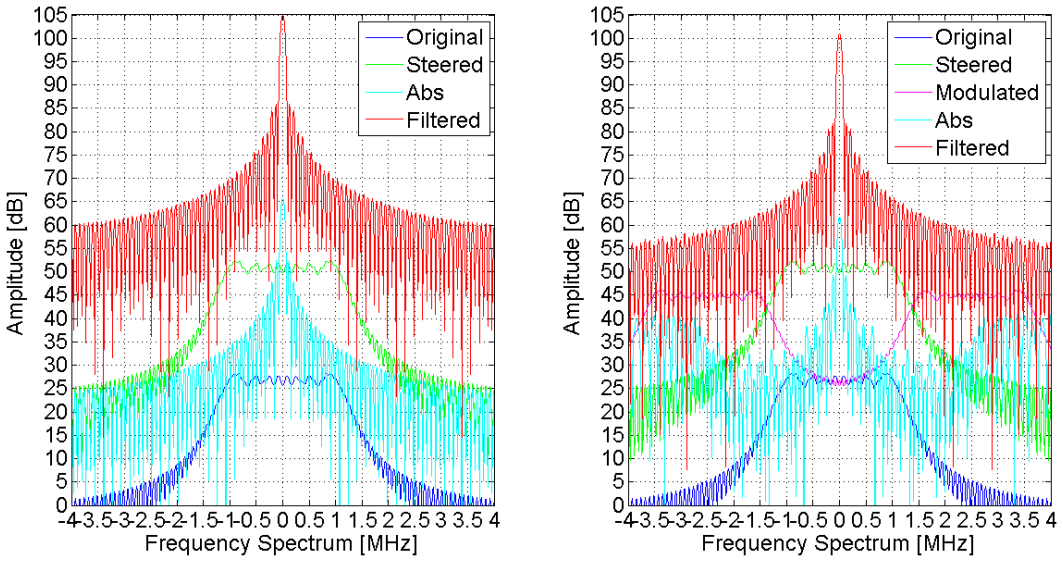
The individual simulation setups are combined to provide an overall comparison of the results. The results are presented in the following section.

4.2 Discussion of Overall Detection Results

The following subsections provide a comprehensive explanation of the notable investigation results which were emphasized in Section 4.1.

4.2.1 Comparison of the Detection Performance of the CVR and the ZIFR

As expected, the ZIFR outperforms the CVR by approximately 5 dB. In other words, the ZIFR is able to detect the phased array radar and MIMO radar signals at a 5 dB lower SNR than the CVR. The 5 dB difference is due to the CVR only considering the instantaneous amplitude of the transmitted modulated signal. Figure 4.13 illustrates the spectra of the radar signal at various points in the processing of the ES receiver. The final low-pass filtered result demonstrates the approximately 5 dB difference between the two ES receivers. Thus, the ZIFR is expected to always outperform the CVR.



(a) ZIFR case. (b) CVR case.

Figure 4.13: Comparison of the spectra at various points in the processing chain of CVR versus ZIFR with a 16-element phased array case with 0.5λ inter-element spacing.

4.2.2 Comparison of the Detectability of MIMO and Phased Array Radar

The detectability of the phased array radar and MIMO radar is also expected. Consider the case of a phased array and MIMO array, both with a single antenna element. The detectability would be similar, depending on the transmitted signal. In the case of a 2-element array, the phased array signal's coherent combination would double the signal gain. This is as compared to the MIMO array signal's coherent combination of instantaneous phasors which may not combine in the same direction, which would result in approximately the same signal gain as a single antenna element. The doubling of the phased array's signal gain would result in a 3 dB difference in the detectability of the phased array signal. The results show that the 16-element phased array radar is approximately 6 dB more detectable than the 4-element phased array radar. This is as compared to the detectability of MIMO radar, where the detectability of a 16-element array is approximately the same as the detectability of the 4-element array. Therefore, the 16-element phased array is 12 dB more detectable than the 16-element MIMO array. The slight difference in MIMO radar detectability can be attributed to the varying combinations of the transmitted signals.

The differing inter-element spacing in the phased array effectively lowers the mean PD. This is as a result of a narrower main beam, the side lobes and the grating lobes. The MIMO array's mean PD remains approximately the same. The slight difference in detectability can again be attributed to the varying combinations of the transmitted signals.

In the ideal antenna case of phased array radar versus MIMO radar, the phased array radar is more detectable than the MIMO radar. However, due to the steering limitations of the phased array, the smaller side lobes effectively lower the average PD of the phased array cases. As a result, the larger the inter-element spacing, the slower the phased array PD results curves reach unity. This allows the MIMO radar to reach $P_d = 1$ faster than the phased array radar.

The theoretical patch antenna case for both phased array radar and MIMO radar is similar in comparison with the ideal omnidirectional antenna case. However, the resulting cross-over of detectability of the MIMO radar and the phased array radar is not as extreme. This is due to the antenna pattern of the patch antenna reducing the effects of the side lobes and grating lobes.

4.2.3 Comparison of the ES Receiver's Detection Result to a Theoretical Benchmark

The ZIFR PD result is comparable to theoretical benchmark for ES receivers. Barton illustrated a family of curves which serves as a basis to determine PD, PFA and detectability factor for all types of radar signals and detection procedures [38]. A few sample points are extracted and presented in Table 8.

Table 8: Detection Probability and detectability for P_{fa}=10^{-4} *[38]*.

PD	0.5	0.6	0.7	0.8	0.9	0.99	0.999
SNR [dB]	9.4	10	10.5	11.05	11.8	13.3	14.2

The ZIFR results from Figure 4.17 are evaluated at $P_d = 0.6$, which corresponds to a detectability factor of approximately -4 dB. For a single sample detection (thresholding directly after taking the absolute value of the sample), a detectability factor of 10 dB can be expected for $P_d = 0.6$ and $P_{fa} = 10^{-4}$. The 14 dB difference between the ZIFR results and the theoretical benchmark can be attributed to the noncoherent integration gain from taking the absolute value of the signal followed by the low-pass filter over the entire radar signal pulse length.

Noncoherent integration gain results from the integration of the absolute values of the signal samples [43]. Peebles presented an empirical formula that approximates the noncoherent integration gain, G_{nc} in dB, for the case of a square-law detector, given by:

$$G_{nc} = 6.79(1 + 0.253P_d)\left(1 + \frac{\log_{10}(1/P_{fa})}{46.6}\right)(\log_{10} N) \ldots$$
$$\ldots (1 - 0.14\log_{10} N + 0.0183\log_{10}^2 N), \tag{4.1}$$

where N is the number of samples. It should be noted that this approximation is accurate to 0.8 dB for $N \in [1,100]$, $P_d \in [0.5,0.999]$ and $P_{fa} \in [10^{-8}, 10^{-2}]$. Furthermore, the detection performance of a linear versus a square-law detector varies by approximately 0.2 dB [44]. A comparison of simulation results using single antenna element phased arrays and MIMO arrays with varying values of N versus their respective theoretical benchmarks is illustrated in Figure 4.14.

As shown in Figure 4.14, the simulation results are similar to the theoretical benchmarks More specifically, it is shown that even though the simulation case of $N = 121$ is outside of the approximation's boundaries, the results remain comparable with an error of approximately 0.4 dB. The approximate 14 dB difference for the case of $P_d = 0.6$, $P_{fa} = 10^{-4}$ and $N = 121$ is accounted for by the noncoherent integration gain calculated G_{nc} = 13.93 dB using (4.1). Therefore, it can be concluded that the results are well calibrated and are comparable to their respective theoretical benchmarks.

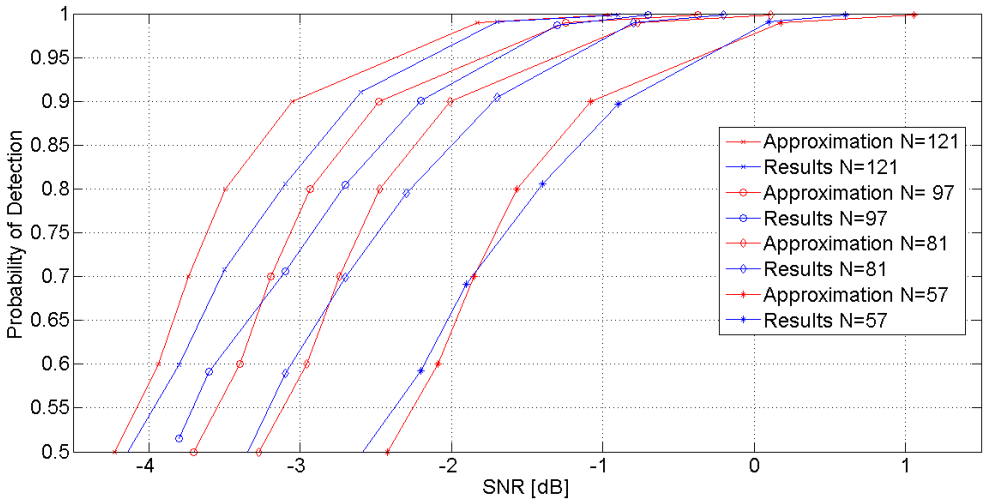


Figure 4.14: Detectability of simulation results versus theoretical benchmarks for interpolated Hadamard codes with lengths of 8, 11, 13 and 16.

4.2.4 Comparison of ES Receiver and Radar Detection Ranges

Recall that this investigation focussed on the detectability of the radar signals by ES receivers in terms of the relative SNR. This is done irrespective of the radar detection range due to the fact that the full MIMO radar has the same detection range as its phased array radar counterpart (both have the same number of array elements). This implies that the

during the time required for the phased array radar to scan the entire space, the full MIMO radar can accrue sufficient target energy to obtain the same detection range [45].

The radar's received power is given by

$$P_R = \frac{P_T G_T G_R \lambda^2 \sigma}{(4\pi)^3 R^4 L_R}, \tag{4.2}$$

where R is the range, P_T is the transmitted power, G_T is the transmit antenna gain, G_R is the receive antenna gain, σ is the radar cross section, L_R is the loss factor for the radar and P_R is the power received [1]. Solving for range:

$$R = \sqrt[4]{\frac{P_T G_T G_R \lambda^2 \sigma}{P_R (4\pi)^3 L_R}}. \tag{4.3}$$

The noise power of the radar is given by

$$P_N = kTB_R N_R, \tag{4.4}$$

where k is Boltzmann's constant, N_R is the radar receiver noise figure, taken at the reference temperature T, and B_R is the bandwidth of the radar receiver. The SNR at which the radar senses a given target is then given by

$$\mathrm{SNR_{dB}} = 10\log_{10}\left(\frac{P_R}{P_N}\right) = 10\log_{10}\left(\frac{P_S G_T G_R \lambda^2 \sigma}{(4\pi)^3 R^4 L_R k T B_R N_R}\right). \tag{4.5}$$

Similar to the radar equation, the ES receiver's equation is given by

$$P_R = \frac{P_S G_T G_E \lambda^2}{(4\pi)^2 R^2 L_E}, \tag{4.6}$$

where G_E is the ES receiver's antenna gain and L_E is the loss factor for the ES receiver. Solving for range:

$$R = \sqrt[2]{\frac{P_S G_T G_E \lambda^2}{P_R (4\pi)^2 L_E}}. \tag{4.7}$$

The noise power of the ES receiver is given by

$$P_N = kTB_E N_E, \tag{4.8}$$

where B_E is the bandwidth of the ES receiver and N_E is the ES receiver noise figure [46]. The SNR at which the ES receiver senses the radar's transmitted signal is then given by

$$\mathrm{SNR_{dB}} = 10\log_{10}\left(\frac{P_R}{P_N}\right) = 10\log_{10}\left(\frac{P_S G_T G_E \lambda^2}{(4\pi)^2 R^2 L_E k T B_E N_E}\right) \tag{4.9}$$

It is important to note from (4.2) and (4.6), the radar is working against a factor of R^4, whereas the ES receiver is working against a factor of R^2.

A numerical example for a single sample detection (includes pulse compression gain, but excluding any pulse-to-pulse signal processing gain) is used to illustrate the detection ranges of phased array radar and MIMO radar. The parameters used in the example are provided in Table 9. Note that at the listed power levels and antenna numbers, this would be more suited towards short range surveillance radar applications.

The detection ranges for this numerical example are illustrated in Figure 4.15. The phased array radar and MIMO radar are shown to have identical detection ranges. It is evident that ES receivers have the clear detection advantage over radars.

Table 9. Example radar and ES receiver parameters.

Radar parameter	**Value**
Number of array elements	16
Single antenna element transmit power	1 W
Single antenna element gain	1 (0 dB)
Radar loss factor	1
Radar centre frequency	1 GHz
Temperature	290 K
Radar bandwidth	2 MHz
Radar noise figure	3 dB
Radar cross section	10 m^2
ES receiver bandwidth	5 MHz
ES receiver noise figure	8 dB
ES receiver gain	0.63 (-2 dB)
ES receiver loss factor	1

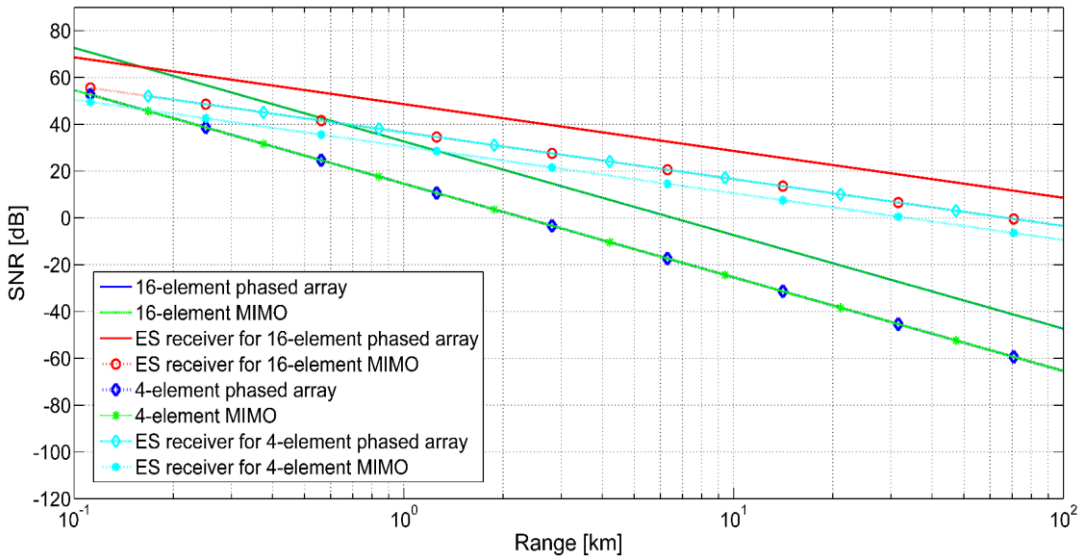
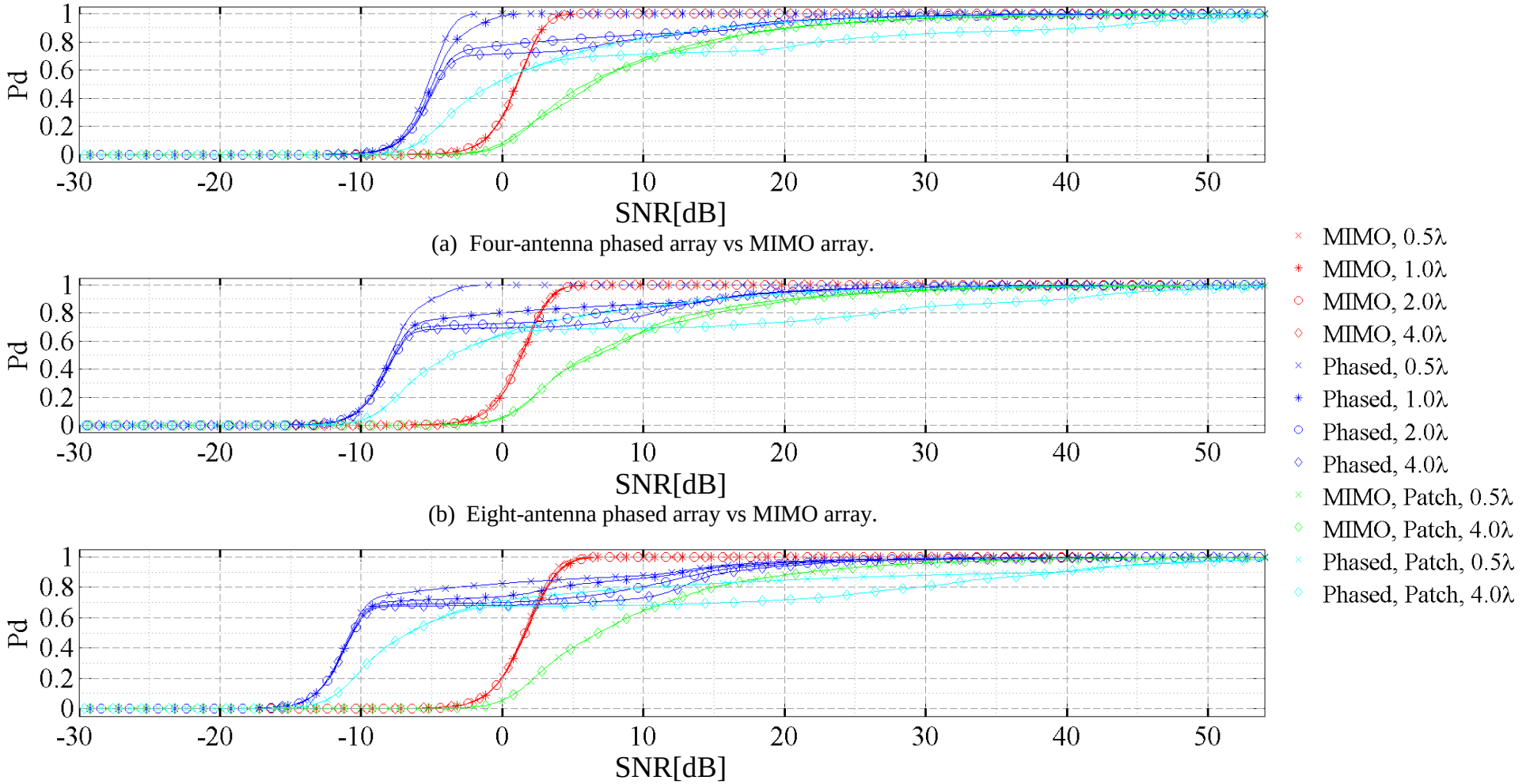


Figure 4.15: Comparison of detection ranges of radar versus ES receivers.

4.2.5 Overall Detection Results

The overall comparison of the detection results for the CVR and ZIFR are given by Figure 4.16 and Figure 4.17 respectively. The findings noted in the previous sections are also highlighted in Figure 4.18 and Figure 4.19.

The main question of this investigation is the detectability of the MIMO using conventional ES receivers such as the CVR and the ZIFR. The basic case of a 4-element MIMO radar case is less detectable than the equivalent phased array radar case by approximately 6 dB, which is a substantial difference (6 dB doubles the range at which the phased array radar can be detected). The loss between the detectability of the phased array radar and MIMO array radar widens as the number of antenna elements in the arrays increase. The 16-element MIMO radar case is found to be 12 dB less detectable than the phased array case. This result alone indicates that the research into MIMO radar signal-specific ES receivers could be necessary in future. Given that the detection range of phased array radar and its comparable MIMO radar counterpart, the results imply that there would be an advantage to using MIMO radar when faced with the CVR and ZIFR, assuming MIMO radar was practically feasible to implement. A more comprehensive investigation into the matter could possibly shed more insight into the necessity of ES receiver algorithms which are designed to detect MIMO radar signals.

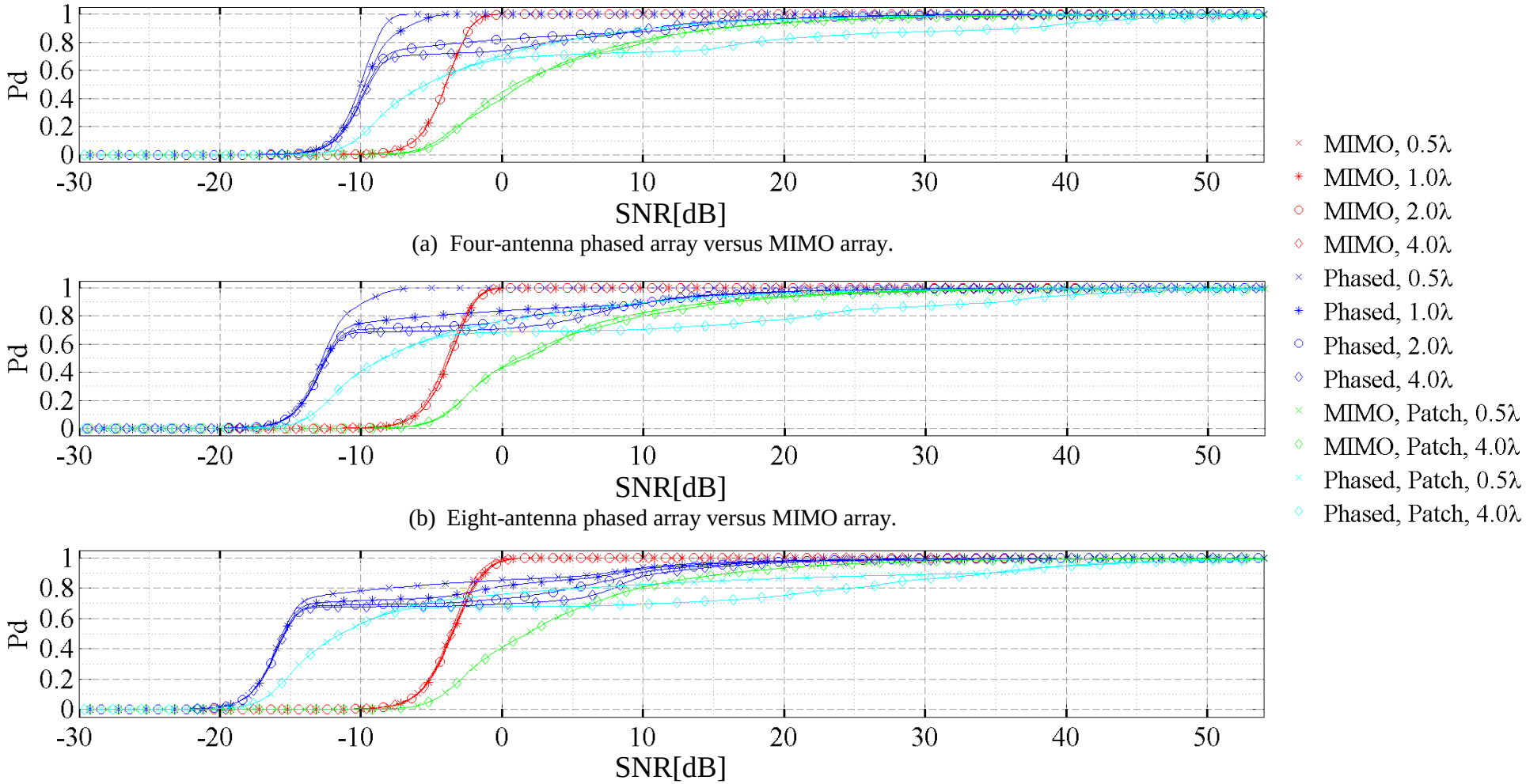


(a) Four-antenna phased array vs MIMO array.

(b) Eight-antenna phased array vs MIMO array.

(c) Sixteen-antenna phased array versus MIMO array.

Figure 4.16: Overall CVR PD result averaged over all DOAs.



(a) Four-antenna phased array versus MIMO array.

(b) Eight-antenna phased array versus MIMO array.

(c) Sixteen-antenna phased array versus MIMO array.

Figure 4.17: Overall ZIFR PD result averaged over all DOAs.

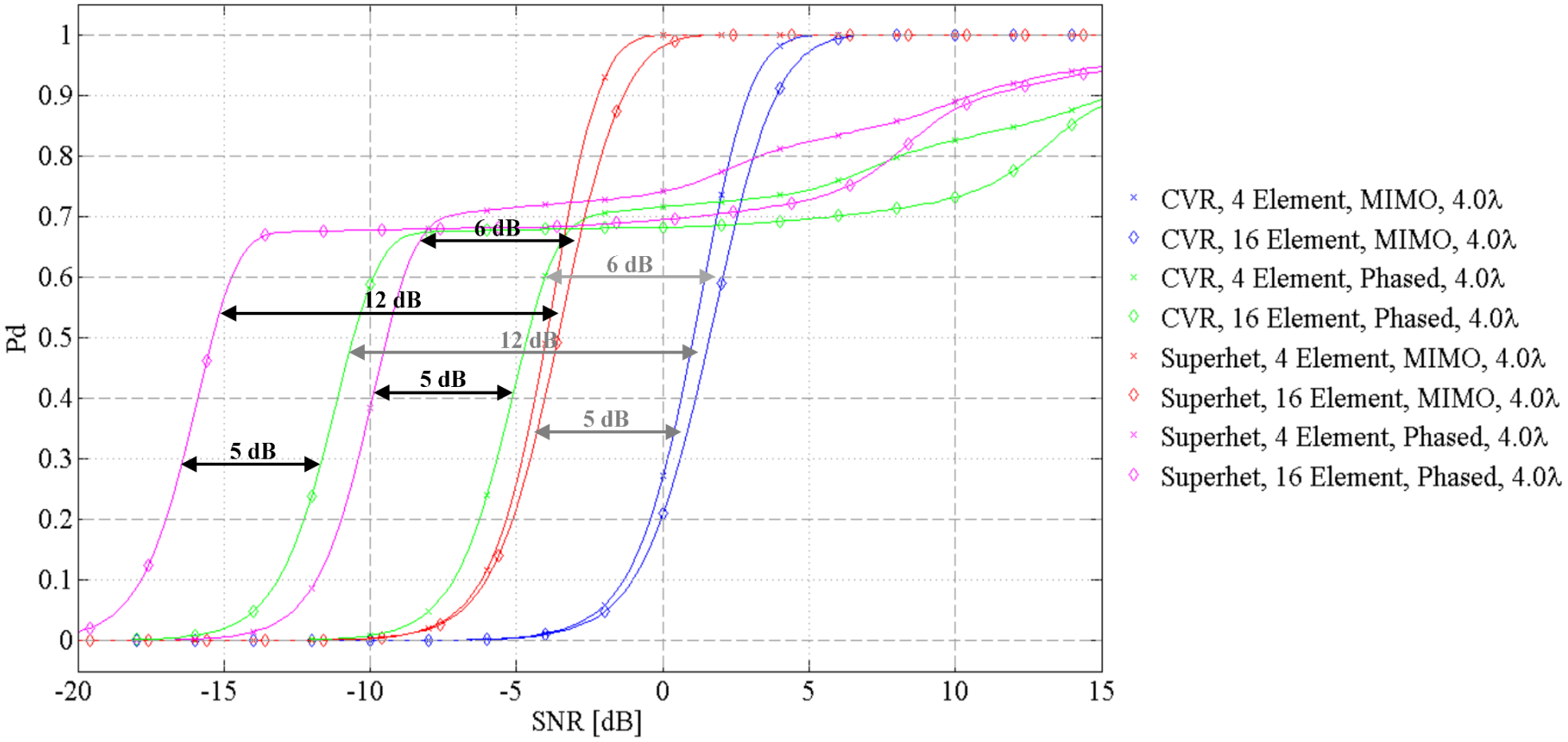


Figure 4.18: Comparison of CVR versus ZIFR PD results (4.0λ only) for the case of ideal omnidirectional antenna array elements.

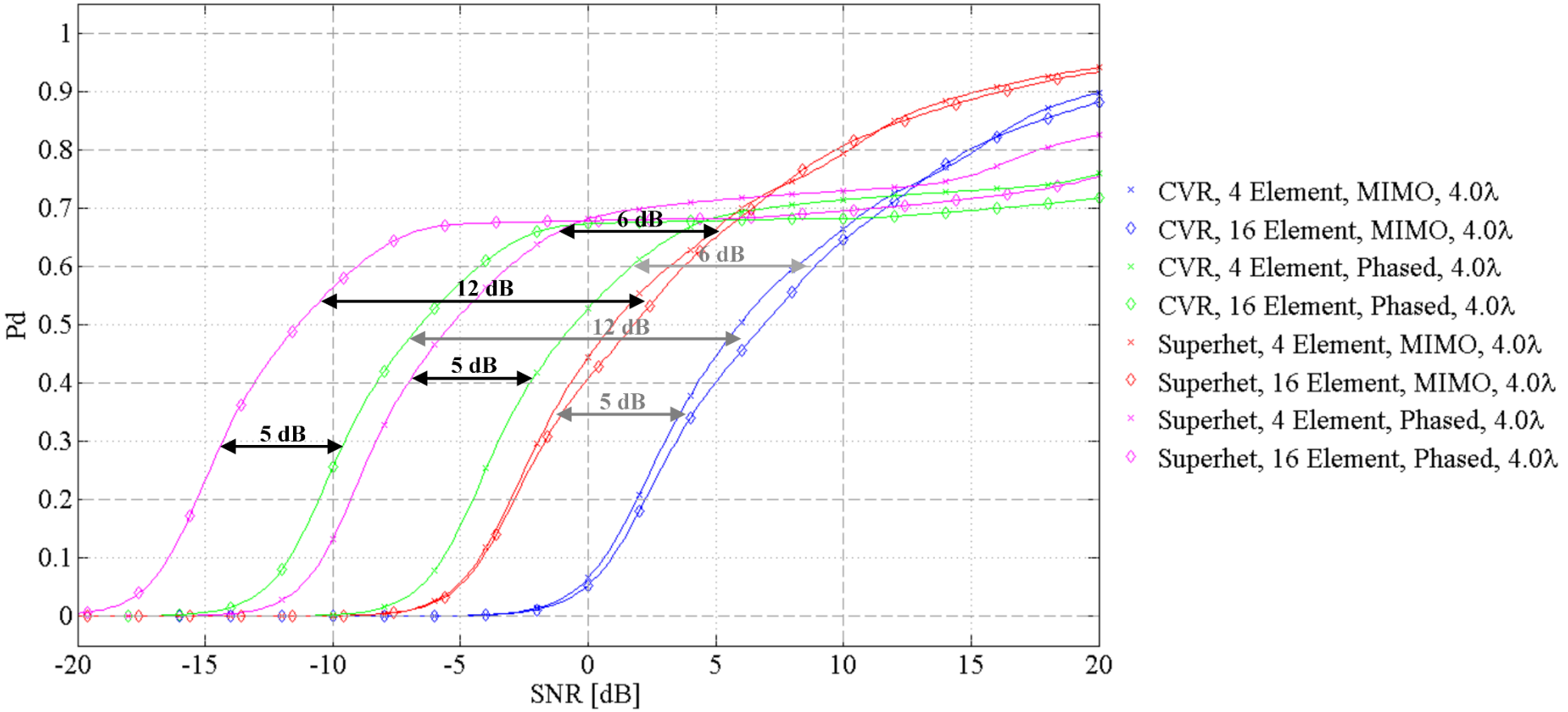


Figure 4.19: Comparison of CVR versus ZIFR results (4.0λ only) for the case of patch antenna array elements.

4.3 Conclusion

To make this chapter more readable, not all of the simulation results were individually presented and discussed. Specific simulation results were chosen to highlight the notable findings of this investigation. A combined overall comparison of all the simulation setups per ES receiver was illustrated, analysed and discussed. This dissertation is summarised in Chapter 5, and recommendations for a more comprehensive investigation are discussed in Chapter 6.

5 Conclusion

The aim of this investigation was to determine the detectability of MIMO radar signals using conventional ES receivers such as the CVR and the ZIFR. This investigation focusses on co-located ULAs and assumes a lossless RF propagation environment. To create meaningful results, the detectability of the MIMO radar signals was compared to the detectability of the equivalent phased array radar signal.

The relevant fundamental background theory was first presented, followed by the development of suitable models for the phased array, the MIMO array, the CVR, and the superhet. More specifically, the type of superhet used in this investigation was the ZIFR, which retains the phase information of the signals. Various simulation setups were investigated, by varying the number of transmit antenna elements in the arrays and by varying the inter-element spacing in the arrays. Several simulation constraints, such as each transmitting antenna element transmits equal power, were introduced to make the comparison between the MIMO radar and phased array radar as fair as possible. The CVR and ZIFR implementations were then presented. It should be noted that the radar pulse length is assumed to be known a-priori, and the low-pass filter for both ES devices was matched to the radar pulse length.

The results of this investigation show that the MIMO radar signals are less detectable than the phased array radar signals. This is due to the coherent constructive combination of phased array radar signals, which results in a signal gain. The signal gain increases as the number of antenna elements increases. In contrast, the coherent constructive and destructive combination of the MIMO radar signals results in a varying signal power over the length of the radar pulse. This signal gain remains approximately constant as the number of antenna elements is increased. Therefore, as the number antenna elements increases in both the phased array radar and the MIMO radar, the difference in detectability increases as well.

The detectability of the phased array radar and the MIMO radar was considered at $P_d = 0.6$ and $P_{fa} = 10^{-4}$. The 4-element comparison resulted in a 6 dB detectability difference, and the 16-element comparison resulted in a 12 dB detectability difference. Therefore, each doubling of the number of antenna elements resulted in a 3 dB detectability difference. Over all the simulation setups considered, the phased array setups were found to always be more detectable than its MIMO counterpart at the specified PD of 0.6. However, it should be noted that for scenarios where PD is greater than 0.6, some MIMO cases are found to be more detectable than the phased array. This result can be attributed

to the inclusion of the sidelobe region of the antennas in the simulation setup by limiting the scanning angle to between -60 and 60 degrees. If the detection results were only analysed between -60 and 60 degrees, the phased array setups would be consistently more detectable than its MIMO counterparts over the full range of PDs.

The ZIFR was found to outperform the CVR in detecting both types of signals by a margin of 5 dB. This is due to the ZIFR being a quadrature receiver, thus being able to detect the maximum possible amplitude for any sample. However, both ES receivers struggle to detect MIMO radar signals in comparison to detecting phased array radar signals. This result suggests that research into MIMO radar signal specific ES receivers may be necessary should the need arise to detect MIMO radar signals in future.

6 Future Recommendations

The results of the investigation suggest that conventional ES receivers such as the CVR and the superhet (specifically the ZIFR) are not well suited to detecting MIMO radar signals. Many assumptions and simplifications were made in this investigation. Thus, a more comprehensive investigation into the detectability of MIMO radar signals could be necessary to justify research into MIMO radar specific ES receivers. A list of future recommendations to take this investigation forward is presented below.

- A more comprehensive investigation into the CVR and ZIFR. Many simplifying assumptions were used in this analysis and investigation. The results of a fully modelled CVR and ZIFR would be interesting to compare with.
- This investigation assumed a lossless RF propagation environment. It would be interesting to incorporate the effects of RF propagation such as multipath and atmospheric effects.
- This investigation was performed entirely via computer simulation. It would be interesting to see this investigation implemented and performed via hardware.
- Only two conventional ES receivers were explored. The detection performance of other conventional ES equipment such as the Instantaneous Frequency Measurement (IFM) receiver would be interesting.
- This investigation only used the Hadamard matrix to generate MIMO signals. As seen in the results, the different combination of MIMO signals can have an effect on the outcome. It would be interesting to investigate the effects of MIMO signals generated from other kinds of orthogonal codes such as Frank-Zadloff-Chu sequences and Generalised Chirp-Like sequences.
- Stationary platforms are assumed in this investigation. The effects of a moving platform (for example an airborne case) and its effect thereof would be interesting. In reality, either transmitter or receiver or both could be airborne.
- Co-located ULAs were used in this investigation. The extension of the investigation to 2D spatial coverage and spatially separated (not co-located) antennas and the corresponding results would be interesting.
- This investigation suggests that research into the ES receivers optimised for MIMO radar may be necessary. This depends largely on whether or not any other existing ES receiver could be suitable for detecting MIMO radar signals.

- These results might lead to new applications where MIMO and phased array techniques are used in the same radar, but each is used depending on the tactical situation. For example, MIMO could be used for a stealthy approach and then phased array for accurate target tracking and engagement.
- It is hypothesized that standard pulse length measurement algorithms may not work on MIMO radar signals. This needs to be clarified.

These recommendations form the logical next steps (in no particular order) to furthering the investigation into the detectability of MIMO radar signals and the use of MIMO techniques in radar systems.

References

[1] G. W. Stimson, Introduction to Airborne Radar, SciTech Publishing, Inc., 1998.

[2] D. Adamy, EW 101: A First Course in Electronic Warfare, Artech House Inc., 2001.

[3] "Joint Publication 3-13.1 Electronic Warfare," United States Military, 2007.

[4] L. A. Miller and A. Surlykke, "How Some Insects Detect and Avoid Being Eaten by Bats: Tactics and Countertactics of Prey and Predator," *BioScience,* vol. 51, pp. 570-581, 2001.

[5] T. Jeffrey, Phased-Array Radar Design: Application of Radar Fundamentals, Institution of Engineering and Technology, 2009.

[6] F. Daum and J. Huang, "MIMO Radar: Snake Oil or Good Idea?," *Waveform Diversity and Design Conference,* pp. 113-117, 2009.

[7] J. Li and P. Stoica, "MIMO Radar with Colocated Antennas," *IEEE Signals Processing Magazine,* vol. 24, pp. 106-114, 2007.

[8] C. Y. Chong, "Signal Processing for MIMO Radars: Detection Under Gaussian and Non-gaussian Environments and Application to STAP," Supelec, 2011.

[9] J. Li and P. Stoica, MIMO Radar Signal Processing, John Wiley & Sons Inc., 2009.

[10] S. Howard, S. Sirianunpiboon and D. Cochran, "Detection and Characterization of MIMO Radar Signals," in *International Conference on Radar,* 2013.

[11] J. E. Cilliers, Y. Huang and M. A. van Wyk, "On the Detectability of Multiple Input Multiple Output (MIMO) Radar Signals Using Conventional Electronic Warfare Support (ES) Receivers," in *IEEE Radar Conference,* Johannesburg, 2015.

[12] H. Krim and M. Viberg, "Two Decades of Array Signal Processing Research: The Parametric Approach," *IEEE Signal Processing Magazine,* vol. 13, no. 4, pp. 67-94, 1996.

[13] D. Dudgeon and R. Mersereau, Multidimensional Digital Signal Processing, Prentice-Hall, 1984.

[14] B. R. Mahafza, Radar System Design and Analysis using MATLAB, Chapman and Hall, 2000.

[15] H. Urkowitz, Signal Theory and Random Processes, Artech House Inc., 1983.

[16] J. Proakis and D. Manolakis, Digital Signal Processing, Prentice Hall, 1996.

[17] "IEEE Standard Radar Definitions," *IEEE Std 686-2008,* May 2008.

[18] J. Hudson, Adaptive Array Principles, Peter Peregrinus Ltd., 1981.

[19] C. A. Balanis, Antenna Theory Analysis and Design, John Wiley & Sons Inc., 2005.

[20] M. S. Smith, "Phased Array Fundamentals," *IEE Tutorial Meeting on Phased Array Radar,* vol. 1, pp. 1-133, 1989.

[21] B. Van Veen and K. Buckley, "Beamforming: A Versatile Approach to Spatial Filtering," *IEEE ASSP Magazine,* vol. 5, no. 2, pp. 4-24, 1988.

[22] S. Middleton, "The Design and Implementation of An Acoustic Phased Array Transmitter For The Demonstration of MIMO Techniques," University of the Witwatersrand, Johannesburg, 2011.

[23] O. I. Frost, "An Algorithm for Linearly Constrained Adaptive Array Processing," *Proceedings of the IEEE,* vol. 60, no. 8, pp. 926-935, 1972.

[24] F. Robey, S. Coutts, D. Weikle, J. McHarg and K. Cuomo, "MIMO Radar Theory and Experimental Results," *Conference Record of the Thirty-Eighth Asilomar Conference on Signals, Systems and Computers,* vol. 1, pp. 300-3004, 2004.

[25] E. Brookner, "MIMO Radars and Their Conventional Equivalents," in *2015 IEEE Radar Conference,* 2015.

[26] K. J. Horadam, Hadamard Matrices and Their Applications, Princeton University Press, 2007.

[27] H. Zepernick and A. Finger, Pseudo Random Signal Processing: Theory and Application, John Wiley & Sons, 2013.

[28] M. Jamil, L. Linde, J. Cilliers and D. van Wykt, "Comparison of Complex Spreading Sequences Based on Filtering Methods and Mean Square Correlation Characteristics," *Transactions of the SAIEE,* 1998.

[29] R. E. Crochiere, "Interpolation and Decimation of Digital Signal: A Tutorial Review," *Proceeedings of the IEEE,* vol. 69, pp. 300-331, 1981.

[30] T. J. Rouphael, RF and Digital Signal Processing for Software-Defined Radio, Oxford: Elsevier Inc., 2009.

[31] M. Lotter, "A Generalized Linear Root-of-Unity Interpolation," in *COMSIG 95,* 1995.

[32] M. Lotter and L. Linde, "Constant Envelope Filtering of Complex Spreading Sequences," *Electronics Letters,* vol. 31, no. 17, pp. 1406-1407, 1995.

[33] Navy, Electronic Warfare and Radar System Engineering Handbook, Naval Air Systems Command: Avionics Department, 1999.

[34] A. G. Stove, "Radar and ESM: The Current State of the LPI Battle," in *1st EMRS DTC Technical Conference,* Edinburgh, 2004.

[35] R. Wiley, Electronic Intelligence: The Interception of Radar Signals, Artech House Inc., 1985.

[36] J. Edwards, "Sensitivity of Crystal Video Receivers," *Communications, Radar and Signal Processing, IEE Proceedings F,* vol. 132, pp. 233-244, 1985.

[37] D. Heeger, "Signal Detection Theory," Stanford University, 1998.

[38] D. K. Barton, Modern Radar System Analysis, Artech House Radar Library, 1988.

[39] J. E. Cilliers and J. C. Smit, "Pulse Compression Sidelobe Reduction by Minimization of Lp-Norms," *IEEE Transactions on Aerospace and Electronic Systems,* vol. 43, pp. 1238-1247, 2007.

[40] G. Galati, Advanced Radar Techniques and System, IEE Radar, Sonar, Navigation and Avionics, No 4, 1993.

[41] J. Proakis, Digital Communications, McGraw-Hill Book Co., 1989.

[42] W. Stutzman and G. Thiele, Antenna Theory and Design, John Wiley & Sons, 2012.

[43] M. A. Richards, Fundamentals of Radar Signal Processing, New York: McGraw-Hill, 2005.

[44] P. Z. Peebles, Radar Principles, John Wiley & Sons, 2007.

[45] Y. Qu, G. S. Liao, Q. Zhu, X. Y. Liu and H. Jiang, "Performance Analysis of Beamforming for MIMO Radar," *PIER 84*, pp. 123-134, 2008.

[46] F. Potgieter, "Low Probability of Intercept (LPI) Radar," CSIR EW Research and Applications Group, Defense, Peace, Safety & Security, Johannesburg, 2015.